ANL-6291

Argonne National Laboratory

HEAT TRANSFER TO A MIST FLOW

by

Jerald D. Parker and Richard J. Grosh

DISCLAIMER

Price $3.00 . *Available from the Office of Technical Services, Department of Commerce, Washington 25, D.C.*

ANL-6291
Engineering and Equipment
(TID-4500, 16th Ed.)
AEC Research and
Development Report

ARGONNE NATIONAL LABORATORY
9700 South Cass Avenue
Argonne, Illinois

HEAT TRANSFER TO A MIST FLOW

by

Jerald D. Parker* and Richard J. Grosh

Purdue Research Foundation

Lafayette, Indiana

January 1961

Argonne National Laboratory Subcontract 31-109-38-704
September 1959 to August 1960
Technical Report No. 5

*Work reported here formed the basis of a Ph.D. Thesis in Mechanical Engineering at Purdue University.

Operated by The University of Chicago
under
Contract W-31-109-eng-38

NOTE

The definition of the term quality, which appears in this thesis, is based upon mass flow rates. This follows the convention most commonly observed in the current literature and differs from the definition given in some thermodynamic texts.

ACKNOWLEDGMENTS

The author is grateful to the National Science Foundation and to the Atomic Energy Commission for the financial assistance that made possible his graduate work at Purdue University.

He is sincerely appreciative of the advice, the encouragement, and the assistance of his advisor, Professor Richard J. Grosh.

The friendly cooperation of the technicians in the Mechanical Engineering Laboratory is acknowledged with thanks.

The frequent help and advice given by fellow graduate students at Purdue were important in the completion of this work and are gratefully acknowledged.

To his wife, Verna Lee, who furnished continuous encouragement and understanding, the author expresses his deepest and most sincere thanks.

TABLE OF CONTENTS

Page

APPENDICES

LIST OF TABLES

LIST OF ILLUSTRATIONS

ABSTRACT

Parker, Jerald Dwain. Ph.D., Purdue University, January, 1961. Heat Transfer to a Mist Flow. Major Professor: Richard J. Grosh.

An experimental and analytical study was made of the heat transfer characteristics of a mist flow of steam and water droplets flowing vertically upward in a round tube. A simplified analytical model, based on momentum, mass, and energy considerations, was developed which shows qualitatively that severe temperature fluctuations are characteristic of such flows under constant wall heat flux conditions.

The experimental investigation was made with steam at 30 psia flowing through an electrically heated one-inch ID copper tube, four feet in length. The quality was varied by the injection of water into the steam prior to its entry into the heated section. Total mass flow rates of 200, 300, and 400 lbs per hour were maintained for the tests. Heat fluxes were varied from 3,020 to 20,700 Btu/hr square feet, and inlet qualities were varied from 89 to 100 percent.

The experimental data showed that the analytical model gave a fairly accurate qualitative description of the tube wall temperature variation with length. The analysis of the data seemed to indicate that the assumptions of equilibrium between phases and constant values for the mass transfer coefficient for droplets were incorrect.

An electronic spray analyzer used in the investigation proved to be useful for the detection of droplets but was of little value in determining droplet spectrums.

Very high values of heat transfer coefficient were found for the annular-mist flow region that exists just upstream from the mist flow region. In the mist flow region two distinct types of heat transfer were noted, depending upon whether the spheroidal state existed for the droplets striking the heated tube wall. For wall temperatures below a certain value heat transfer coefficients 3 to 6 times those for dry steam were noted. For wall temperatures above this critical value the heat transfer coefficients were almost identical to those for dry steam, even with considerable moisture present in the mist.

INTRODUCTION

The transfer of heat to an evaporating fluid is a common problem in many modern engineering processes. In many of these processes the energy for heating is supplied by a nuclear reaction, a chemical reaction, or by electrical heating. In such cases, the energy supplied per unit area is usually constant or nearly constant over the heat transfer surface. Thus, a sharp decrease in the heat transfer coefficient could cause overheating at some position on the surface, in some cases leading to a condition called "burnout" where the surface is permanently damaged.

One type of burnout which occurs with high heat-flux boiling systems is that due to a transition from nucleate to film boiling. Extensive work has been done during recent years on methods of predicting the occurrence of this type of burnout in evaporator tubes.

Another type of burnout, sometimes called net boiling burnout or two-phase burnout, occurs in systems with relatively high qualities present and in some cases even with moderate heat fluxes. Several investigators have attributed this sudden change in heat transfer coefficient to a change in the two-phase flow pattern brought about by the vaporization process. That is, a change from an annular-mist flow pattern,

where the tube wall is wet, to a dispersed or mist flow where the tube wall is relatively dry, appears to be a logical explanation for the observed decrease in film coefficients.

Although a number of investigators have noted this transition, no one has yet made a careful study of the transition phenomena. No detailed information is available for values of heat transfer coefficients in the liquid deficient region where a dispersed or mist flow is assumed to occur. In this region there is insufficient liquid present at the wall to completely cover the wall with a liquid film. It is the objective of this thesis, therefore, to investigate the heat transfer mechanism of a mist flow of steam and water droplets flowing vertically upward through a round tube at constant wall heat flux. A round, vertical tube was chosen in order to eliminate the complexities caused by corners and by gravitational forces.

Mists of various types occur in many industrial processes and yet very little information is available on their heat transfer characteristics. One of the more important and recent applications where mists are important is in rocket motors with molten fuel droplets suspended in the stream. Studies of mist have long been of importance in the field of meteorology.

This investigation may help to shed some light on this area of the rather complex subject of heat transfer to two-phase flows. It is hoped that this study may also lead to a better understanding of the transition

region between annular and mist flow, which may in some way lead to a better understanding of two-phase burnout in evaporator tubes.

LITERATURE SURVEY

Very little information was found in the literature pertaining directly to the subject of heat transfer to mists. As late as 1957, Collier (10), made a thorough review of the existing two-phase heat transfer literature. In the summary he stated that there was no available experimental data for local conditions in the liquid deficient region of evaporator tubes. It is in this region that mist flow occurs. No articles having a direct bearing on the subject were found for the period from 1957 to the present. Therefore, the literature surveyed and discussed in the following sections has to do only with background materials and thus includes material on the subjects of two-phase flow, two-phase burnout, spray and droplet behavior, and droplet measurement techniques.

Two-Phase Flow

In recent years, several articles have appeared summarizing the work done in the field of two-phase flow and listing most of the important references on the subject. Among these summaries are those of Gresham (2o), Santalo (59), Bennett (6), Isbin, et al (33), and Boggs and Fitch (o). Since these articles include fairly complete bibliographies, only the two-phase flow references that are of more recent date or those

which have an important bearing on the subject of this thesis will be reviewed.

Much of the work done in the field of two-phase flow has been directed toward the identification of the various flow patterns that can exist and toward the prediction of pressure drop during isothermal flow of gas-liquid systems. A comparison of the flow patterns presented by many of the investigators has been made by Ambrose (3). This comparison indicated good agreement considering that the transitions between flow patterns are vague and were detected visually. Ambrose lists the following patterns which were generally observed to occur as the gas-phase mass velocity was increased:

1. Pure liquid
2. Bubble flow (bubbles move along the upper part of the pipe at about the same velocity as the liquid).
3. Plug Flow (alternate plugs of gas and liquid).
4. Stratified flow (vapor flowing above the liquid).
5. Wavy flow (vapor above a wavy liquid surface).
6. Slug flow (periodic frothy slugs pass through the pipe at a greater velocity than the average liquid velocity).
7. Annular flow (liquid flows in a film around the inside wall of the pipe and the gas flows at a higher velocity as a central core).

8. Mist or spray flow (gas with liquid entrainment flowing in a pipe with wetted walls).

9. Pure gas.

Of course, some of the above patterns apply only to horizontal flow.

In a system in which a boiling occurs, the ratio of liquid to vapor changes with distance from the entrance of the tube, and the flow patterns therefore change. At sufficiently high qualities one would expect the mist or spray flow to eventually develop.

It is interesting to note that the description of mist flow given by Ambrose includes wetted walls. It should more properly be given the name of annular-mist flow. It is probable that a true mist flow would exist in adiabatic flow only under unusual conditions. Droplets dispersed in the turbulent gas core usually diffuse toward the duct wall and build up a liquid film. This would not be the case of course if sufficient heat were being added at the wall to evaporate the droplets as they struck. In some cases the liquid film may be so thin as to be practically invisible to the eye, especially if the surface of the film is laminar. This author, (J.D.P.), observed thin water films on the inside of glass tubes with a 20 power microscope that were barely noticeable to the eye.

One of the investigators who studied the various flow patterns for a number of liquid gas combinations was Baker (4). Baker utilized the information of Jenkins, Gazley, Alves, and Kosterin to make the plot

shown in Fig. 1, using $\frac{G_g}{\lambda}$ as the ordinate and $\frac{G_L}{G_g}\lambda\psi$ as the abscissa,

where

$$\lambda = \left[\left(\frac{\rho_g}{0.075}\right)\left(\frac{\rho_L}{62.3}\right)\right]^{1/2}$$

and

$$\psi = \left[\left(\frac{73}{\sigma}\right)\mu_L\left(\frac{62.3}{\rho_L}\right)^2\right]^{1/3} .$$

The lines shown on Baker's chart do not represent sharp boundaries between flow regimes but instead they show the general area where transition occurs.

Since the ratio of steam to water flowing is determined by the quality of the mixture, the quality should determine the flow pattern that might exist. Assuming that Baker's chart would apply for steam-water mixtures, a calculation was made for the minimum quality that could exist with a mist or dispersed flow. The calculation was made for the lowest gas-phase mass flow rate shown on the chart. If it is assumed that saturated steam and water at 30 psia flows through a one-inch pipe, then

$$\lambda = 0.954$$

and

$$\psi = 0.897 .$$

From the chart a minimum value of $\frac{G_g}{\lambda} = 3 \times 10^4$.

This gives a value of $G_g = 2.86 \times 10^4$.

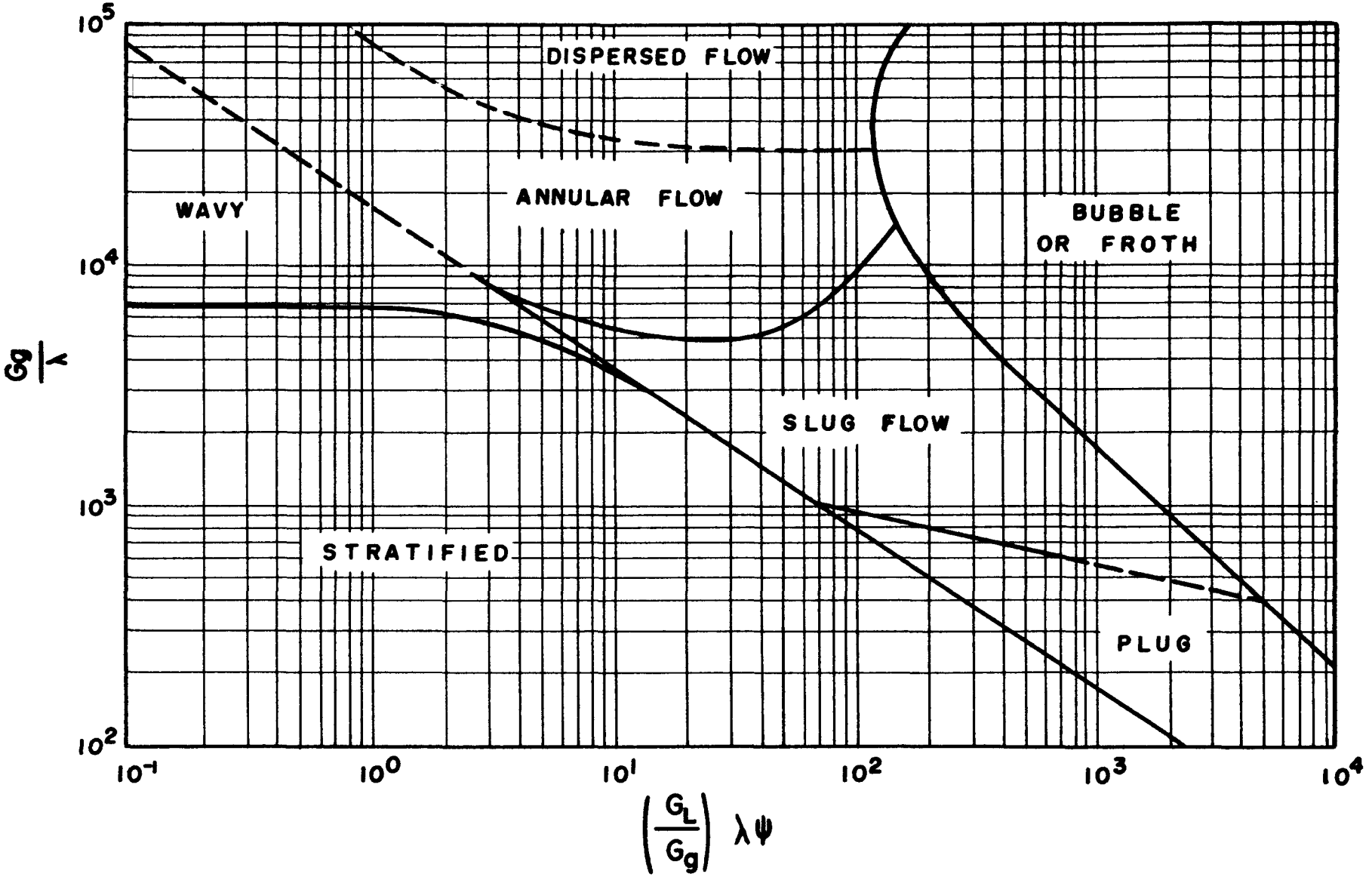

FIG. 1 FLOW REGIMES AS DESIGNATED BY BAKER.

The maximum liquid rate occurs when $\frac{G_L}{G_g} \lambda \psi = 120$ according to the chart. Therefore the maximum liquid rate for dispersed flow when $G_g = 2.86 \times 10^4$ would be

$$G_L = \frac{120\, G_g}{\lambda \psi} = 4 \times 10^6 \quad .$$

The quality would be

$$X = \frac{G_g}{G_g + G_L} = 0.0071 \quad .$$

This is a surprising result since it represents a steam-water volume ratio of only 5.75 at the assumed conditions. Of course Baker's chart may not be valid for the conditions that we have stated.

An even more surprising result that can be obtained from the chart is that it predicts a change from the dispersed pattern to the annular pattern with a decreasing liquid flow rate, assuming that the gas rate remains constant. This would indicate that as an annular film becomes thicker with increasing liquid rate a point would eventually be reached where the film of liquid would be broken up by the action of the gas and dispersed as drops in the core. There must be some definite limit to the thickness of an annular film if there is to be no dispersion of droplets into the core. This factor must be considered in the design of film cooled rocket motors (79).

It is indeed surprising, considering the high degree of importance of two-phase flows in industrial equipment, that so little has been done to carefully describe the two-phase flow regimes in any general manner. Even the most generalized work, due to Baker, is still a far cry from the type of definition needed.

Two-Phase Flow Pressure Drop

Most of the work done in the area of two-phase flow has been directed toward the prediction of pressure drop. One of the earliest studies on local pressure drops in boiling was that of McAdams, Woods, and Bryan (43), who investigated the evaporation of water flowing through a four-pass, horizontal, steam-jacketed one-inch copper pipe. Each pass was four feet long and contained three separate steam jackets. Low mass flow rates permitted nearly all of the entering liquid to be vaporized when desired. Pressure drops measured in this investigation were used in a later report (44) to determine apparent friction factors as a function of steam quality. The results are shown in Fig. 2. At the right side of the chart is shown the range of friction factors for the flow rates of the experiment, assuming that the substance flowing is all vapor. On the left is shown the range of friction factors for the various mass flow rates, assuming that the substance is all liquid. In the range of qualities from 0.4 to 1.0 the values of the apparent friction factor are not much higher than would be obtained by a linear interpolation between

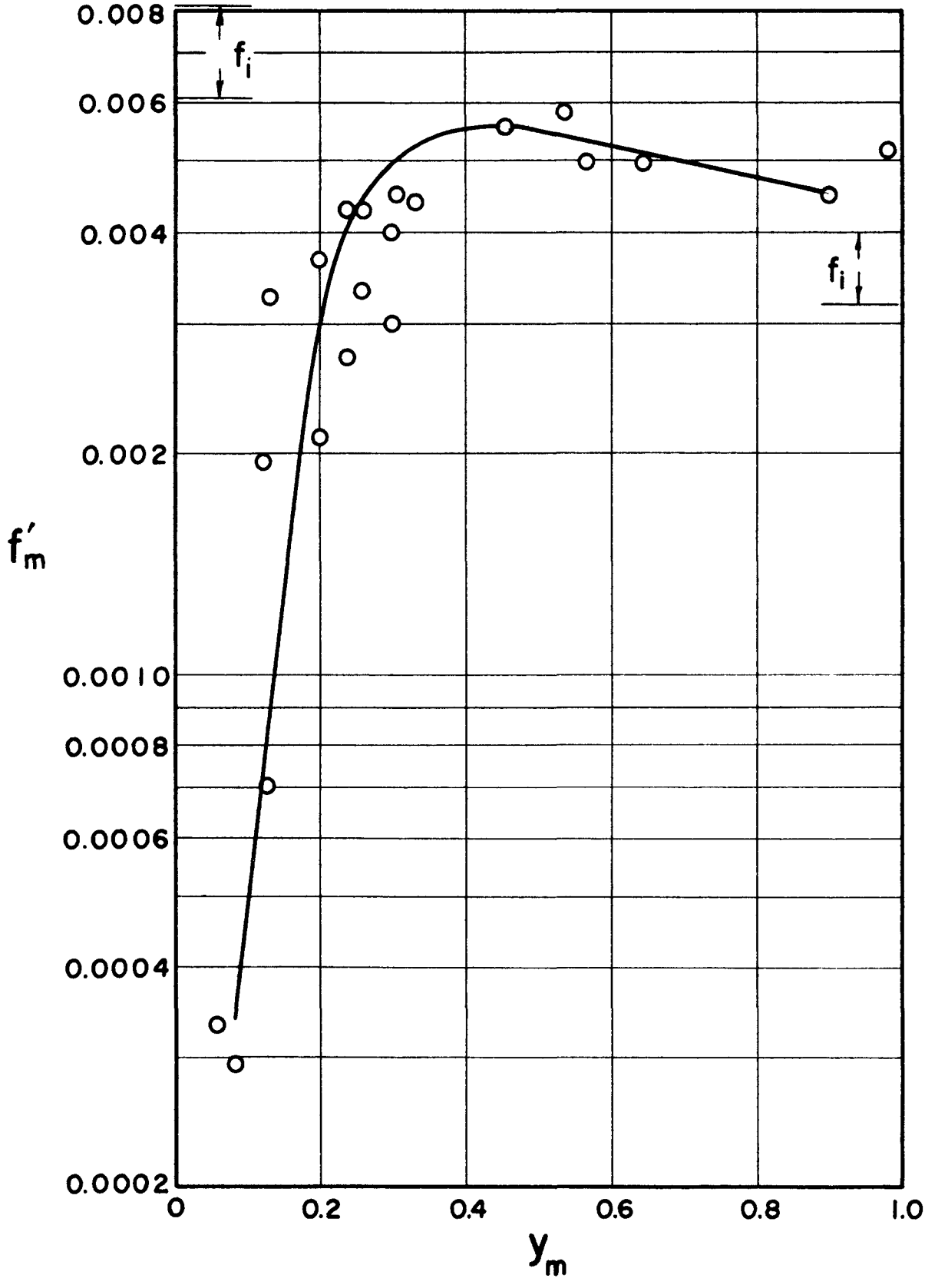

FIG. 2 APPARENT FRICTION FACTOR ACCORDING TO McADAMS, ET. AL.

these terminal values of f. The authors stated that for values of f in the range of qualities from zero to 0.4 it is likely that the abnormally low values of f can be due to the error of assuming no slip between the liquid and vapor phases. At very low qualities this assumption of no slip is completely invalid.

The conclusion of the investigation therefore was that for high qualities the friction factor can be computed from Reynolds number based on a mean viscosity of the mixture. The mean viscosity would be a function of the quality

$$\frac{1}{\mu_m} = \frac{1 - X}{\mu_d} + \frac{X}{\mu_v} \quad .$$

Thus , for very high qualities, such as might exist with a mist flow, the friction factor would be very near the value for one-phase flow of the vapor at the same mass flow rate.

Various schemes have been tried by investigators to develop friction factors for the prediction of two-phase pressure drops. For example, Davidson et al (13), obtained a fairly good correlation of apparent friction factors for forced convection boiling of water by plotting them against the product of the Reynolds number and the ratio of inlet specific volume to outlet specific volume. They suggested that the specific volume ratio corrects for the effects of separation of the mixture, bubble slip, etc. However, such a scheme appears to be of little value in attempting to predict local pressure drops, such as for example,

the pressure drop in the mist flow region of the evaporator tube.

A very extensive investigation of pressure drop in isothermal, two-phase flow systems was conducted by Martinelli and others (37), (40), (41). The work eventually led to a correlation which made use of the parameters ϕ_L and X where

$$\phi_L = \frac{(\Delta P/\Delta L)_{TP}}{(\Delta P/\Delta L)_L}$$

$$X = \frac{(\Delta P/\Delta L)_L}{(\Delta P/\Delta L)_G}$$

The functional relation between ϕ and X depended upon which of four arbitrarily defined types of flow existed. These flows, in turn, depended upon the Reynolds number for the flow of each phase. The types were designated as viscous-turbulent, viscous-viscous, turbulent-viscous, and turbulent-turbulent, depending upon the values of the Reynolds numbers. Mist flow, for example, where the liquid rate is low and the gas rate is high, would usually come under the classification of viscous-turbulent. The four types of flow defined by Lockhart and Martinelli do not necessarily distinguish the flow patterns that have been identified visually. In fact, experiments (40) in which the liquid surface tension was changed by Nekal B-X indicated changes in the flow patterns observed at given flow rates, but did not indicate appreciable changes in pressure drop. Although it seems strange , this

tends to support the idea of Martinelli and Lockhart that the type of flow should be defined by Reynolds numbers instead of by visually observed patterns when making pressure drop calculations.

Martinelli and Nelson (42), combining the previous results for isothermal, two-phase flow with the experimental data of (44) and (13), developed a method for predicting pressure drop during boiling in evaporator tubes. In boiling, the quality changes with length and therefore the value of Γ in the Martinelli-Lockhart correlation changes with length. By using the relationships developed previously and by assuming that the pressure drops correlated by the relationships were entirely due to friction, the following relationship was obtained:

$$\frac{\left[\frac{dP}{dL}\right]_{TPF}}{\left[\frac{dP}{dL}\right]_{O}} = (1 - X)^{1.75} \phi_L^2 \quad .$$

It was found that the high pressure data of (13) was overestimated when the equation above was integrated and applied to determine total pressure drop over the tube length. It was also noted that at the critical point the value of $\frac{\Delta P_{TPF}}{\Delta P_O}$ should have approached unity, but instead, the value of 5 was obtained. Therefore the correlation for ϕ_L used previously had to be corrected by extrapolation from the critical pressure to include the effect of pressure. This gave a new plot for

ϕ_L with pressure as a parameter. With this new curve they were able to compute local values of $(\frac{dP}{dL})_{TPF} \Big/ (\frac{dP}{dL})_O$ versus quality for various pressures. The resulting curve for local friction pressure drop is shown in Fig. 3. The curve is based upon the assumption that the general Martinelli-Lockhart type of correlation can be applied to non-isothermal, steam-water systems and that the method of extrapolation used to determine the effect of pressure is valid.

By further assuming that saturated water entered the tube, that a linear relationship existed between quality and length, and that a point-to-point evaluation of ϕ_L and $(\frac{dP}{dL})_O$ was valid, the authors were able to integrate the relationship for local pressure drop along the tube. This gave a relationship for the total friction pressure drop as a function of exit quality. The result of the integration is shown in Fig. 4.

Throughout their derivation the authors assumed the flow was turbulent-turbulent. In many mist flows the flow type would likely be viscous-turbulent, and under such conditions the curves shown in Figs. 3 and 4 would not be valid.

Martinelli and Nelson also calculated values of pressure drop due to momentum changes during evaporation. The derivations were made for each of the two possible extreme exit conditions:

1. Liquid and vapor completely mixed (mist).

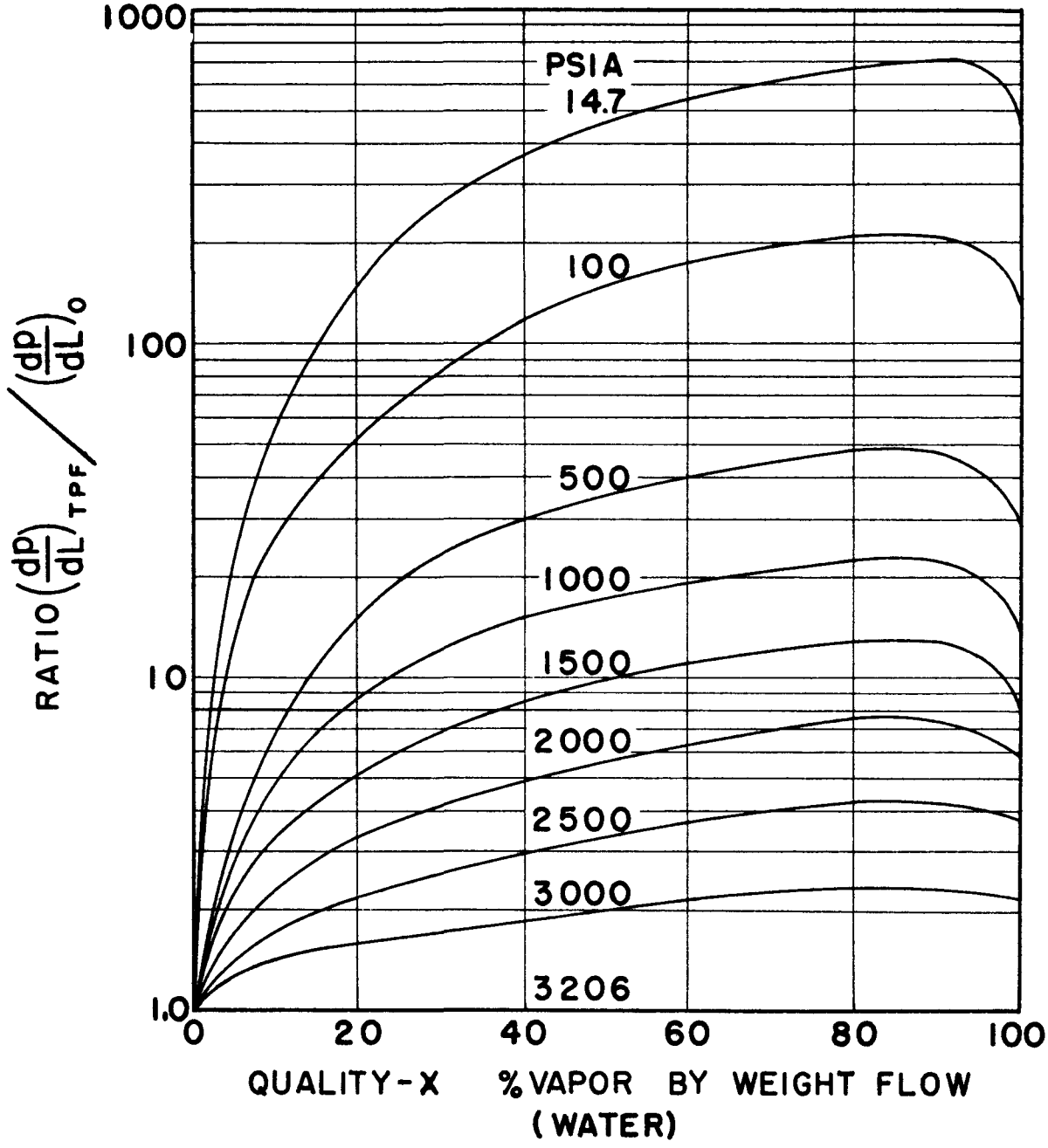

FIG. 3 LOCAL TWO-PHASE PRESSURE GRADIENT ACCORDING TO MARTINELLI-NELSON

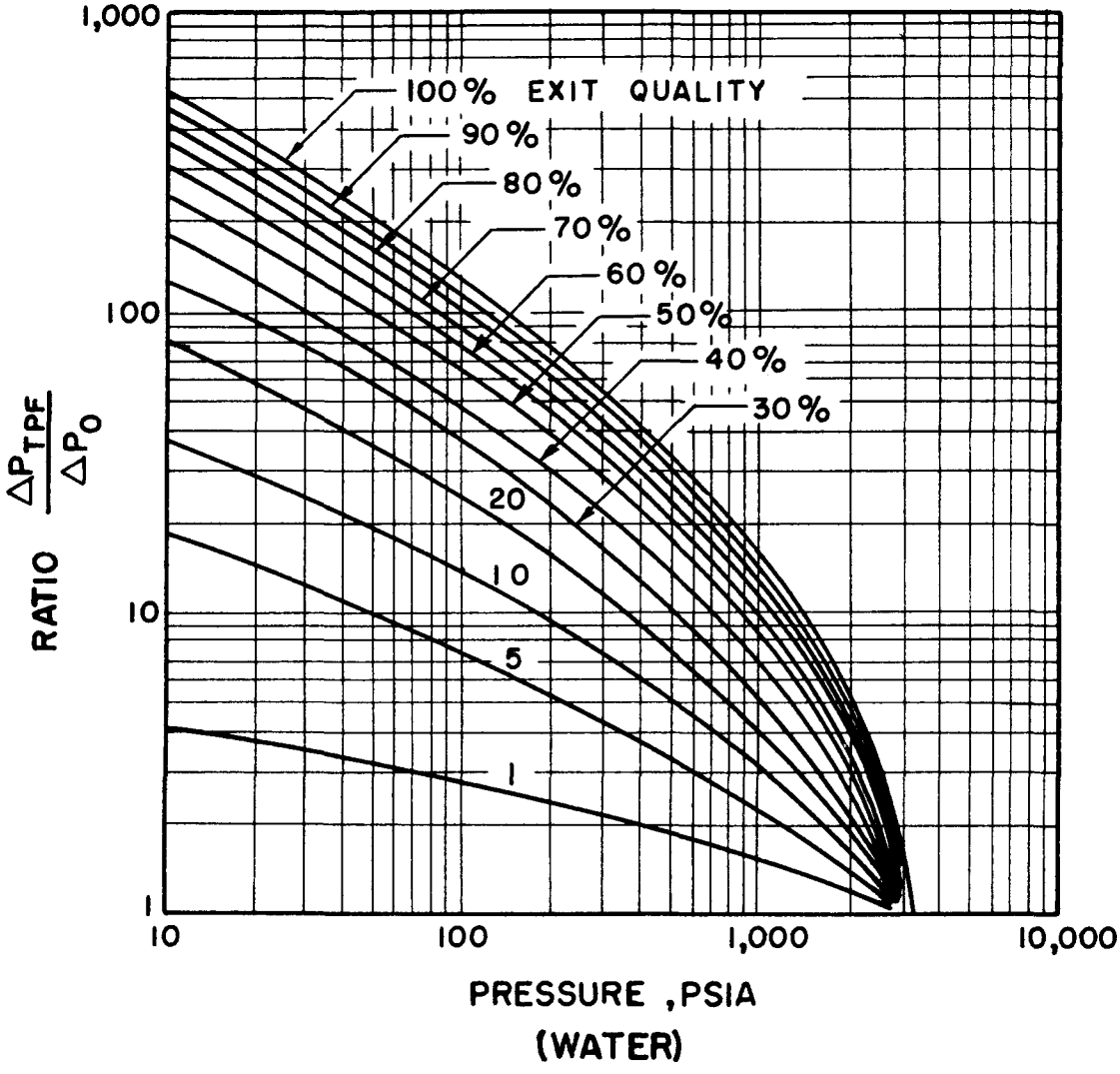

FIG. 4 FRICTION PRESSURE DROP FOR VARIOUS EXIT QUALITIES BY MARTINELLI – NELSON METHOD.

2. Liquid and vapor completely separated and moving at different velocities.

The value of the actual pressure drop due to acceleration would probably lie between these two extremes.

The total pressure drop in an evaporator tube can be obtained by adding the acceleration drop to the friction drop. The curves presented previously for friction pressure drop are also strictly applicable only to a horizontal tube of constant diameter.

In comparing the predicted values of acceleration pressure drop with the measured values of (44), Martinelli and Nelson noted that in the cases where the vaporization was gradual the derivation based on the assumption of separated phases was most applicable. In those runs where the vaporization was more rapid a better correlation was obtained with the assumption of complete mixing of the phases. This would indicate that a mist flow may be more likely to occur at a given quality if the heating has been rapid.

Dengler (16) measured pressure drops for vaporizing water in a 20 foot vertical copper tube of one inch inside diameter. Heat was supplied by five closely spaced steam jackets and pressure drops were measured by means of manometers connected to taps located between the jackets. Feedwater entered the tube near the saturation condition and at rates of 240 to 5,550 pounds per hour. Exit quality varied from 0 to 100 percent, exit pressure from 7.2 to 29 pounds per square inch

absolute, and temperature difference between the condensing steam and the vaporizing water from 0 to 40 degrees F. In order to determine the local volume fraction of the mixture Dengler added a radioactive tracer to the liquid feed. By the use of a Geiger-Mueller counter, variations in radioactivity were noted at various positions along the tube, and these variations were related to the volume fraction. The volume fraction was used to obtain the pressure gradients due to gravitational and acceleration effects. From these and the measured total pressure drop the frictional pressure drop was obtained. Values of the parameter ϕ_L obtained in this manner were found to be about 20 percent higher than those obtained by Lockhart and Martinelli. When the temperature difference was greater than that necessary to initiate nucleate boiling in the tube, values of ϕ_L were found to be up to three times the predicted values.

Weiss (71) studied two-phase pressure drop using a heated 0.174 inch stainless steel tube. The range of pressures covered was from 20 to 1,400 psia and the heat fluxes were from 100,000 to 500,000 Btu per hour square foot. Exit qualities at the two-phase burnout points were greater than 75 percent. His data agreed within plus or minus 30 percent with the values predicted by the Martinelli-Nelson method. The results seemed to indicate that the exit flow was closer to a mist type of flow than to the separated type of flow, although this was not determined experimentally.

One of the few studies directed primarily to the investigation of flowing mists was that of Leonard (36). He investigated pressure drops for mists of air and water flowing vertically upward through a 12 foot long pyrex tube with an inside diameter of 0.301 inches. Pressure taps were centered 10 feet apart on the tube. The following correlation, which was determined by digital computer techniques, correlated the pressure drops to within five percent of the measured values:

$$\left[\frac{\Delta P}{\Delta L}\right]_{mist} = \phi_{mist} \left[\frac{\Delta P}{\Delta L}\right]_{g}$$

where $\phi_{mist}^{0.293} = (0.00436)\ \chi_{mist}^{0.257} + 0.562$

and $\chi_{mist} = N_{Re} \frac{W_L}{W_g} \frac{\rho_L}{\rho_g} \frac{\mu_d}{\mu_v}$.

The range of values studied by Leonard were:

W_g = 0.376 to 1.29 pounds per minute

W_L = 0 to 0.667 pounds per minute

N_{Re} = 25,700 to 88,300 .

Leonard stated that Martinelli's (37) correlation for viscous-turbulent flow did not seem to apply to mist flow. It seems, however, that Leonard may not have taken into account the acceleration and gravitational effects, since his correlation is for total measured pressure drop.

Discussions of two references on mist flow given by Leonard will

be repeated here since translations of the articles were not available. They are investigations by Yagi and Sasaki (75) and Yagi and Kato (74).

Yagi and Sasaki investigated pressure drops in vertical mist flow using glass tubes of 8, 10.25, and 17.5 mm inside diameter. They used air and various liquids for their experiments. They concluded that the pressure drops could be correlated by

$$\left[\frac{\Delta P}{\Delta L}\right]_{mist} = 5000\, \rho_{avg} \left[\frac{u_d^2}{2gD}\right]^{0.75} \left[\frac{GD}{\mu_d}\right]^{-0.6}$$

This equation is difficult to use, since in most cases the velocity of the drops and therefore the average density of the mixture are unknown.

Yagi and Kato (74) gave the following expression for pressure drop in horizontal mist flow:

$$\left[\frac{\Delta P}{\Delta L}\right]_{mist} = \left[\frac{\Delta P}{\Delta L}\right]_{g} \left(1.5 + 0.83\, \frac{\mu_d}{D}\right) \left(1 + \frac{u_d}{u_g}\, \frac{P_{avg}}{P_i}\right)$$

$$\left(1 + \frac{Q_L}{Q_g}\right)^{0.8} \frac{P_i}{P_{avg}} \quad .$$

As in the equation of Yagi and Sasaki, it is necessary to know the slip velocity between phases in order to utilize this expression. Thus this equation seems to have little practical value in predicting pressure drops to mists, since pressure drops are easier to measure than slip velocities.

Because such a meager amount of experimental data is available, evaluation and comparison of the various schemes for prediction of pressure drop in mist flows cannot be made. It appears that more studies are needed in this area.

Two-Phase Burnout

Two-phase burnout is sometimes called net boiling burnout, and is distinguished from local boiling or film boiling burnout. It has been known for many years that for evaporator tubes operated at high exit qualities the heat transfer coefficients are relatively low near the exit end. Under such conditions a change probably occurs in the flow pattern due to the changing liquid-vapor ratio, and there results a sharp decrease in the heat transfer coefficients. If heat is being added to the tube at a constant or near constant rate, the tube will undergo a sharp temperature increase in the region where the coefficients decrease. When the temperature rise is sufficient to cause damage to the tube, two-phase burnout is said to occur.

Although evaporator tube performance has been studied by numerous investigators, most of the earlier studies were directed toward performance of the entire tube. Many investigators studied only the inlet and outlet conditions of the tube and measured mean overall temperature differences. Most of the more recent studies have been directed toward determination of local conditions in evaporator tubes.

However, very few of these studies have been concerned with local conditions of the high quality or liquid deficient region where mist flows occur.

McAdams, et al (43), using the equipment described previously, measured the overall heat transfer coefficients to boiling water, using steam at various pressures in the jackets. The condensing steam side resistance was minimized by using octyl thiocyanate to promote drop-wise condensation, and therefore the overall coefficients were thought to be near the values of the inside film coefficients. One result of the investigation is shown in Fig. 5. The value of the coefficients decreases sharply with increasing percent of feed vaporized above 40 percent. The authors attributed this decrease to the fact that there was insufficient liquid left to completely wet the inner walls of the tube. Observations made at the glass bends of the apparatus indicated that the flow had changed to a mist pattern when the low coefficients were experienced. Because the flow had to make a 180 degree turn at the end of each 12 foot run, the droplets in the flow were thrown against the outer wall at the turn and high coefficients were noted in the first jacket downstream from the bend.

A sharper, earlier decrease in the coefficient was noted for the cases where the wall temperature was high, that is, where the steam jacket pressure was 71 psig. The higher wall temperature may have caused the spheroidal state to exist, resulting in the lowered

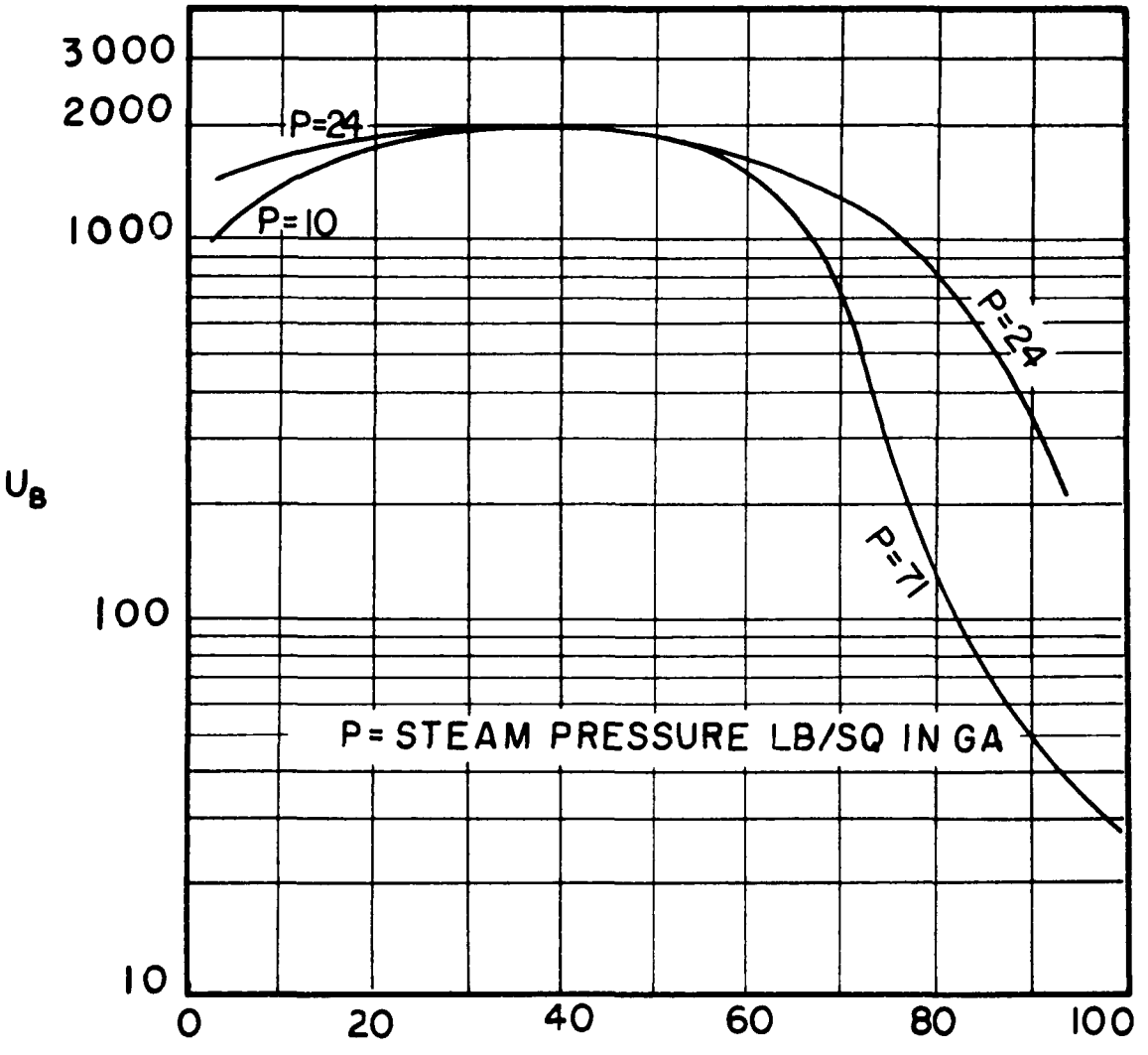

FIG.5 LOCAL OVERALL COEFFICIENT FOR BOILING ACCORDING TO McADAMS

coefficients. With 71 psig in the steam jackets the temperature difference between the wall and the boiling fluid would have been about 105 degrees F.

The use of condensing jackets for heating prevented any detailed observation of the local heat transfer coefficients. The values obtained are actually average values over a distance of approximately three feet.

In 1946 Witzig, Penny, and Cyphers (73) evaporated Freon-12 in an electrically heated, horizontal tube evaporator. The tube was 0.305 inches inside diameter and 27.5 inches long. In one series of runs the mass flow rate was held constant at 11.9 pounds per hour and the power was constant at 3,540 Btu per hour square foot based on outside area. In that series of runs the wall temperature was very nearly constant up to the point where the quality was approximately 70 percent. There the wall temperature increased sharply from about 80 degrees F to over 300 degrees F, indicating a decrease in heat transfer coefficient apparently due to a dry wall condition.

E. R. Wolfert of Westinghouse Corporation in commenting on the paper stated, "Further information on heat transfer rates in the region beyond the point where 70 percent of the Freon is evaporated is needed as an evaporator must usually carry the heat transfer to a point where the gas is not only all evaporated but actually superheated."

Fikry (21) measured heat transfer rates to wet steam flowing through an electrically heated constantan tube of 0.25 inch inside

diameter. The four foot long tube was heated over a length of three feet. The quality of the mixture was varied from 2 to 85 percent. The heat added varied from 6,000 to 30,000 Btu per hour square foot, but was never enough in any given run to change the quality by more than two percent.

Preliminary runs with water indicated good agreement with the Dittus-Boelter equation.

Fikry varied the inlet quality by spraying cold water on the outside of the bare steam line upstream from the test section. The flow rates of steam in the pipe varied from 4.14×10^4 to 7.47×10^4 pounds per hour square foot.

Fourteen iron-constantan thermocouples, welded to the outside of the constantan tube, measured the outside wall temperature. This reading was corrected to obtain the inside wall temperature. This represented a rather large correction since the temperature difference between the wall and the fluid was usually in the range of from 2 to 3 degrees F.

The coefficients determined from these measurements ranged from 580 to 2,740 Btu per hour square foot. The results were correlated in terms of Reynolds and Nusselt numbers using the physical constants of dry saturated steam.

$$N_{Nu} = cN_{Re}$$

The value of c in the equation was a function of the steam quality. Fikry arbitrarily divided the qualities into three ranges and determined the value of c for each range to be

70 - 80 percent quality	0.904
55 - 65 percent quality	0.887
40 - 50 percent quality	0.840 .

On this basis of correlation the coefficients for a given Reynolds number are much higher for wet steam than those for water or for dry steam flowing alone. Above 80 percent quality the coefficients decreased markedly from their maximum value.

Dengler (16), in the same study in which he was measuring the previously described pressure drops, also investigated the heat transfer mechanism. Three different mechanisms were used to explain his heat transfer results. At low qualities nucleate boiling seemed to be the controlling mechanism. At high qualities forced convection seemed to mask out the effect of nucleate boiling. At qualities ranging from 47 percent at a mass velocity of 0.171×10^6 pounds per hour square foot to 84 percent at 0.044×10^6 pounds per hour square foot, Dengler noticed a sharp decrease in heat transfer coefficients. He attributed this to a liquid deficient condition in which the tube wall had become essentially dry. This conclusion was supported by the readings taken with the Geiger-Mueller counter. At one point he noted a sudden increase in the counting rate of the counter, which indicated a deposit of

radioactive salt inside the tube. This was suggestive that the tube wall had become dry at the region where the film coefficients had decreased.

Mumm (49) investigated heat transfer to boiling water forced through an electrically heated, horizontal, stainless steel tube which was 0.465 inch inside diameter and 7 ft long. The investigation covered a range of pressures from 45 up to 200 psia, heat fluxes from 50,000 to 250,000 Btu per hour square foot, and flow rates from 250,000 to 10^6 pounds per hour square foot. Mumm noted that the local heat transfer coefficients increased with increasing quality up to a quality near 50 percent. In that region the coefficients decreased rapidly toward a value near those of dry vapor at about 70 percent quality.

Vanderwater (69) proposed an analytical model to predict conditions under which two-phase burnout would occur. His model supposed that a spray-annular type of flow occurred upstream from the region of burnout. Droplets were assumed to be constantly disappearing by diffusing into the liquid film, and the boiling action in the liquid film was assumed to be constantly forming droplets that are entrained in the core. Burnout was assumed to occur at the point in the tube where the liquid film disappeared. Vanderwater developed an equation to predict the liquid distribution and hence burnout. The model was used to correlate burnout data of several investigators for vertical, upward flow of steam-water mixtures in round and rectangular channels.

The values of the mass transfer coefficient for the droplets k_d and the re-entrainment function E in his equation could not be determined except by trial and error means, using the burnout data which was to be correlated. The distribution of the liquid at some point along the tube length also had to be assumed, which introduced a parameter z_o in the equation.

The mass transfer coefficient was assumed to be of the form $k_d = b\,G^j$ where G is the mass velocity of the total flow. Vanderwater concluded that j could not be greater than 1.0 since his equation would then predict the wrong relation between mass velocity and quality at burnout. The value of j was also noted to influence the effect of inlet subcooling on burnout. This pointed to a negative value of j as being desirable. From the burnout data he concluded that the best value of j was $-\frac{1}{2}$, and the value of b varied with the experimental conditions. The value of j for molecular mass transfer is ordinarily 0.8. Vanderwater explained possible reasons for the difference and stated that droplets could not be expected to diffuse in the core in exactly the same manner as molecules. Also the evaporation of droplets at the tube wall could have formed vapor whose motion away from the wall hindered the droplet motion to the wall. This vapor motion was described by means of a "boiling velocity" defined as

$$V_B = \frac{v_{fg}\, q''}{h_{fg}} \quad .$$

The mass transfer coefficient k_d should decrease as V_b increases. Vanderwater stated that V_b increases as the mass velocity increases (the reason is not apparent); therefore k_d should also decrease with increasing G.

The mean size of the droplets, which could change with mass velocity, could also affect the relationship.

It was found that, in general, the coefficient b decreased with an increase in pressure, and the effect was greatest at the higher pressures.

The re-entrainment function was described for round tubes by the relationship

$$E = E' V_b^{0.25}$$

where E' is a constant. This predicted a large re-entrainment effect at low mass velocities and a small effect at high mass velocities. Values of E' determined from the burnout data varied by a factor of about 15, due primarily to a pressure effect. The study seemed to indicate that the re-entrainment effect should be smaller for rectangular tubes than for round tubes.

Vanderwater made no attempt to correlate the parameter z_o representing the fraction of the liquid initially dispersed at some reference location.

He concluded that the tendency for a mist type flow would be greater during two-phase flow with heat transfer than without, primarily due to the effect of the boiling velocity.

Droplet Behavior

Three informative texts on the general properties of disperse systems have been published in recent years. The first, published in the United States in 1946, was written by Dallavalle (12). The second, published in the Netherlands in 1953, was by Hermanns (30). The third was a British publication of 1957, and was written by Green and Lane (27).

These books have very useful information on the basic principles of drop and particle behavior. The discussions include topics such as adiabatic evaporation, diffusion, drag coefficients, drop size and spectrum determination, atomization, dusts, powders, foams, gels and liquid-liquid suspensions. Each book has a very complete bibliography on the subject However, they contain little or no information on the behavior of droplets in their own vapor, non-adiabatic systems, heat transfer mechanisms, surface behavior, wall effects, and flow in confined spaces.

Miesse (47) discussed the recent advances in spray technology in an article published in 1956. He summarized the subject under the following topics:

1. Droplet formation.
2. Stream penetration (distance that a droplet penetrates into a stagnant gas layer).
3. Secondary atomization (breakup of droplets into smaller droplets).
4. Evaporation and ballistics.

Although most of the discussion is limited to liquid sprays in air, the general principles could be most useful in the study of flowing mists. Miesse also made the following conclusions:

1. The phenomena of droplet formation, spray penetration and secondary atomization can be characterized principally by the Weber number, with secondary viscosity effects represented by the Reynolds number.
2. The ballistics of an evaporating droplet is dependent upon the ratio of air viscosity to the product of liquid density and evaporation rate; the variation of evaporation rate due to relative velocity effects was represented adequately by the Schmidt and Reynolds numbers.
3. The relative ignorance in the following fields provides ample opportunity for extensive fundamental research:

a. Atomization by jet impingement

b. Coalescence of droplets

c. Determination of the size distribution from physical properties of the liquid, injector, and surrounding atmosphere.

An excellent bibliography is included with the article.

One of the most thorough and complete works on droplet behavior is included in a publication on injection and combustion of liquid fuels (5) prepared by the Battelle Memorial Institute in 1957 for the United States Air Force. This monograph, which contains 723 pages, was the work of a group of scientists who were experts in their fields. The six parts of the publication are:

1. Atomization of liquid fuels
2. Ballistics of droplets
3. Evaporation of droplets
4. Fluid dynamics
5. Homogeneous combustion
5. Heterogeneous combustion .

Each part includes a critical summary of the work done in that area and a list of significant references.

A listing of the more important investigations pertaining to sprays was prepared by the Pennsylvania State College and published by the Texas Company in 1948 (14). This bibliography, which includes

abstracts on most of the articles, was enlarged and published in a second edition in 1953 (53). This second edition included about 600 entries and nearly as many abstracts. The abstracts were of a non-critical nature.

Most of the material in the second edition mentioned above was included in a book edited by DeJuhasz (15) and published by the American Society of Mechanical Engineers in 1959. This book contains over 1,300 references to work done on sprays by investigators in twenty four countries and includes the period from 1880 to 1958 inclusive. Included are references to articles having a bearing on the theoretical and experimental studies of sprays such as, for example, studies of powders and dusts. Many of the abstracts are quite detailed. DeJuhasz had compiled many of the abstracts as a reviewer for Applied Mechanics Reviews and was given permission to use these abstracts in his book.

Because most of the important references on droplet behavior are included in (5), (15), (47), and (53), only those investigations that have an important bearing on this thesis will be discussed.

The three most common mathematical expressions for drop size distribution in sprays are the Rosin-Rammler, Nukiyama-Tanasawa, and the log-probability equations. They may be written:

Rosin-Rammler $$\frac{d(v)}{d(d)} = \frac{\delta d^{\delta-1}}{\bar{d}^{\delta}} e^{-(\frac{d}{\bar{d}})^{\delta}}$$

Nukiyama-Tanasawa $$\frac{d(v)}{d(d)} = \frac{b^{\frac{6}{\delta}}}{\Gamma\frac{6}{\delta}} d^5 e^{-bd^{\delta}}$$

log-probability $$\frac{d(v)}{d(d)} = \frac{\delta}{\sqrt{\pi}} e^{-(\delta \ln \frac{d}{\bar{d}})^2} .$$

The Rosin-Rammler (55) expression was obtained from a mathematical investigation of size distribution in powdered coal and other pulverized material. It has been found to be quite useful, however, in many instances for the study of spray distributions.

The Nukiyama-Tanasawa (52) distribution equation resulted from an extensive investigation of the characteristics of sprays produced by various air-atomizing nozzles. Their equation has been found to fit various data reasonably well, even where the mechanism of droplet formation was entirely different from that in the investigations of Nukiyama and Tanasawa. These authors also developed an expression for the prediction of the Sauter (48) mean diameter of a spray produced by an air-atomizing nozzle. This equation is probably the only generally used equation for the prediction of mean drop sizes produced by a nozzle. The equation is:

$$d_{32} = 585 \frac{\sqrt{\sigma}}{\Delta v \sqrt{\rho_d}} + 597 \left(\frac{\mu}{\sqrt{\sigma \rho_d}}\right)^{0.45} \left(1000 \frac{Q_L}{Q_g}\right)^{1.5} .$$

All properties are for the liquid. The Nukiyama-Tanasawa expression is entirely empirical in nature and, as may be noted, is not dimensionally correct.

The log-probability distribution equation is the result of ordinary statistical analysis.

A comparison and discussion of the methods of expressing droplet size distribution are given by Bevans (7) and by Mugele and Evans (48). The latter authors introduced a new distribution equation called the upper-limit equation, based on the equation of the normal or Gaussian distribution. The distributed quantity is y and

$$y = \ln \frac{bd}{d_m - d} \quad .$$

Mugele and Evans indicated that their equation fit the available spray data well and also predicted the various mean diameters accurately.

Some consideration was given to using the Nukiyama-Tanasawa equation to predict mean droplet size in the experiments of this thesis. Ingebo (32) used a simple orifice injector system, similar to the one used in the investigation of this thesis, to study spray vaporization rates and drag coefficients of iso-octane sprays in turbulent air streams. His measurements indicated that it was doubtful that the Nukiyama-Tanasawa equation could be used to predict initial droplet size over a wide range of operating conditions with such an injection

system. It is also very likely that heat transfer, which is a function of droplet radius, would severely modify the drop size distribution of a spray produced in a high temperature gas or vapor stream.

Longwell and Weiss (38) made a study of the mixing and distribution of liquids in high velocity air streams. They state that inertia effects cause the diffusion rate of droplets in a gas stream to be less than the diffusion rate for molecules at the same condition. A rough illustration of this effect was given, assuming that the velocity fluctuations in turbulent flow were sinusoidal and that Stokes law applies for the drag on the drop. The equation of motion of the drop became

$$m \frac{d^2Z}{d\theta^2} = 3\pi\mu_v d(U\cos\omega\theta - \frac{dZ}{d\theta})$$

where Z was the drop displacement from the mean position, and U was the peak velocity of the turbulent gas fluctuation relative to its time average velocity. Defining B by

$$B = \frac{3\pi\mu_v d}{m}$$

a solution to the above equation was obtained:

$$Z = \frac{BU}{\omega}\left(\frac{B\sin\omega\theta - \omega\cos\omega\theta}{\omega^2 + B^2}\right) .$$

By differentiating, the maximum amplitude Z_m was found. Dividing Z_m by Z_o where $Z_o = \frac{U}{\omega}$ they obtained:

$$\frac{Z_m}{Z_o} = \left(\frac{B^2}{\omega^2 + B^2}\right)^{\frac{1}{2}} .$$

The frequency of motion of the drop was the same as that of the gas and therefore the velocity would be reduced in proportion to the amplitude. The eddy diffusion coefficient is proportional to the product of velocity and amplitude, therefore

$$\frac{\alpha_d}{\alpha_g} = \left(\frac{Z_m}{Z_o}\right)^2 = \frac{B^2}{\omega^2 + B^2}$$

where $\frac{\alpha_d}{\alpha_g}$ is the ratio of the diffusivity of the drop to that of a gas which could follow the motion of the gas stream exactly.

The authors illustrated this effect by assuming a typical drop of 45 micron diameter in a 300 ft per second air stream. The frequency for a 6 inch duct with fully developed turbulence was assumed to be 300 radians per second. For a kerosene drop these conditions gave a diffusivity ratio of $\frac{\alpha_d}{\alpha_g}$ of 0.35.

The authors presented some experimental data for point injection of both naphtha and Diesel fuel. The naphtha vaporized much more readily than the Diesel fuel so that it was primarily in the gaseous state during spreading whereas the Diesel fuel was primarily in the form of droplets. The data showed higher diffusivity rates for the

naphtha and also confirmed the general trend of frequency influence shown in the derived equation.

The assumptions that Stokes law is valid and that the turbulence is sinusoidal in nature could possibly lead to erroneous results. As more information becomes available on the drag coefficients of accelerating spheres and on the nature of turbulence, a more sophisticated analysis should be possible.

Alexander and Coldren (2) studied the deposition of drops from a turbulent air stream to the inner walls of a 1.86 inch ID pipe. The spray was produced by an atomizing nozzle located at the entrance to the pipe. A constant air and water rate flowed through the nozzle, and the authors used the Nukiyama-Tanasawa (52) equation to predict the mean drop size produced. This estimated drop size of 27 microns was maintained through all of the tests, and varying amounts of air were mixed with the spray at the pipe entrance. Air velocities in the pipe varied from 80 to 295 ft per second, and the constant water rate was 0.106 gpm. Liquid distribution measurements were made at distances of from approximately 8 to 68 inches from the nozzle.

In discussing their results, Alexander and Coldren divided the test section into two zones. In the first zone, the first one-third of the pipe, the profiles of local mass velocity of suspended liquid across the cross section were bell shaped. By assuming negligible resistance to the transfer of droplets at the wall and that the eddy diffusivity of the

main body was controlling, they were able to derive the following equation for droplet depletion in that zone:

$$\frac{d(\ln G_d)}{d(L)} = \frac{-4R_1^2 \alpha_d}{D^2 u_{avg}} .$$

Values of eddy diffusivity of water droplets in zone 1 were given as a function of the average air velocity. They ranged from 0.088 to 0.119 ft squared per second. These values should be considered as characteristic of this particular system only, since the intensity of turbulence would be affected by the presence of the nozzle in this region, and the turbulence has a strong effect on the droplet motion.

In the second zone, the local mass velocity profiles were flat over 75 percent of the duct radius and dropped sharply toward zero near the wall. This indicated that the main resistance to droplet transfer was in the gas layers near the wall. The data in this region was correlated by means of the equation

$$k_d = 12.06 (u_{avg})^{1.17}$$

where k_d is the mass transfer coefficient for drops.

It is intersting to note that this positive exponent of 1.17 differs from the $-\frac{1}{2}$ exponent used by Vanderwater in his analysis of burnout. This would seem to indicate that the boiling velocity has a tremendous effect on the rate of droplet diffusion to the wall.

This value of k_d determined by Alexander and Coldren is 10 to 20 times the values for common gases under equivalent flow conditions.

Friedlander and Johnstone (23) studied the deposition of suspended particles from turbulent gas streams. In their experiments they used iron particles with mass median diameters of approximately 3 and 5 microns, aluminum particles of approximately 5 micron mean diameter, and lycopodium spores with a mean diameter of approximately 30 microns. The particles were mixed with air and passed through various sized glass and brass observation tubes. Observation sections for the glass tubes were made by grinding a flat surface on the outer tube wall. Observation sections for the brass tubes were made by cutting out sections and replacing them with new pieces. The particles were made to adhere to the observation sections by the use of either glycerol jelly or pressure sensitive tape with adhesive on both sides. Concentrations were determined by the use of filters downstream from the observation tube. Direct observations made during the runs with a microscope gave results which agreed with the information obtained with the adhesive. Runs where re-entrainment was observed were not used in the presentation of their results.

In the analysis of their data Friedlander and Johnstone used an analogy similar to that used by von Karman (70). In this analogy the flow was assumed to be made up of three layers: a turbulent core, a buffer layer, and a laminar sublayer. Reynolds' analogy was assumed

to hold in the turbulent core. Thus, for the turbulent core,

$$\frac{\rho M}{\tau g_c} = \frac{dC}{d\bar{u}} \quad .$$

By assuming that the diffusion rate of the particles was the same as that of the carrier gas, the authors were able to use the relationship above to predict the rate at which particles would diffuse in the turbulent core. Further, in the cases where the particles were large enough to penetrate the buffer and laminar layers, all particles diffusing from the turbulent core would strike the wall. In such cases, by assuming zero concentration and velocity at the wall, integration of the first equation led to

$$\frac{k_d}{\bar{u}} = \frac{f}{2}$$

where f, the friction factor is defined by

$$f = \frac{2\tau_w}{\rho \bar{u}^2} \quad .$$

To determine whether a particle of a given size could penetrate the relatively stagnant buffer and laminar layers after diffusing from the turbulent core the authors assumed that Stokes law was valid. Equating the viscous and inertia forces acting on the particle an expression was obtained for the distance that a particle of given size and initial velocity would travel before coming to rest. The result was

$$L = \frac{d^2 \mu_o \rho_L}{18 \mu_v} \quad .$$

To estimate the initial velocity of the particles entering the buffer layer from the turbulent core the authors used the results of Laufer's (35) investigation. Laufer made a careful study of velocity components for turbulent flow in a 10-inch tube at Reynolds numbers of 50,000 and 500,000. Figure 6 shows the variation of v', the root mean square of the radial component of the fluctuating gas velocity as a function of the friction velocity u^* and the generalized coordinate r^+. The curve levels off to values of $\frac{v}{u^*} = 0.9$ in the turbulent core ($r^+ > 30$).

In all of their calculations, Friedlander and Johnstone assumed that the particles diffused to within one stopping distance of the wall. In every case the stopping distance was calculated by using an initial velocity of the particle equal to $0.9\ u^*$. For the reference conditions, the calculated stopping distances were always less than the thickness of either the laminar sublayer or the combined thickness of the laminar and buffer layers. Thus they had to account for diffusion of the particles in these layers. For these layers they used the following values of eddy diffusivity:

For the laminar sublayer, $r^+ = 0$ to $r^+ = 5$

$$\alpha_d = \nu \left(\frac{r^+}{14.5}\right)^3$$

For the buffer layer, $r^+ = 5$ to $r^+ = 30$

$$\alpha_d = \nu \left(\frac{r^+}{5} - 0.959\right) .$$

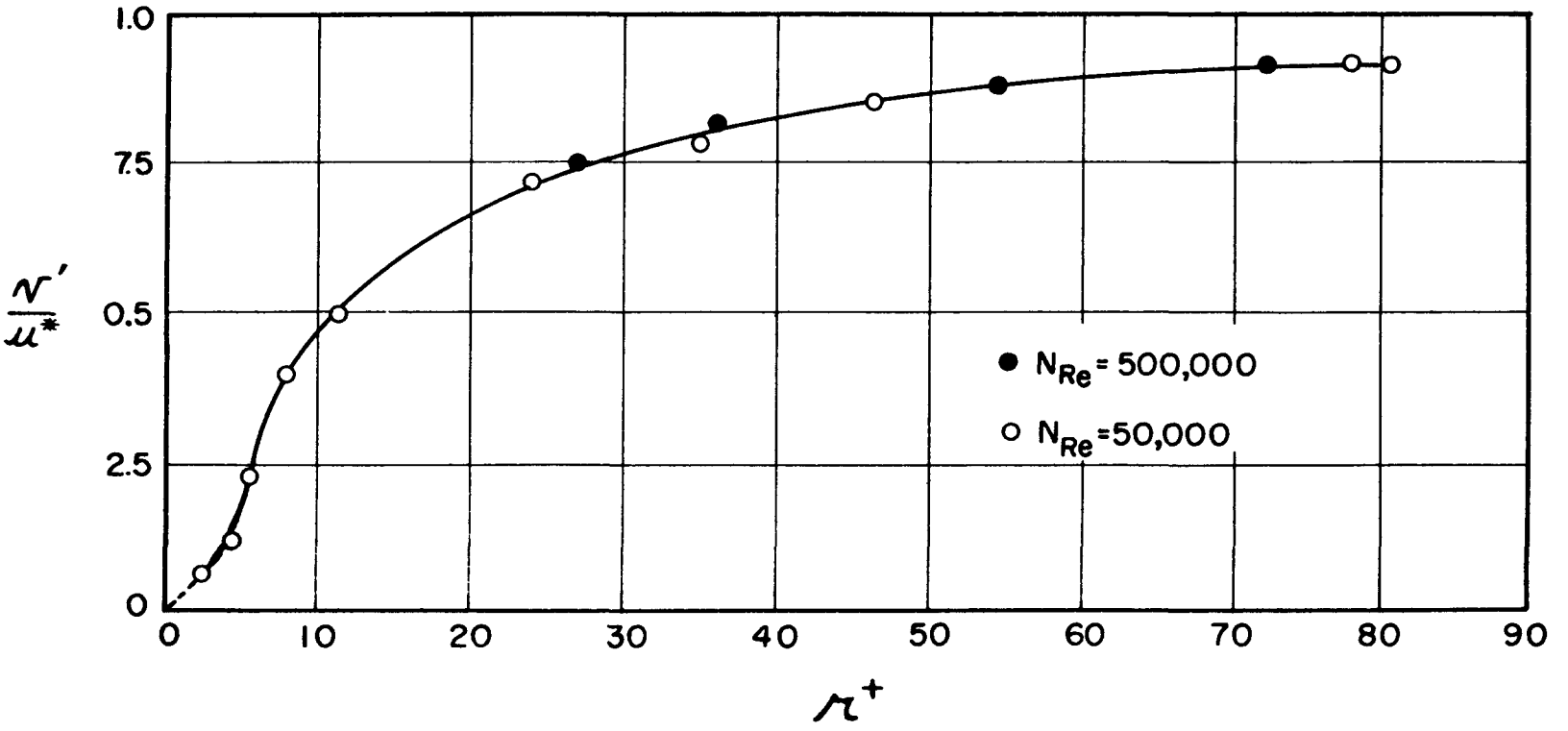

FIG. 6 , ROOT MEAN SQUARE RADIAL COMPONENT OF VELOCITY NEAR WALL, ACCORDING TO LAUFER

Defining a nondimensional stopping distance by

$$L^+ = \frac{Lu_{avg}}{\nu}\sqrt{\frac{f}{2}}$$

and using the procedure outlined by von Karman they derived the following expression for the base where the stopping distance was calculated to be less than the thickness of the laminar sublayer:

$$\frac{k_d}{\bar{u}} = \frac{\frac{f}{2}}{1 + \sqrt{\frac{f}{2}}\left(\frac{1525}{L^+} - 50.6\right)} .$$

In case the stopping distance is small the equation reduces to

$$\frac{k_d}{\bar{u}} = \sqrt{\frac{f}{2}}\,\frac{L^+}{1525} = \frac{\rho^2 d^4 \rho_L^2 u_{avg}^4}{6.1(10)^5 \mu_v^4}\left[\frac{f}{2}\right]^{\frac{5}{2}} .$$

The following equation was derived for the base where the nondimensional stopping distance was between 5 and 30:

$$\frac{k_d}{\bar{u}} = \frac{\frac{f}{2}}{1 + \sqrt{\frac{f}{2}}\left\{5 \ln\left[\frac{5.04}{\frac{L^+}{5} - 0.959}\right] - 13.73\right\}} .$$

The experimental results with the smaller particles fit the derived equation reasonably well. The data for the larger lycopodium particles fell well below the curve predicted by the theory. No observations were made where the stopping distance was greater than the combined laminar and buffer layer thickness.

In order to determine which of the equations would probably apply in the case of a mist of steam and water droplets, calculations for stopping distances of droplets were made. The assumptions were made that the flow was at 30 psia in a one-inch tube. The friction factors used were based on Reynolds numbers assuming the flow to be dry saturated steam. Calculations of the stopping distance for various size drops and of the thickness of the laminar sublayer and buffer layers were made for three different Reynolds numbers. Initial velocities used in calculating stopping distances were assumed equal to 0.9 u^*. The results are shown in Table 1.

TABLE 1

A Comparison of Particle Stopping Distances with Laminar Sublayer and Buffer Layer Thicknesses

	Stopping Distance				Laminar Sublayer	Buffer Layer
N_{Re}	d = 1 micron	d = 10	d = 100	d = 250	$y^+ = 5$	$y^+ = 30$
10^4	3.25×10^{-6}	3.25×10^{-4}	3.25×10^{-2}	.188	6.77×10^{-4}	40.6×10^{-4}
10^5	24.8×10^{-6}	24.8×10^{-4}	24.8×10^{-2}	1.55	$.885 \times 10^{-4}$	5.31×10^{-4}
10^6	196×10^{-6}	196×10^{-4}	196×10^{-2}	12.2	$.112 \times 10^{-4}$	$.672 \times 10^{-4}$

From these calculations it would seem that drops greater than 10 micron diameter, for example, could easily penetrate both the laminar and buffer layers at a Reynolds number of 10^5.

There seemed to be one inconsistency in the analysis of Friedlander and Johnstone. The root mean square of the radial component of the fluctuating gas velocity decreases with r^+ as shown in Fig. 6. Thus the particles would be expected to decrease in velocity as they approach the wall. The value of the initial velocity to use in calculating the distance for stopping the particle depends upon the position from which the stopping distance is to be calculated. By their analysis, the value of the stopping distance determines the point at which eddy diffusion is assumed to become unimportant and therefore determines the value of the diffusion coefficient. This should more correctly be handled by a trial and error solution. Friedlander and Johnstone always assumed that the initial velocity of the particle approaching the wall was equal to $0.9\ u^*$ regardless of the value of the stopping distance computed. It would seem that a considerable error could be introduced by this simplification.

Their conclusion, that the rate of transfer of particles is always less than, or at most, equal to the rate of transfer of the common gases, seems to be contradictory to the conclusion of Alexander and Coldren (2). The latter concluded that the value of k_d is 10 to 20 times the value for common gases under equivalent flow conditions.

The assumption made by Friedlander and Johnstone, that the particles follow the gas eddies exactly, does not agree with the simple analysis of Longwell and Weiss (38), especially for larger particles.

In 1952 Ryley (56) made a study of the flow of wet steam through nozzles, and he developed a new method for determination of ideal discharge coefficients. In defending gross simplifications made in his method Ryley claimed that he had made some advance on the existing theories and had been able to avoid certain anomalies of some of the older methods. He further stated, "Any rigorous theory would have to take cognizance of differences in drop size, velocity, etc., and would have to be approached from a statistical standpoint. Existing knowledge of the behavior of drops is quite inadequate to enable such a theory to be elaborated." It would seem that a similar statement could be made at the present time about elaborating a rigorous theory for heat transfer to wet steam.

In discussing the transfer of heat from vapor to small drops Ryley stated that the small size probably limited the heat transfer to conduction. Both theory and experiments indicate that heat is transferred with extreme rapidity to or from drops of very small size, (10^{-8} to 10^{-9} ft diameter) but takes longer with larger drops, especially for temperature differences less than two degrees F.

In a later article (57) Ryley extended his theory to the case where dry steam entered the nozzle and moisture precipitated as droplets as the stream neared the exit.

In 1954 Ryley (58) presented a theoretical treatment of the behavior of water globules in steam. The subjects that he discussed

were the trajectory of globules, slip velocities, descent of globules, and fracture of globules.

Ryley divided water globules in steam into three size categories:

1. Clusters of less than 8×10^{-8} inches diameter (less than 150 molecules). These do not exhibit the usual equilibrium vapor pressure, viscosity, or surface tension of water.
2. Droplets between 8×10^{-8} inches and 10^{-2} inches diameter. These act as rigid spheres and have a small terminal velocity which is attained rapidly.
3. Drops greater than 0.01 inch diameter which tend to settle out or break into droplets and hence are rare. Ryley stated that this last boundary is somewhat arbitrary since the maximum stable droplet size depends upon the relative velocity between the droplet and the steam.

He stated that because of the impossibility of bringing a sufficient concentration of energy on the body, clusters and the smaller size droplets were immune from fracture. For water the smallest droplet that has been formed by fracture that has been detected was about one micron (3.3×10^{-6} ft), and was produced by a spray nozzle.

Ryley presented a fracture chart for water based on the assumption of breakage of the drop on a diametral plane perpendicular to the flowing vapor direction. For values of drag coefficients used in the calculations he used the conventional chart of drag coefficient versus

Reynolds number for spheres in steady flow. His chart is shown in Fig. 7. It gives the droplet diameter produced in fracture by a certain relative velocity between the steam and the drop, with pressure as a parameter. The sharp breaks in the curves are due to the fact that as the Stokes region boundary is reached the relative velocity becomes independent of droplet diameter, since

$$\pi d q_L = 3\pi \mu_v d(\Delta u)$$

$$(\Delta u) = \frac{q_L}{3\mu_v} \quad .$$

When the relative velocity reaches this value it might seem at first that the globule would undergo complete and continuous atomization to formation size. However, three considerations oppose this idea:

1. The relative velocity would not be preserved for each new globule formed from a parent globule.
2. Most physicists believe that the surface tension increases with decreasing diameter for very small drops.
3. Common sense prohibits the acceptance of an abrupt discontinuity in the curves. It seems logical that the curves in the aerodynamic region should continue steadily increasing with decreasing droplet size.

In discussing practical applications of his presentations Ryley suggests that steam separators should be situated at the bottom of a

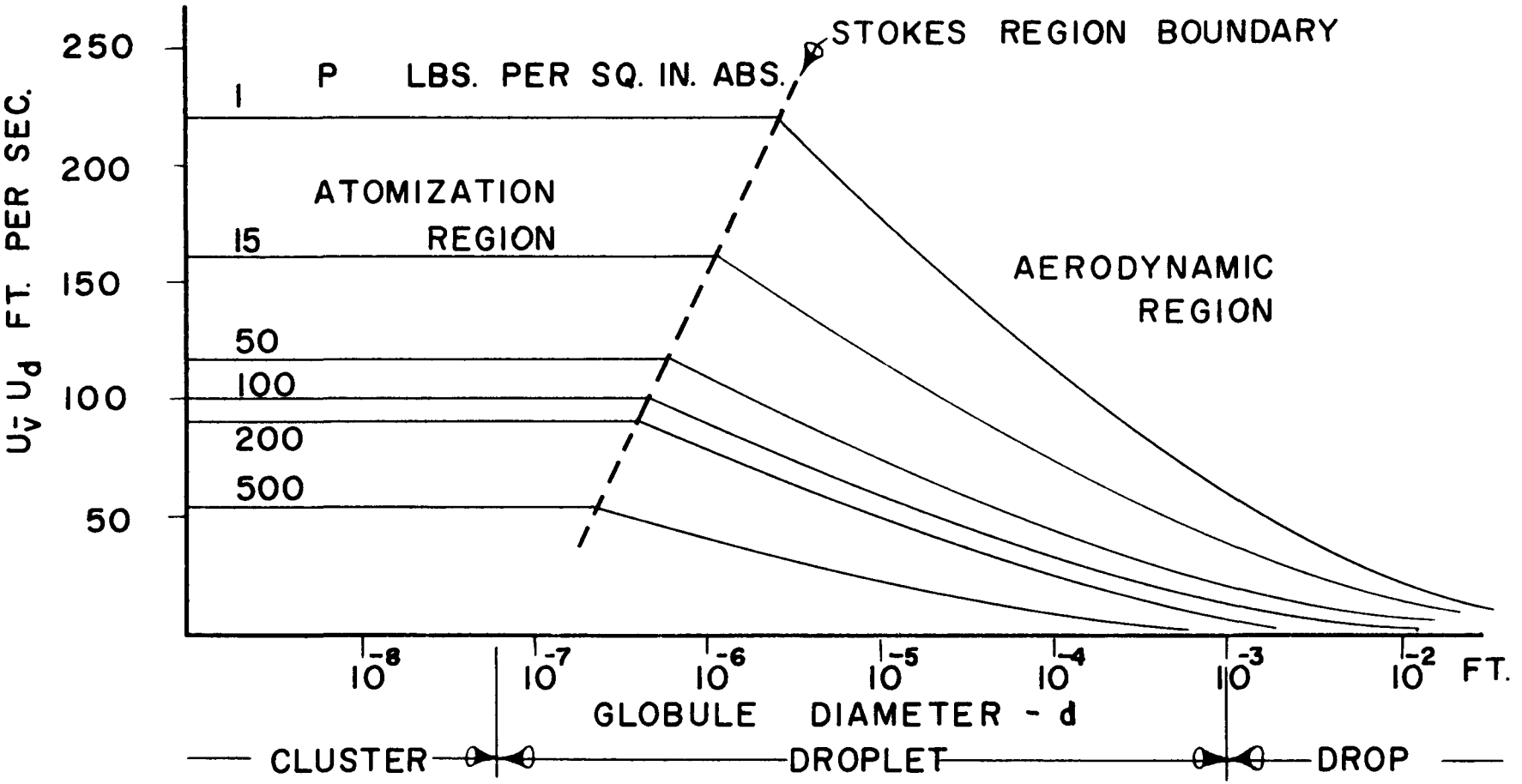

FIG. 7 GLOBULE FRACTURE CURVES OF RYLEY (58)

vertical main in which steam is descending. There is a tendency for the globules to slide toward the axis under the influence of the velocity gradient. This would suggest that heat transfer rates to mists might be quite different for the two possible cases of vertical flow, depending upon whether the flow were upward or downward.

Ryley's statement about the globules tending to slide toward the axis for downward flow seems to be in contradiction to the recent study of Young (78). In this study observations of the flow of aqueous suspensions of fine spherical glass particles in vertical glass tubes revealed a pronounced coring effect near the transition velocity between laminar and turbulent flow. For upward flow all the particles collected near the center of the tube. For downward flow the particles collected along the wall of the tube. Young proposed the idea that the effect was due to a lateral force on the particles, caused by the velocity gradient in the pipe.

Hottel, William, and Simpson (31) made an investigation of the combustion of droplets of heavy liquid fuels. In their presentation they discussed the factors affecting the amount of heat transferred to drops by radiation. Figure 8 shows one result of their calculation, a comparison of the ratio of heat transferred to a drop by radiation to that transferred by convection. The Figure shows that radiation is of minor importance for low surrounding temperatures and small drop sizes. Although the Figure applies to oil drops at 100 degrees C, the values

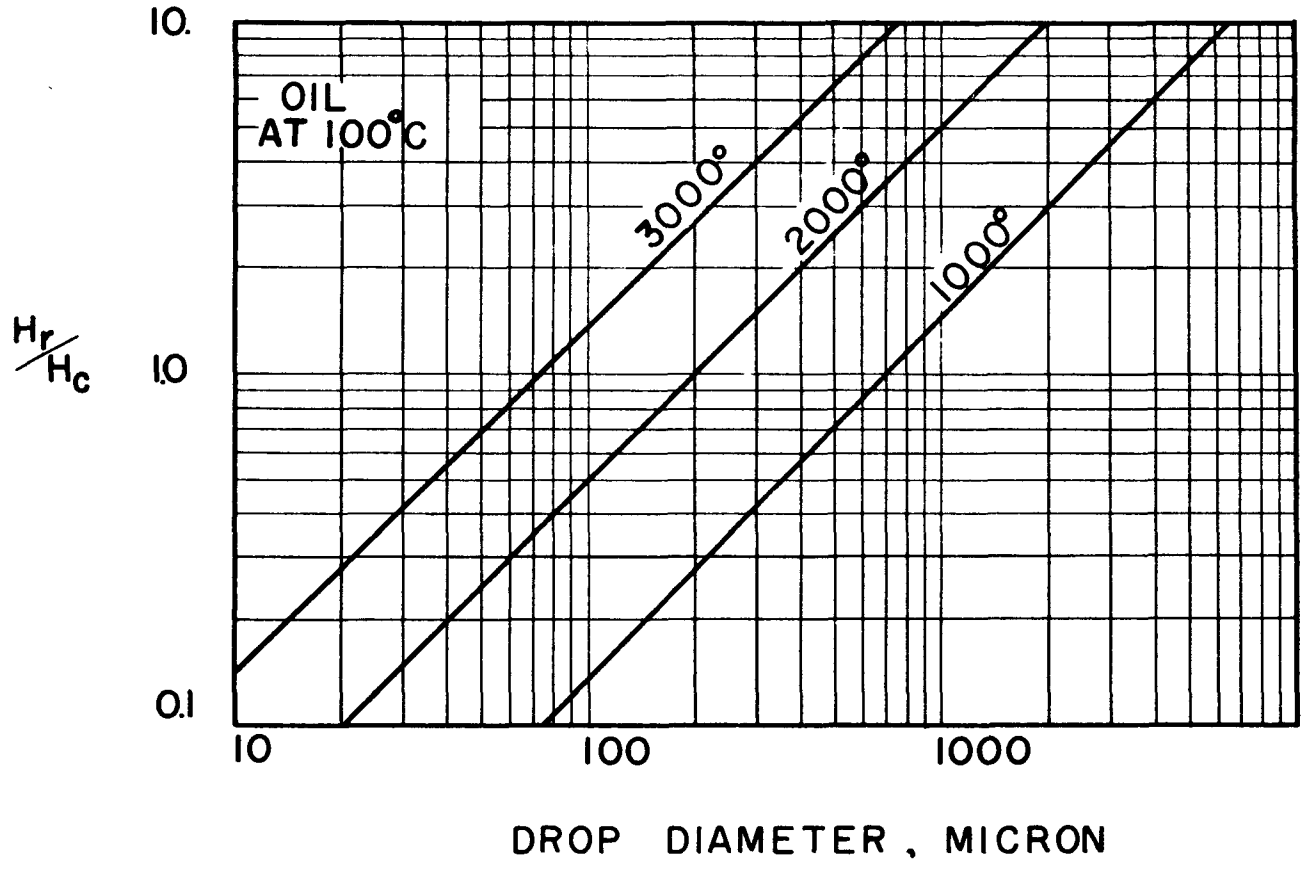

FIG. 8 THE EFFECT OF DROP SIZE AND SURROUNDING TEMPERATURE ON THE RATIO OF THERMAL RADIATION INCIDENT ON A DROP TO HEAT TRANSFER TO THE DROP BY CONVECTION ACCORDING TO (31).

are approximately correct for water drops. Radiation is generally an unimportant mode of heat transfer in evaporator tubes at normal conditions.

A recent literature survey on film boiling was presented by McFadden and Grosh (46). In their survey the authors reviewed the more important points of previous surveys on the subject. They noted that early studies of film boiling were concerned primarily with droplets dancing on a hot surface. Many investigators have noted that droplets often take a long time to evaporate when placed in contact with a very hot plate, whereas lowering of the plate temperature can cause the droplet to evaporate very rapidly, sometimes explosively. This phenomenon became known as the spheroidal state (often called the Leidenfrost effect) and has been defined by Drew and Mueller (19) as: "A non-equilibrium condition assumed by two or more bodies of solid or liquid when an attempt is made to bring them together while their temperatures differ by more than a determinant amount; it is characterized by the subsistence of a layer of vapor between the bodies which resists and prevents their being brought into direct contact."

In spite of the fact that many of the investigations with droplets were crude and the results were difficult to reproduce, the following points seem to be true:

1. The roughness and material of the solid surface determine the minimum surface temperature necessary for the

spheroidal state to exist with drops of a given diameter and substance.

2. The liquid does not need to be at the saturation temperature for the spheroidal state to exist.

3. The droplet does not touch the plate at all times but is held up by a vapor layer.

One of the more recent studies of heat transfer to drops of liquid in the spheroidal state was by Gorton (26). Drops of distilled water, distilled water plus Duponol C, 95 percent ethyl alcohol, and carbon tetrachloride and of 0.2, 0.3, and 0.4 inch diameter were fed onto a hot stainless steel or platinum surface and photographed. Gorton concluded from his study that smaller drops have higher heat transfer coefficients, even when the liquid temperature, plate temperature, and temperature difference are the same. Decreasing surface tension increased the heat transfer coefficient, seemingly because the spreading of the drop affected the vapor film thickness.

Savic and Boult (61) made a theoretical and an experimental study of the fluid flow associated with the impact of liquid drops with solid surfaces. Their primary interest was in obtaining information about the mechanism of turbine blade cooling by means of impinging drops. However, this study dealt primarily with the impact of drops on unheated surfaces.

Drops approximately 3/16 inch in diameter were dropped from a

height of 6 feet in air at reduced pressures. Using ideal fluid theory they obtained an expression for the spreading of the drops that agreed well with the high speed photographs taken of the actual drop impact.

In one series of runs the drops were allowed to impact against a silver surface at 1,300 degrees F, in a chamber at 0.5 inches Hg absolute. The photographs indicated that the spreading drops contained two zones of violent boiling, separated by an intermediate zone of relatively slow evaporation. The central portion of the drop produced a single growing bubble, which ultimately burst and tore the upper part of the drop apart. The outer edges of the drop were raised by the vapor formed in the evaporation at the outer region.

Savic (60), making a further study of the photographs of drops impinging on hot surfaces, concluded that the mode of heat transfer was primarily nucleate boiling for the conditions of his experiments. He noted that a fine spray, shooting upward, originated at the outer edge of the spreading drop and progressed rapidly toward the center, eventually enveloping the entire drop. This spray was interpreted to be the result of the breakthrough of steam bubbles across the free surface of the drop. Since the spreading drop was thinnest at the outer edges, the spray originated there. At the time the bubbles began to break through the center portion of the drop, the drop rapidly disintegrated, and the smaller droplets of liquid moved radially outward along the solid surface in the spheroidal state. The temperature of the heater surface

prior to impact was varied between 160 and 600 degrees C, so that the spheroidal state always existed for the drop fragments.

Savic stated that the outer portions of the spreading drop seemed to be in the film boiling state but that the local solid surface was cooled sufficiently to allow nucleate boiling at peak flux conditions to occur immediately behind this region. It was in this nucleate boiling region that the spray seemed to emerge from the free surface. He noted that this point of spray emergence was always at a point where the drop free surface was approximately 0.019 inches above the heater surface. This was true regardless of the location in the drop or of the heater surface temperature.

Calculations made by Savic showed that the maximum bubble radius in water must vary between 0.0135 and 0.027 inches. Therefore he used a value of 0.019 inches above the heater surface to describe the point of breakthrough of the bubbles across the liquid surface of the spreading drop. This value seemed to agree with the values of maximum bubble radius given by Gunther (29) at the assumed convection velocity.

Savic made some approximate calculations as to the cooling effect of the drops. Assuming the drop spread uniformly to a thickness of 0.019 inches, that it adhered to the heater for 1.6 microseconds prior to disintegration, and that a value of peak heat flux was 2.75 Btu per square inch second, he calculated the total heat transfer to be

4.4×10^{-5} Btu. This was considerably less than the total latent heat in the drop of 2.9×10^{-2} Btu. In another calculation he assumed the drop was raised uniformly in temperature to the saturation temperature at which time the bubbles, growing rapidly, would break through a drop of any thickness. This gave a heat transfer of 4.1×10^{-3} Btu, which was much more than the previous calculation but still less than the total cooling effect available in the drop. Savic concluded that the heat transfer process was a very inefficient one, unless one assumed that the small fragments of the drop formed an isolating vapor blanket over the surface and made available for cooling all of the liquid latent heat. He stated that recent observations with spray cooled gas turbine blades seemed to support the latter as the likely mechanism. In a personal communication with this author Savic said that his remark was based on the work of a classified report (51). Another classified report bearing on the same subject was issued in 1954 (50).

Savic's work dealt with large drops (0.115 inches) and with the case of impact at right angles to the solid surface at a particular impact velocity. It would be useful to study this same effect with smaller drops hitting a solid surface at various angles and velocities such as occur with mists flowing through tubes.

In the appendix to (60) the fluid dynamical treatment of the spreading drop given in (61) was extended, showing that the forward edge of the spreading drop can be calculated by a boundary layer type

of treatment, taking account of capillary effects, which could be neglected elsewhere in the drop.

A very thorough and recent study of the fundamental aspects of solid-gas flows was made in a series of articles by Torobin and Gauvin (68). In these articles the authors discuss introductory concepts and idealized motion in viscous regimes, the sphere wake in steady laminar fluids, and the accelerated motion of a particle in a fluid. Although most of the ideas apply strictly to solid spheres, some of the concepts could be applied to two-phase vapor-liquid flows.

The authors critically reviewed and compared many articles on the subject and showed that many discrepancies exist between experiments that have not as yet been explained. The theoretical and experimental information available on the unsteady motion of a particle through a fluid is much more crude and deficient than that available for steady state conditions. Some of the conclusions made were:

1. Potential flow theory can be used to describe events only at the beginning of rectilinear accelerations as well as oscillatory motions involving very small amplitudes.
2. Non-steady motion can cause very appreciable departures from the steady-state drag even for particulate movement in gases where the fluid-particle density ratio is extremely low.
3. Constant and varying acceleration rate experiments do not

give similar drag coefficients and therefore the rate of change of the acceleration must be taken into account.

4. The large decreases in drag noted in some acceleration experiments (32) cannot be explained in terms of present fundamental information which predicts increases in drag only and it is suggested that these data are influenced by phenomena other than acceleration.

There appears to be a great opportunity for research in the field of the fluid dynamics of unsteady particle motion.

In recent years Tchen (67), Lumley (39), and Soo (63) have made analytical studies of turbulent two-phase motion. In each case assumptions were made by the investigators that the particles moved in an isotropic, infinite turbulent field and were affected by drag forces of a viscous nature only. These investigations have been useful in helping to understand the mechanism of momentum transfer in two-phase flows, but direct applications to practical problems are limited due to the simplifying assumptions made.

An experimental determination of the statistical properties of two-phase turbulent motion was made by Soo, Ihrig, and El Kouh(64) in 1959. Glass spheres of 40 to 250 micron diameter were observed as they flowed with air through a three-inch square horizontal duct. The authors studied the gas phase turbulent motion with a tracer-diffusion technique and they studied the particle motion with a unique photo-optical

technique. From the investigations the authors concluded that, for the conditions studied (0.01 to 0.06 lb of solids per lb of air and particles less than 250 microns in diameter), the stream turbulence was not significantly affected by the presence of the particles. The particle motion was nonisotropic, even where the stream motion was nearly isotropic, chiefly due to gravity and wall effects. The intensity of particle motion seemed to be greatly affected by the distribution of stream intensity in the duct. The probability of particle-stream encounter had a significant effect on the particle diffusivity. (Particle-stream encounter is the encounter between the solid particle and the elements of the stream with fluctuating velocities.)

Particle diffusivities were considerably lower than the eddy diffusivity of the air stream in their investigation. This is shown in Fig. 9 where the ratio of particle diffusivity to eddy diffusivity is plotted against the parameter K, where

$$K = \frac{\pi^{\frac{1}{2}}}{18} \bar{N}_{Re} \frac{d}{\ell_1} \frac{\rho_L}{\rho_g} .$$

This result seems to contradict an earlier statement by Soo (63), in which he said, "... and the diffusivity of the particles is greater than the eddy diffusivity of the stream, but tends to the eddy diffusivity of the stream." This is simply an indication of the difference which can exist between the results of studying an ideal system and an actual system.

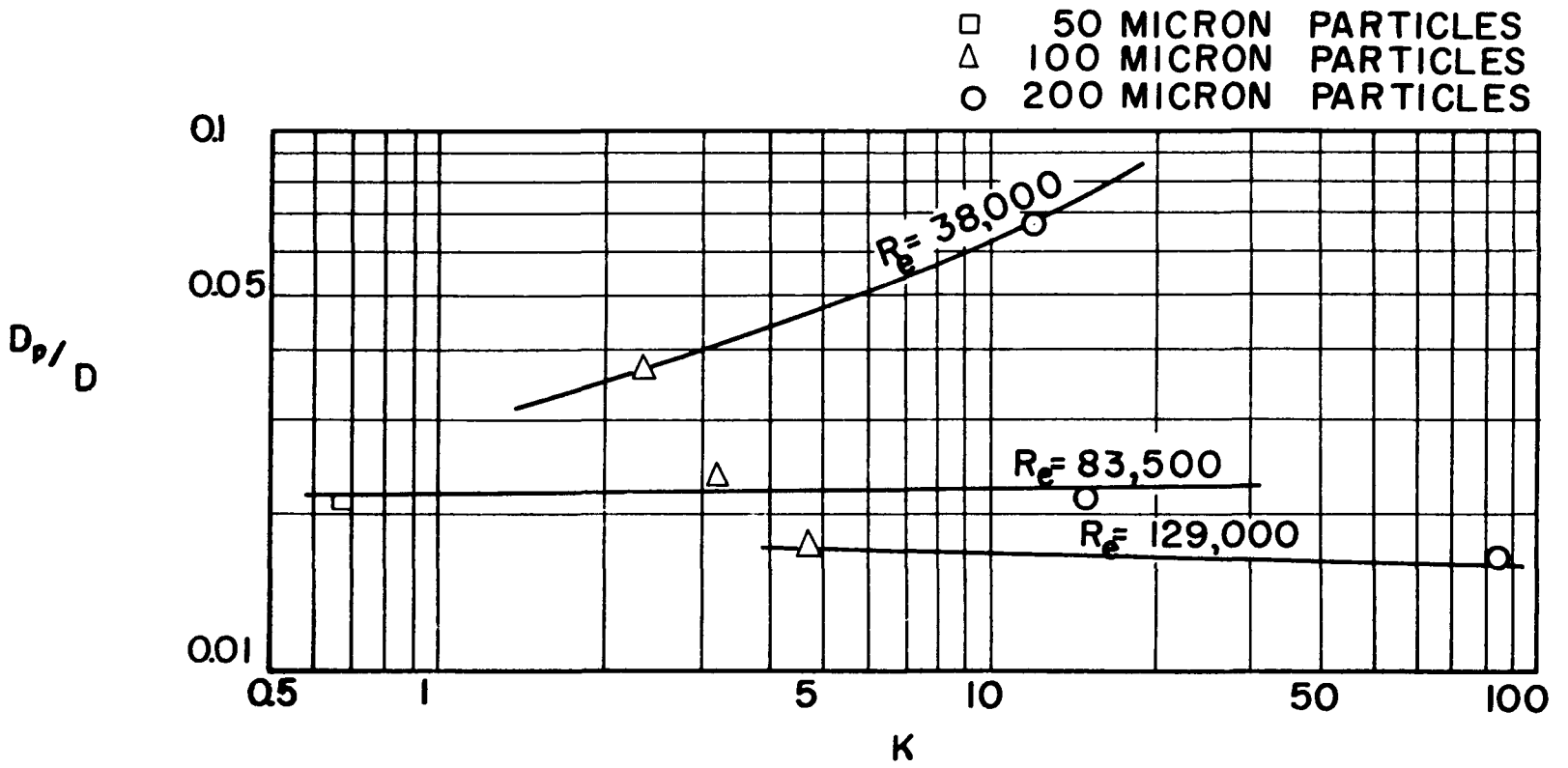

FIG. 9 RATIO OF PARTICLES DIFFUSIVITY TO EDDY DIFFUSIVITY ACCORDING TO (64)

Figure 9 suggests that at high Reynolds numbers the ratio of particle diffusivity to eddy diffusivity is almost a simple function of density ratio only.

Noting from the previous study that the wall seemed to have an effect on the intensity of motion of the particles, Soo and Tien (65) made an analytical study on the effect of the wall on two-phase turbulent motion. From their study they were able to conclude that the presence of a wall affects the intensity of motion of the particles in the mean stream of a two-phase duct significantly, but that the particle diffusivity is not significantly affected by the wall. They further concluded that the intensity of particle motion increases toward the wall, the scale of turbulence of particle motion decreases toward the wall, and the effect of the wall on the mean stream is more predominating for low duct Reynolds numbers than for high Reynolds numbers.

One effect that the authors noted is quite interesting as well as important. The spinning motion of the solid particles due to the fluid velocity gradient leads to the Magnus effect, causing the particle to move away as it approaches the wall. This effect is the most pronounced for particles smaller than the boundary layer thickness. The authors state that this effect explains the fact that a straight run of duct used in the pneumatic conveyance of solids suffers only a small amount of wear over a long time. Such an effect could greatly reduce the heat transfer coefficients to a mist if one assumes that contact between the

wall and droplet is the important factor in the heat transfer mechanism.

Droplet Measurement

The experimental methods for determining drop size distributions of fuel sprays were reviewed recently by Pilcher and Thomas (54). They listed the following six general methods:

1. Microscopic
2. Freezing and sieving
3. Optical methods based on scattering or absorption
4. Electronic and radiographic
5. Photography
6. Selective impaction

A thorough review of the literature and the references listed in (5), (15), (47), and (53), revealed no other general methods of determining liquid particle size. Study of the various methods led to the conclusion that only the methods listed under 4 and 5 above would likely be satisfactory for determining droplet sizes in a steam-water system where the droplets exist in a wide variety of sizes and are moving at high velocities in a hot vapor.

Photographic methods were given some very serious consideration since such methods have yielded satisfactory results in systems where small droplets were moving at high velocity (20), (32), (45). However elaborate optical and lighting equipment was generally utilized in these investigations.

Photographic methods also require a considerable amount of effort in the analysis of the droplet photographs. Although systems are available for the analysis of photographs, the analysis is usually done manually. Since the droplet images are often blurred and fuzzy in the photographs a great deal of human judgment enters into the analysis. Because of the randomness of droplet flow, several photographs usually must be taken in order to obtain a suitable sampling of each flow condition.

Photographic systems also require some means of visualization into the duct and for the provision of a light source. Most mist flows are accompanied by wetted walls, therefore some method is required to keep the windows free of liquid. This is often difficult to do without disturbing the flow pattern.

It was for these reasons that interest was directed toward investigating the electronic spray analyzer. Development of a droplet measuring device that would not have the complexity of photographic methods would be a great contribution to the science of spray technology.

Guyton (25) developed an electronic apparatus for the analysis of slow moving clouds. A sample of the suspension being investigated was aspirated through a tube and emitted at high velocity through a jet onto a grounded wire. The particles apparently became electrostatically charged as they moved through the tube, the charge being proportional to the square of the particle diameter. Electrical pulses were created

as the charged particles hit the grounded wire. The pulses were amplified, sorted by a discriminator circuit, and counted. The device was found to be most successful with nonconducting particles.

In 1951, Geist, York, and Brown (25) reported on their work with an electronic spray analyzer for electrically conducting particles. The report was the result of work done for the Ph.D. thesis by Geist (24).

The analyzer consisted of a charged wire that could be inserted into a moving or stationary suspension of particles. Electrical pulses were generated by the contact of the particles with the wire. An electronic circuit was used to amplify, sort and count the pulses generated at the probe wire. A block diagram of their circuit is shown in Fig. 10 along with the circuit diagram of the cathode follower. The amplifier, discriminator, and scaler-timer were standard items, similar to those used in radioactive counting.

The interceptor was a four-inch piece of 18-gauge copper wire connected directly to the grid of the 6AK5 pentode in the cathode follower. The components of the cathode follower were enclosed in a brass cylinder connected to ground. The brass cylinder and two inches of the probe wire were covered with Plexiglas tubing to reduce surface conduction between the charged probe and the grounded brass cylinder. An electrical potential of up to 430 volts could be placed on the probe wire.

Metal spheres 500 to 6,340 microns in diameter and water drops with diameters of 2,590 to 4,550 microns were used to calibrate the

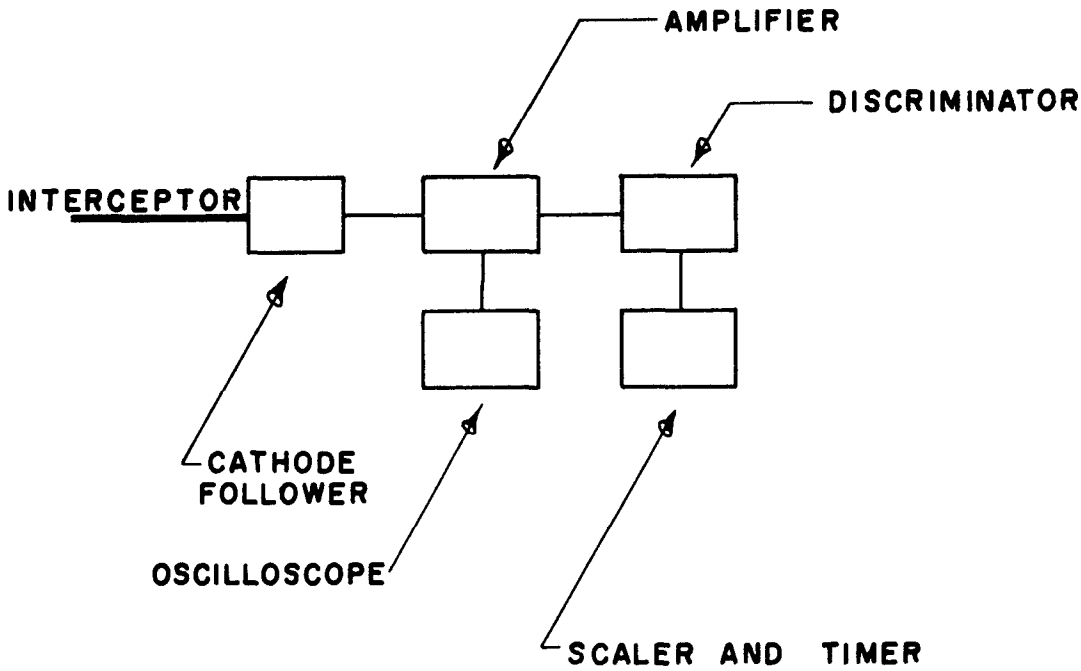

BLOCK DIAGRAM

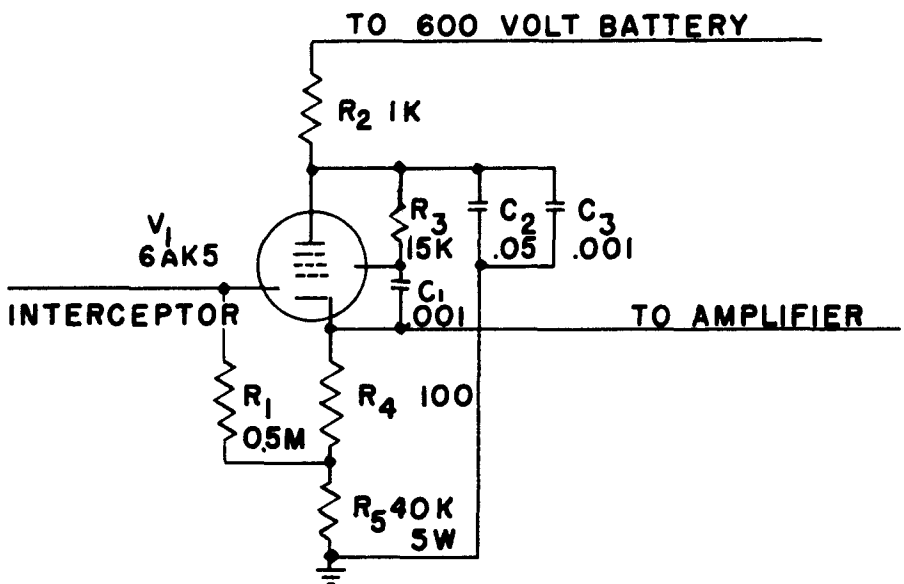

WIRING DIAGRAM OF CATHODE FOLLOWER

FIG. 10 SPRAY ANALYZER OF GEIST (25)

spray analyzer. The investigators found that the size of the pulse produced by the apparatus was proportional to the size of the particle hitting the probe and the potential of the probe, but was also affected by the position along the probe wire at which the particle hit. The relationship between pulse size and particle size for a probe potential of 430 volts is shown in Fig. 11. The variation of pulse size with potential for an 0.125 inch steel ball is shown in Fig. 12.

They found little difference in the size of the pulses produced by the water drops and the steel or solder spheres of the same size. This suggested that the pulse size produced by the instrument would be unaffected by the material of the particle, so long as it was a conductor. Measurements made with non-conducting acetone and alcohol drops showed smaller pulse sizes than for the metal and the water spheres of the same diameter.

Explanation for the production of the pulses was given by assuming that the probe wire could be considered as a capacitor with a fixed charge. For a capacitor,

$$Q = C_E V,$$

which upon differentiating gives

$$dV = -\left(\frac{Q}{C_E^2}\right) dC_E \quad .$$

Thus, for small changes

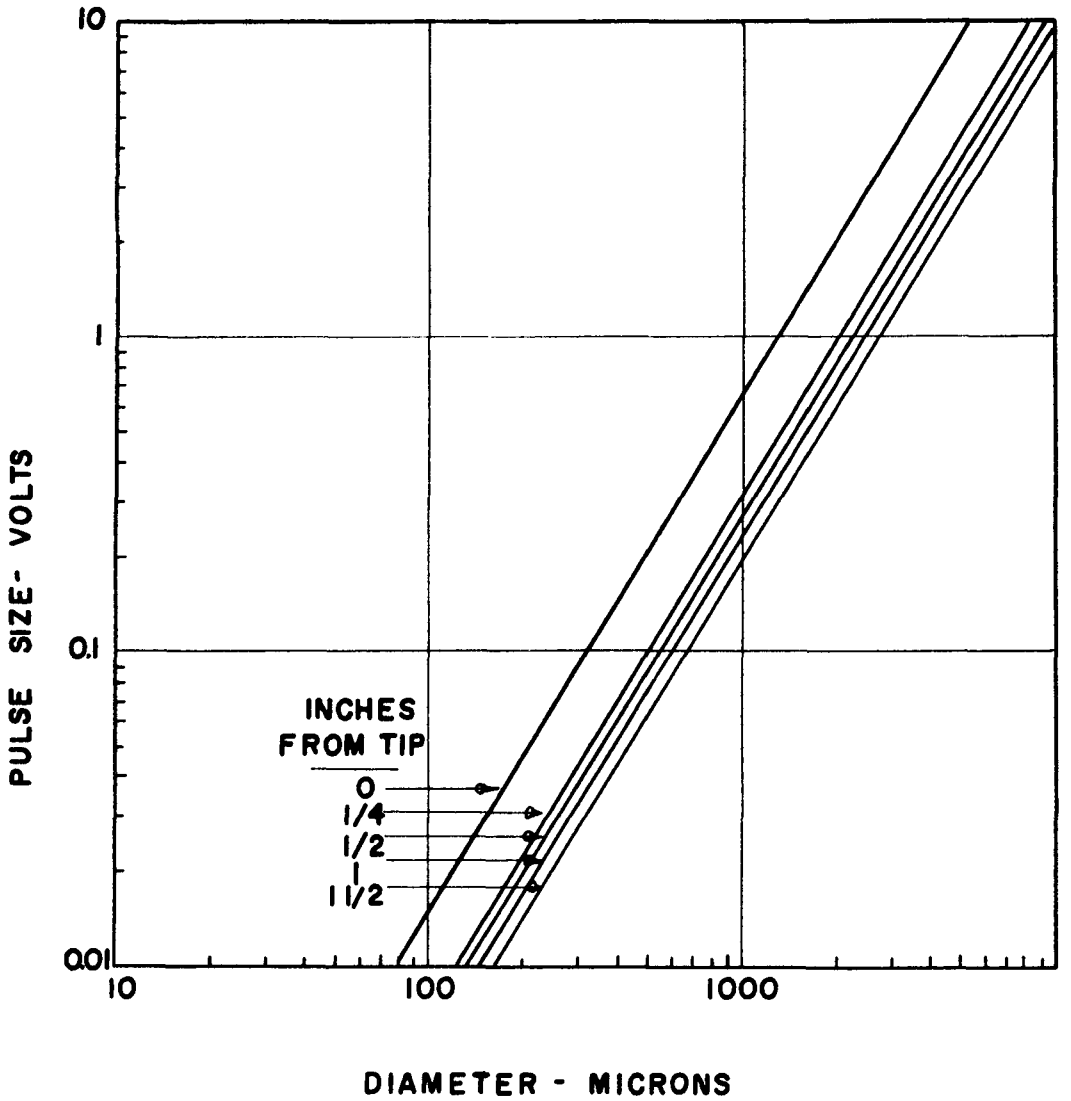

FIG. 11 RELATIONSHIP BETWEEN PULSE SIZE & PARTICLE SIZE FOR PROBE OF GEIST (25)

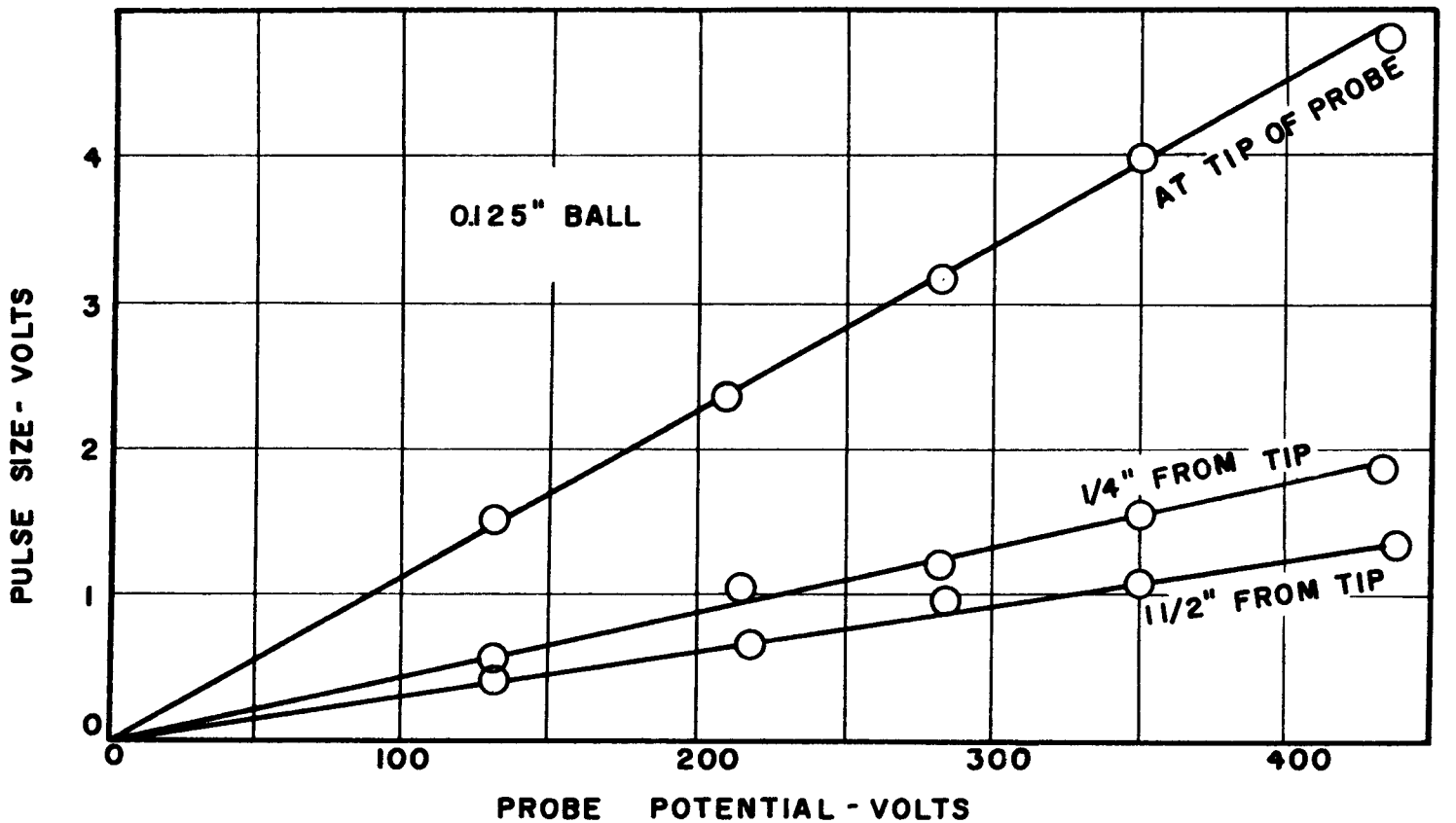

FIG. 12 VARIATION OF PULSE SIZE WITH POTENTIAL FOR PROBE OF GEIST (25)

$$\Delta V = - V \frac{\Delta C_E}{C_E} \quad .$$

Contact of the sphere with the charged probe increases the capacity of the probe slightly and this changes the potential of the probe, according to the above equation. Increasing the probe potential and decreasing the probe capacity results in a larger pulse from a given size particle. This gives an indication of the direction to go in improving the performance of the analyzer.

The biggest disadvantage of the spray analyzer was the fact that the size of the pulse produced was dependent on the position along the wire at which the particle hit. This was because the charge density was unevenly distributed along the surface of the wire due to the physical shape of the probe. This effect made the instrument impractical for use as a droplet measuring device in sprays, since the drops of various sizes would be hitting the probe at various locations. The resulting pulses would have little significance.

Further work on improving the spray analyzer was carried on by York, et al (76), (77), under the sponsorship of the DeVilbiss Company of Toledo, Ohio. The work was directed primarily toward increasing the pulse size produced at the probe by a droplet and in improving the probe geometry so as to eliminate the dependency of pulse size on position of impact. A sensing unit was eventually developed that solved the latter difficulty. This was done by making the probe from a small

metal sphere, 0.020 inch diameter, attached to the end of an 0.010 inch diameter wire. The wire was covered with electrical insulating material, leaving only the front half of the metal sphere exposed.

This design gave a sensing element in which the charge density was uniformly distributed over the exposed surface and made the pulse size independent of position of impact. The basic arrangement of the analyzer, shown in the block diagram of Fig. 10, remained unchanged; however, the cathode follower and the major components of the analyzer were replaced.

A calibration curve obtained for the improved spray analyzer is shown in Fig. 13. The curve shows that the lower limit of drop size detection was limited by the noise level of the circuits. There seemed to be no way to extend this lower level of the analyzer at that time so work on the instrument was temporarily abandoned.

The DeVilbiss Company obtained a United States patent on the electronic spray analyzer that was developed.

In the final report of the investigation by York, et al (77), the authors suggested that a modification of the device might be used to study entrained droplets flowing with vapor through a closed tube. Professor York, in a personal communication, suggested that such a device might actually have a better lower limit capability since the probe could be built with a lower electrical capacity than the model described previously. This is true because the previous model had to be closely

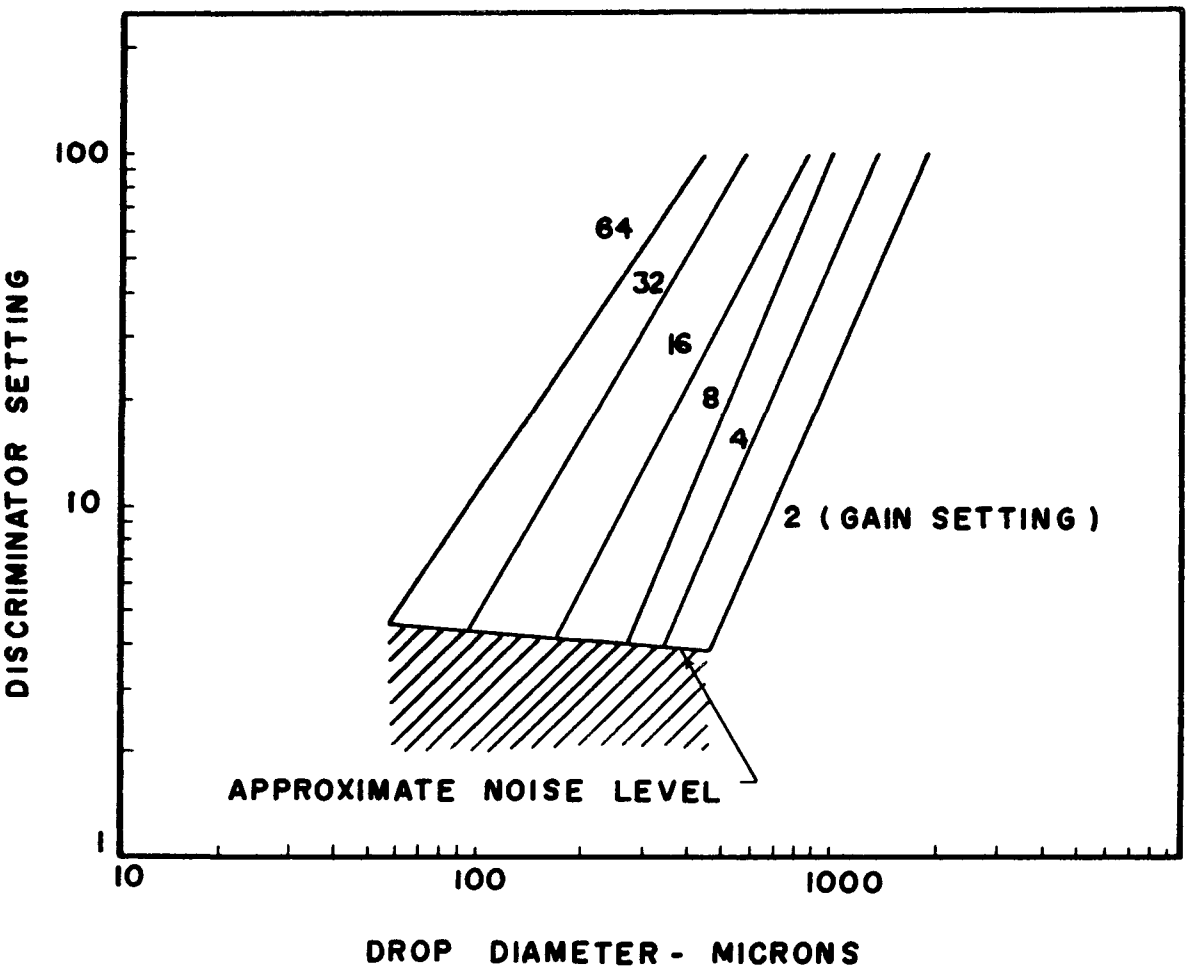

FIG. 13 DEVILBISS ELECTRONIC-DROP-ANALYZER CALIBRATION CURVE

shielded to reduce noise whereas the pipe wall could serve as an excellent shielding in the suggested device.

DEVELOPMENT OF AN ANALYTICAL MODEL

In developing an analytical model with which to predict heat transfer coefficients to a mist flow it seems logical to use the fundamental equations of momentum, energy, and continuity. Combining these equations with certain phenomenological equations could lead to a solution of the temperature distribution existing in the flow, which would in turn yield the desired heat transfer coefficients. However this type of treatment becomes very complex when applied to a mist flow, since two phases exist. The fundamental equations must either be written for both phases, or else the equations must be written as for single-phase flow but using property values that are suitably descriptive of the mist and that assume it to be a homogeneous substance.

In applying the single-phase treatment to a mist flow the assumption would have to be made that both the vapor and the droplets move at the same local velocity, with no relative acceleration between the phases. It is the inertia forces that cause the droplets to have a relative acceleration with respect to the vapor. Drag forces on the droplets tend to decrease this relative acceleration. Therefore, in order to use the single-phase treatment, the inertia forces acting on the droplets should be less than the drag forces. This means that single-phase

treatment would be limited to cases where the Reynolds number is low, the droplets are small, and where differences in the density of the phases are slight. Some types of mist flows would meet these requirements. However, another difficulty arises in determining property values to adequately describe the mixture, especially the properties of thermal conductivity and viscosity. Little information is presently available on this subject.

In a mist flow the gas phase is usually turbulent. This would have to be taken into account in writing the fundamental equations and would further complicate their solution. The effect of the wall on the two-phase turbulent motion would also have to be considered (65).

The alternate method of writing the fundamental equations for each phase requires the introduction of phenomenological equations to describe the action between the two phases and to relate the properties for each phase. The transfer of heat and mass across the interfaces between steam and droplets involves problems that are not completely understood at the present time (58). The effects of acceleration, distortion, and internal circulation on the drag forces acting on a drop are not completely understood. In addition, suitable equations of state for water are fairly complex. Therefore, it does not seem practical at the present time to attempt to solve the problem of heat transfer to a mist by the use of the fundamental equations.

Because of the difficulties described above it was decided to attempt to develop an analytical model for heat transfer from certain simplified assumptions. It is well known that the heat transfer coefficients between a solid and a liquid are quite high as compared to those between a solid and a vapor. In addition it is known that the heat transfer rate is fairly low between a droplet and its own vapor in the case of evaporation. The theoretical minimum value of the Nusselt number for a sphere in a stagnant medium is two. This would give a large value of film coefficient for very small diameter drops if the effect were purely conduction. With evaporation, however, the heat transfer to the drop is in an opposite direction to the mass transfer of vapor away from the drop. At moderate pressures a very large quantity of vapor is produced by the vaporization of a small quantity of liquid. Another effect becomes important for very small drops. The surface tension of the liquid causes the liquid in the drop to be at a higher pressure than the surrounding vapor. Thus it is possible for thermal equilibrium to exist between a superheated vapor and a drop whose liquid is below the saturation temperature. For these reasons, superheated steam frequently contains moisture (11). Jakob and Knoblauch in an investigation to determine specific heats of steam noted that small drops persisted for a long period of time in a superheated vapor atmosphere even after a considerable amount of stirring (66).

The above facts seem to indicate that the heat transfer coefficient to mists is greatly increased by the contact of the droplets with the wall and is influenced strongly by the behavior of the droplets after striking the wall. Thus a satisfactory model must predict the motion of the droplets toward the wall, and it must predict what cooling effect the droplet will have on the wall.

Consideration of the above statements has led to the following simplified model for heat transfer to a mist flow. The assumptions made are:

1. Steady turbulent flow of a mist of steam and water droplets through a straight round tube of constant cross section.
2. Heat is added at a constant rate along the tube length. The quality is assumed to be a linear function of the distance from the start of heating.
3. Entrance effects are negligible.
4. Pressure is constant across the tube. The turbulent core consists of vapor and droplets in thermal equilibrium at a temperature corresponding to the pressure of the vapor phase. Superheated vapor occurs only in a thin layer near the wall.
5. The average axial velocity of the liquid and vapor at any cross section can be estimated from a slip velocity ratio S.

6. The rate of transfer of droplets to the wall can be predicted by use of a mass transfer coefficient k_d and the average concentration of droplets at any cross section.
7. Body forces are negligible.
8. Heat transfer to the mist is equal to the heat added to the vapor phase plus the heat added to the liquid. If the wall temperature is below the critical value for the spheroidal state, all drops striking the wall will be completely vaporized. If the wall temperature is above this critical value, the droplets will undergo a negligible amount of evaporation and will return to the turbulent core. Heat transfer from the wall to the vapor phase is unaffected by the presence of the drops and can be predicted by the use of a suitable equation.

This model predicts coefficients to a mist flow that are higher than for dry steam at the same pressure and mass flow rate. If, however, the wall temperature is above the critical value for the spheroidal state, the heat transfer coefficient is predicted to be approximately the same as for dry steam.

In the case where all of the droplets striking the wall are vaporized, the heat necessary to evaporate these droplets per square foot of tube wall area would be

$$q''_{evap} = k_d C h_{fg} \quad . \tag{1}$$

Then, according to assumption 8 of the model, the wall temperature can be

$$(T_w - T_B) = \frac{q'' - k_d C h_{fg}}{h} \qquad (2)$$

where h is the coefficient of heat transfer to dry steam at the same mass flow rate.

The heat transfer coefficient to the mist flow is defined by

$$q'' = h_{mist} (T_w - T_B) \quad . \qquad (3)$$

Therefore

$$h_{mist} = \frac{q'' h}{q'' - k_d C h_{fg}} \quad . \qquad (4)$$

The water content of wet steam mixtures is usually described by the quality instead of by the concentration. The quality is the pounds of steam flowing per unit time divided by the pounds of mixture flowing per unit time. The concentration is the weight of water per unit volume of the mixture. In the case where there is a slip velocity between the phases the weight of water per unit volume would be higher than that calculated from flow rate measurements. If S is the ratio of average liquid velocity to average steam velocity, then

$$C = \frac{\text{weight of water flowing per unit time}}{S \text{ (volume of mixture flowing per unit time)}} \quad .$$

If the density of the liquid is much greater than the density of the steam ρ_g, the quality can be expressed as

$$X = \frac{\rho_g \text{ (volume of the mixture flowing per unit time)}}{\text{weight of the mixture flowing per unit time}} .$$

Then

$$CX = \frac{\rho_g \text{ (pounds of water flowing per unit time)}}{\text{pounds of mixture flowing per unit time}}$$

or

$$C = \frac{\rho_g}{S} \frac{(1 - X)}{X} . \tag{5}$$

Equation (4) can be written as

$$h_{mist} = \frac{q'' h}{q'' - \frac{k_d \rho_g h_{fg}}{S} (\frac{1 - X}{X})} . \tag{6}$$

Because of assumption number 2, the quality at any cross section can be expressed as a function of the quality X_o at some reference position, the distance L from the reference position, the wall heat flux q'', the mass flow rate of the mixture W, and the tube diameter D. The energy added to the flow per hour for one foot of tube length is

$$q = q'' \pi D . \tag{7}$$

Thus

$$X = X_o + \frac{qL}{Wh_{fg}} = X_o + \frac{q'' \pi D L}{Wh_{fg}} \tag{8}$$

and the expression for the heat transfer coefficient is

$$h_{mist} = \frac{q'' h}{q'' - \frac{k_d \rho_g h_{fg}}{S} (\frac{1}{X_o + \frac{q'' \pi D L}{Wh_{fg}}} - 1)} . \tag{9}$$

The equation for the wall temperature is

$$(T_w - T_B) = \frac{q''}{h} - \frac{k_d \rho_g h_{fg}}{hS} \left(\frac{1}{X_o + \frac{q'' \pi DL}{W h_{fg}}} - 1 \right) . \qquad (10)$$

If the model correctly describes the mechanism, then Equation (10) gives the wall temperatures that would exist for a mist flow at various positions along the tube.

The equations that have been derived apply only for positive values of $(T_w - T_B)$ and only for values of mixture quality $(X_o + \frac{q'' \pi DL}{W h_{fg}})$ less than 100 percent. Negative values of $(T_w - T_B)$ imply that more liquid is arriving at the wall than is being evaporated and thus annular-mist, rather than mist, flow would exist. In the region past the point where the quality is 100 percent the wall temperature remains a fixed value above the bulk temperature, assuming that a constant value of h exists in that region.

It is convenient to use the point of 100 percent quality as a reference. Rewriting Equation (10) in terms of a length L' upstream from the 100 percent quality point, since

$$X = 1 - \frac{q'' \pi DL'}{W h_{fg}} , \qquad (11)$$

then

$$(T_w - T_B) = \frac{q''}{h} - \frac{k_d \rho_g h_{fg}}{hS} \left(\frac{1}{1 - \frac{q'' \pi DL'}{W h_{fg}}} - 1 \right) . \qquad (12)$$

The previous equations and statements lead to some rather interesting results about the variation in wall temperature that might be

encountered in a mist flow. In an example the assumption will be made that the slip ratio S is 1.0 and that a reasonable value of k_d is 1000 ft per hour. A mixture of steam and water droplets at 30 psia is assumed to flow at 200 pounds per hour through a one-inch tube. For the first case to be considered the wall heat flux is assumed to be 3,000 Btu per hour square foot. The value of the film coefficient h can be calculated from the Dittus-Boelter equation using property values for saturated steam and the flow rate of the mixture as an approximation. The result for the assumed conditions is h = 41 Btu per hour square foot degree F.

Equation (12) becomes

$$T_w - T_B = \frac{3000}{41} - \frac{(1000)(945.3)}{(13.746)(41)} \left[\frac{1}{1 - \frac{(3000)\pi (0.0833)L'}{(200)(945.3)}} - 1 \right] \quad (13)$$

Assuming that the bulk temperature and the saturation temperature are the same as long as there is moisture present in the steam, and further assuming that the pressure drop down the tube is small, then the bulk temperature of the saturated mixture remains constant.

Figure 14 shows the results of using Equation (13). Downstream from the point of 100 percent quality the temperature difference $(T_w - T_B)$ is constant since a constant heat transfer coefficient was assumed for dry steam. In the mist region the temperature difference decreases in the direction of decreasing quality until the value of zero is reached. At this point the droplets are assumed to be diffusing to

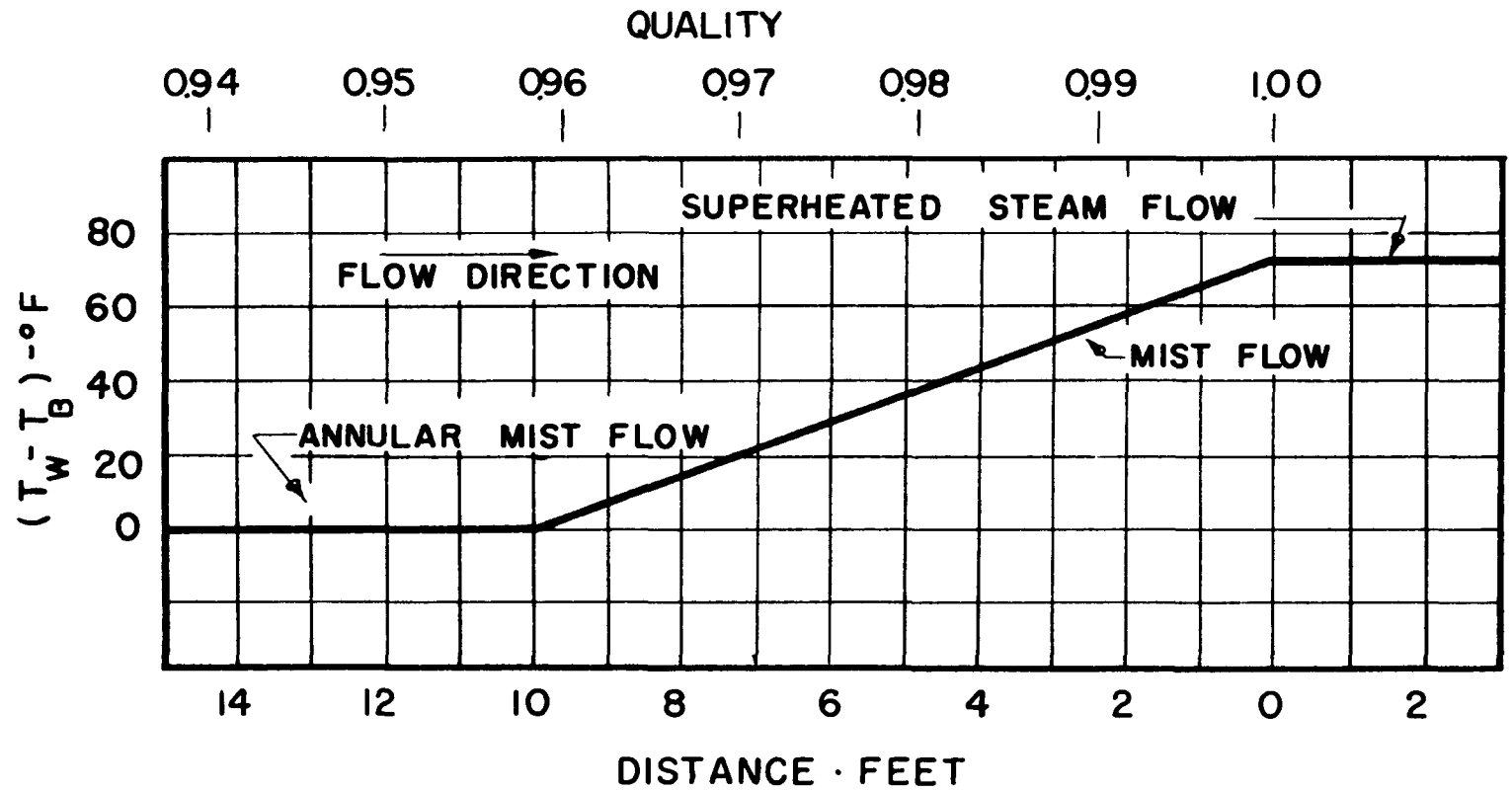

FIG.14 PREDICTION OF WALL TEMPERATURE BY SIMPLIFIED MODEL

the wall at just the right rate to keep the wall at the saturation temperature. Upstream from this point the droplets diffuse to the wall faster than they are evaporated and an annular-mist flow exists. Of course in the actual case the wall temperature will never equal the saturation temperature, since heat is being transferred from the wall to the fluid. For the annular flow which is assumed to occur in this region, however, the heat transfer coefficient is relatively high and the temperature difference is therefore small. This is especially true for very thin, turbulent films of liquid (1).

Thus, for the assumed conditions, the temperature difference will change rapidly in the region of mist flow as the quality changes, and will change very little in the regions of annular and superheated flow. The rate at which the temperature difference changes in the mist region for given flow conditions will depend upon the value of the wall heat flux. The curve for temperature difference in the mist region approximates a straight line very closely for the chosen parameter values.

In some applications the ratio of quantity of water in the annular film to that dispersed in the core may be such that there will be insufficient droplets to keep the wall temperature near saturation just downstream from the point where the film disappears. This could be the case, for example, if the film had been formed due to droplet diffusion to the wall in an adiabatic section prior to the start of heating. In this case the film of liquid on the wall could be the result of a

depletion of droplets in the core. (Re-entrainment of the droplets from the film to the core are neglected in this analysis.) In such cases the wall temperature would remain near saturation until the annular liquid film is evaporated and at that point the wall temperature would jump to the value predicted by Equation (10). The amount of the temperature rise would depend upon the position (or quality) at which the film disappears. Such an example is shown in Fig. 15, making the same assumptions as before except that the liquid film is assumed to persist up to a quality of 98 percent. For the case of pure annular flow, Equation (13) predicts that the wall temperature would rise sharply at the disappearance of the liquid film to the value computed for dry vapor.

Increasing the wall heat flux for the stated flow conditions results in a steeper temperature gradient in the mist region, since the quality is changing more rapidly. The result for a wall heat flux of 10,000 Btu per hour square foot is shown in Fig. 16, assuming that the film disappears at a quality of 90 percent. Here a new phenomenon must be taken into account. As the wall temperature rises above the bulk temperature of the fluid, a point will soon be reached where the spheroidal state starts to exist. When this happens the droplets no longer can be considered to evaporate completely and they have little cooling effect on the wall. The wall temperature jumps to near the value that would exist for dry steam flowing alone. This value of critical temperature

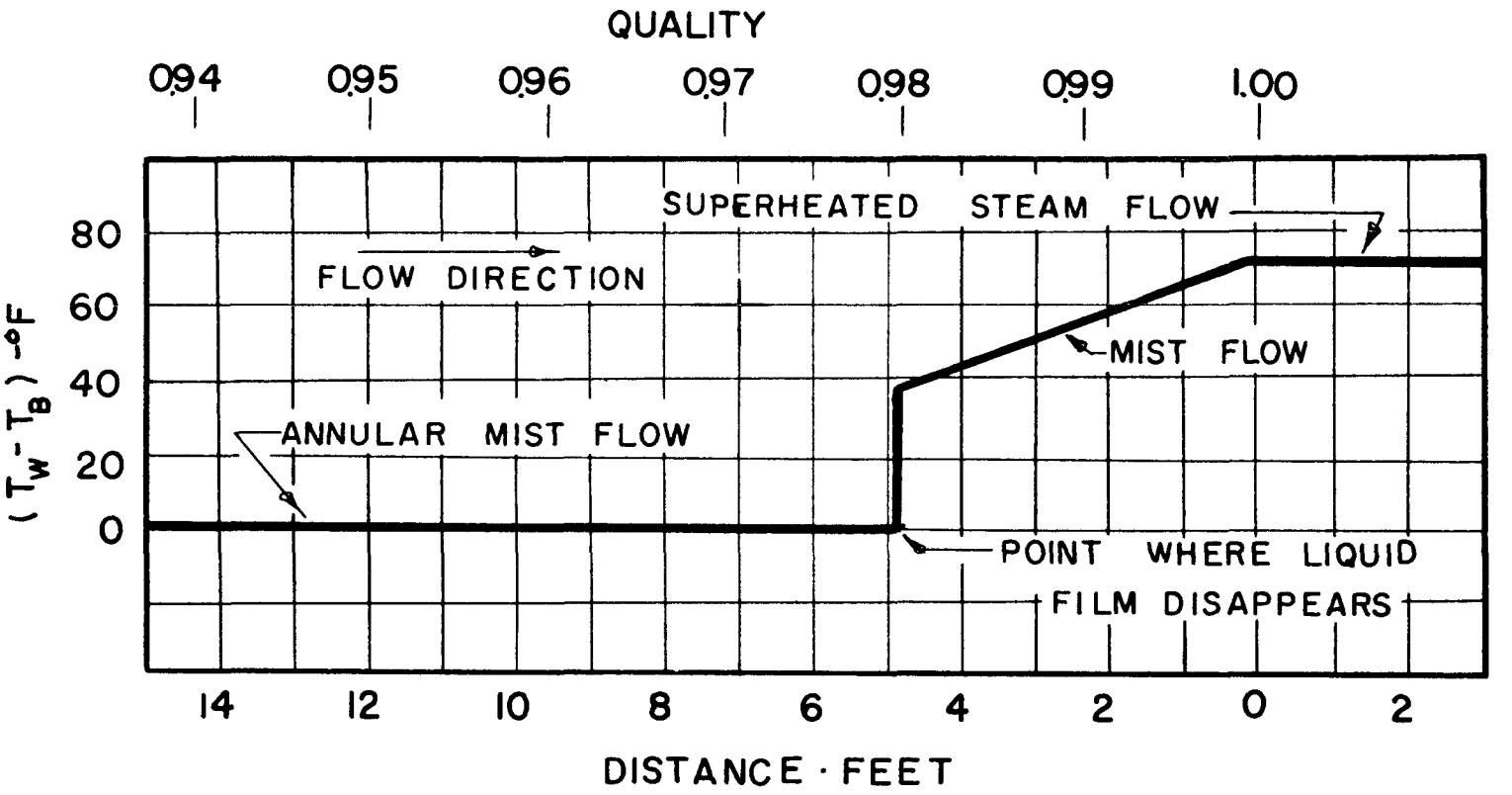

FIG.15 PREDICTION OF WALL TEMPERATURE BY SIMPLIFIED MODEL

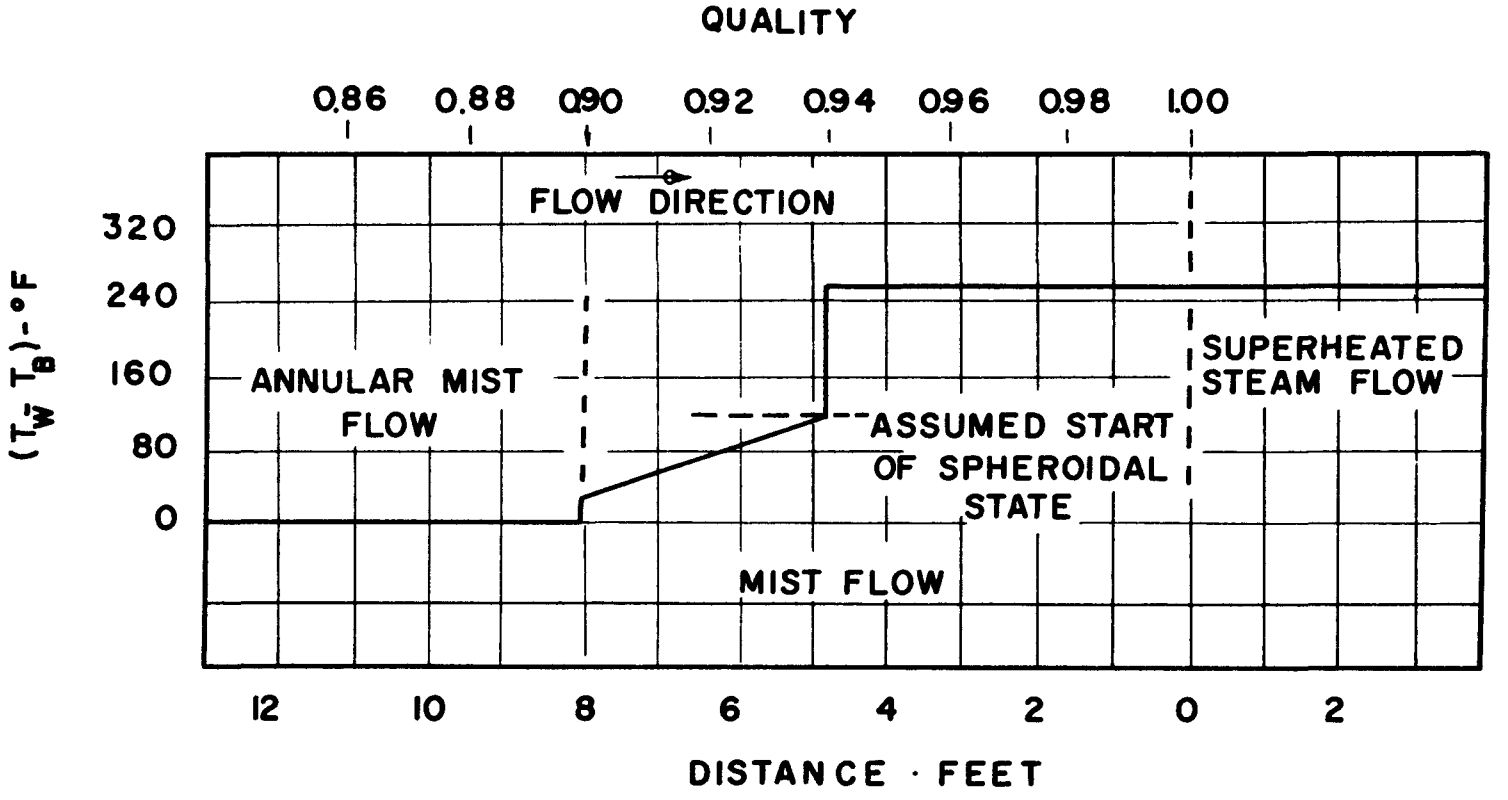

FIG. 16 WALL TEMPERATURE PREDICTED BY SIMPLIFIED MODEL WITH SPHEROIDAL EFFECT

difference for the spheroidal state is a function of surface condition and droplet size (26); but, in the figure it is shown as beginning abruptly at $(T_w - T_B)$ equal to 100 degrees F. At that point the wall temperature is assumed to jump immediately to the value for dry steam.

In the actual case, of course, temperatures and temperature gradients do not change sharply, but are smoothed out due to conduction effects in the wall and in the boundary layer. This conduction effect tends to shift the start of the spheroidal state upstream, causing the temperatures to climb more rapidly than predicted by Equation (10) just prior to the estimated point of inception of the spheroidal state. The spheroidal state does not begin at a distinct location along the tube since in the real mist flow a variety of drop sizes exists. Also the droplets have some cooling effect even in the spheroidal state. Taking these factors into account, the actual temperature profile might appear as shown in Fig. 17, for the example shown in Fig. 16.

In the equations that have been derived there are two terms that are not readily determinable. They are the mass transfer coefficient k_d and the slip velocity ratio S. Since both terms are likely a function of the average droplet diameter, it is desirable to know something of the droplet spectrum for the flow.

Even if the drop size distribution were well known for a particular flow, the mass transfer coefficient could not be determined directly for

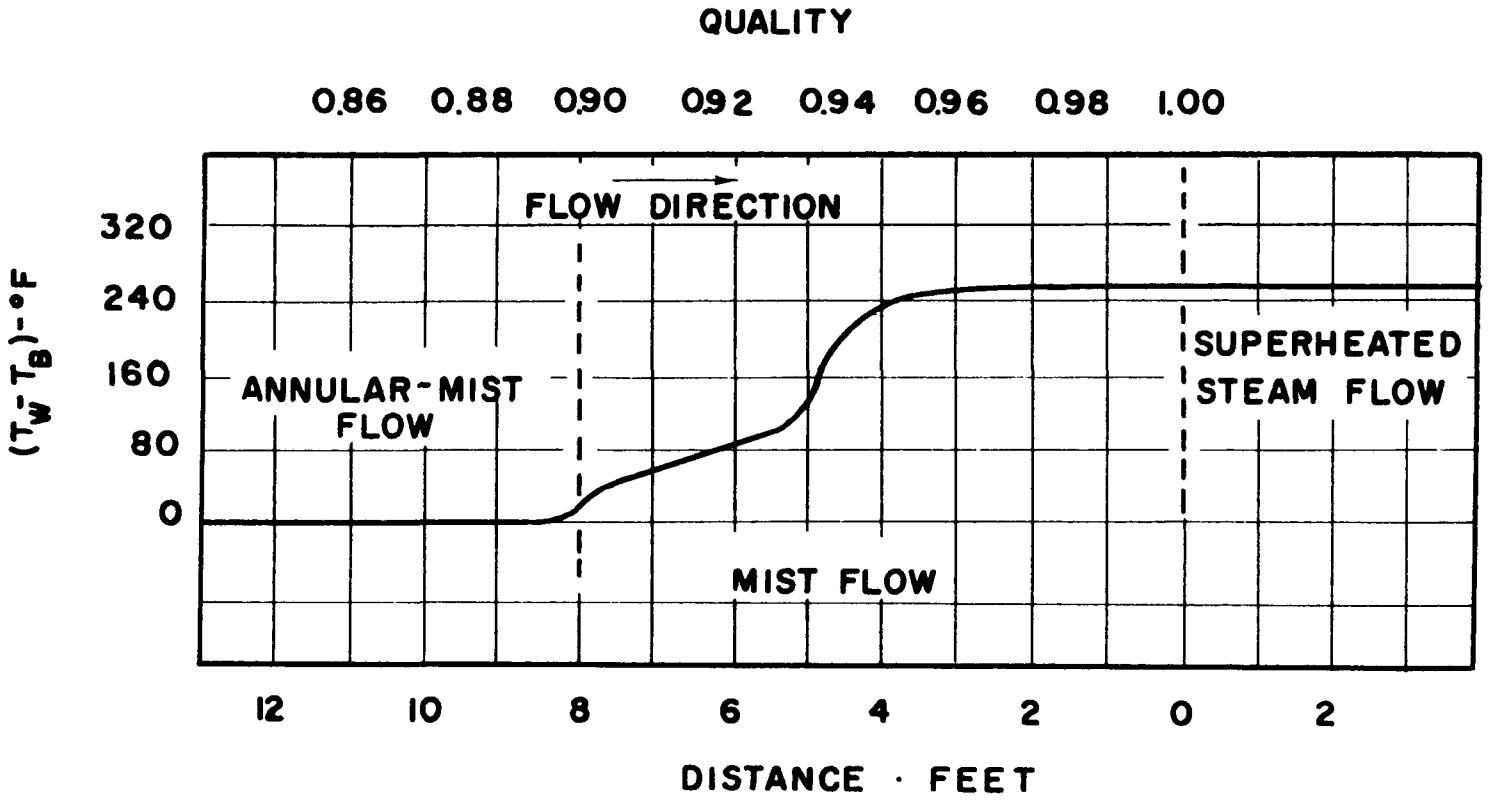

FIG. 17 WALL TEMPERATURE PREDICTED BY MODEL AFTER CORRECTION FOR CONDUCTION & SPHEROIDAL COOLING EFFECTS

the real case. This is because of the present lack of understanding of the mechanism of droplet transfer in turbulent gas streams. The use of an analogy such as was described by Friedlander and Johnstone (23) depends upon the assumption that the droplets follow the motion of the gas eddies. This is actually not true for any except the very smallest droplets (64).

The "exploding" of the droplets striking the tube wall into a large volume of vapor would most likely have an effect on the value of k_d. This effect would be similar to the effect of the boiling velocity discussed by Vanderwater (69). The creation of expanding vapor volumes at separated locations along the tube wall would create additional turbulence in the stream which would also have some effect on k_d. The analogy between mass and momentum transfer may be completely invalid.

The mass transfer coefficient k_d may not be a constant value with length as was assumed. The changing of the flow pattern from annular to mist might cause an effect on the dispersion in the core that would require a certain length before "fully developed" conditions are established.

The slip velocity ratio term must either be estimated or measured experimentally. Experimental methods of determining slip ratios for mist flows are fairly difficult to carry out. One method of estimating slip velocity ratios is to equate the inertia and drag forces acting on a

droplet, using an empirical expression for the drag coefficient. A similar analysis was used by Ingebo (32).

Thus

$$ma = \frac{1}{2} \rho_g A (\Delta u)^2 C_D \quad . \tag{14}$$

For the conditions of his experiments Ingebo found that the drag coefficient for small accelerating spheres could be found from the relation

$$C_D = \frac{27}{(\bar{N}_{Re})^{0.84}} \quad . \tag{15}$$

By making appropriate substitutions and integrating, the following expression is obtained:

$$L = 0.0585 \frac{\rho_L}{\rho_g} d (\bar{N}_{Re})^{0.84} \left[(1-S)^{0.84} + 5.25(1-S)^{-0.16} - 6.25 \right] \tag{16}$$

The derivation of this equation is given in Appendix A.

Thus an expression has been obtained for the distance L that a droplet of given diameter d must travel in order to attain a certain slip velocity ratio S. The results for this equation have been calculated for various droplet diameters, and various vapor velocities for steam at 30 psia, and are shown in Table 2.

In cases where the mist consists of small droplets and the Reynolds number is low, the slip velocity ratio approaches 1.0 for very small values of L. This means that in many instances the slip velocity ratio term can be neglected in Equations (9) and (10), particularly at

TABLE 2

Distance Necessary to Obtain a Certain Slip Velocity Ratio

Droplet Diameter = 1 Micron

(Distance, Feet x 10^4)

Initial Velocity	150 fps	300 fps	600 fps
Slip Ratio			
0.1	0.0274	0.049	0.0879
0.2	0.0970	0.211	0.311
0.3	0.211	0.376	0.676
0.4	0.513	0.916	1.645
0.5	0.884	1.580	2.83
0.6	1.435	3.12	4.44
0.7	2.41	4.30	7.71
0.8	4.07	7.29	13.10
0.9	7.52	13.40	24.1
1.0	∞	∞	∞

Droplet Diameter = 10 Micron

(Distance, Feet x 10^2)

Initial Velocity	150 fps	300 fps	600 fps
Slip Ratio			
0.1	0.0189	0.0338	0.0608
0.2	0.0668	0.119	0.215
0.3	0.1450	0.260	0.467
0.4	0.354	0.634	1.140
0.5	0.609	1.090	1.960
0.6	0.990	1.770	3.18
0.7	1.660	2.97	5.34
0.8	2.81	5.03	9.05
0.9	5.18	9.27	16.70
1.0	∞	∞	∞

TABLE 2 (Cont'd.)

Droplet Diameter = 100 Micron

(Distance, Feet)

Initial Velocity	150 fps	300 fps	600 fps
Slip Ratio			
0.1	0.0131	0.0227	0.0405
0.2	0.0462	0.0802	0.1430
0.3	0.1010	0.1740	0.311
0.4	0.244	0.425	0.758
0.5	0.421	0.731	1.310
0.6	0.685	1.190	2.12
0.7	1.150	1.990	3.56
0.8	1.950	3.38	6.03
0.9	3.58	6.21	11.10
1.0	∞	∞	∞

large distances from the point of droplet formation. This assumes of course that the vapor stream is not accelerating greatly due to vapor formation.

The formation of vapor from the droplets at the wall could also have a tremendous effect on the dry vapor film coefficient in the vicinity of the evaporating droplet. The effect might be similar to that in nucleate boiling, where the hot fluid is lifted away from the wall by the expanding vapor bubbles. In the mist flow the cooler saturated vapor from the droplet would tend to displace the hotter, superheated vapor away from the wall and into the turbulent core. This forced mixing could lead to values of film coefficient h higher than predicted by an equation such as the Dittus-Boelter equation. This effect should be

greatly affected by the rate at which the droplets hit the wall per unit area; i.e., h should be affected by the quality and the mass transfer coefficient.

In order to get an idea as to how rapidly droplets might be striking the wall, a few assumptions will be made. Reynolds' analogy for mass transfer predicts mass transfer coefficients of the order of 1,000 ft per hour for steam flowing at a Reynolds number of 10^5 and a velocity of 140 feet per second. A mass mean droplet diameter of 30 microns seems to be a reasonable value for droplets produced by an air atomizing nozzle under ordinary conditions. Using these values for 30 psig steam at 95 percent quality the value obtained for the number of droplets striking one square foot of wall per second is 36.3×10^6. Multiplying this number by the projected area of one drop gives an area of approximately one fourth of a square foot. This gives approximately the fraction of the surface that is touched by a drop per second. Unless the persistence time of a drop at the wall is very low, this would indicate a rather crowded condition of droplets which could strongly influence the dry film coefficients. This influence could only be determined by experimental methods.

It is concluded, however, from our simplified model, that sharp temperature variations will likely occur in mist flows, particularly at the points where the annular liquid film disappears and at the point where the spheroidal effect starts to occur. High values of wall heat

flux would likely cause a sharp change directly to spheroidal conditions very near the point where the annular film disappears.

DESCRIPTION OF APPARATUS

An apparatus was constructed to test the general validity of the proposed model and to obtain values of film coefficient for various flow conditions. The apparatus consisted of two systems:

1. A system to measure heat transfer coefficients to mists at certain flow conditions.
2. A system to measure the droplet size of mists flowing through the test section.

Flow System

The schematic diagram of the first system is shown in Fig. 18 and a photograph of the system is shown in Fig. 19. Steam, entering the system at approximately 150 psig and near 100 percent quality, was supplied from the University power plant through underground lines.

The raw water furnished to the power plant has a hardness of approximately 23 grains per gallon, and is treated by a lime and soda hot process. Nalco 35 is added to keep the average ph at 7.6.

The steam was passed through a separator to remove excess moisture before it was passed through a flow measurement nozzle. The separator was found necessary in order to maintain a consistent

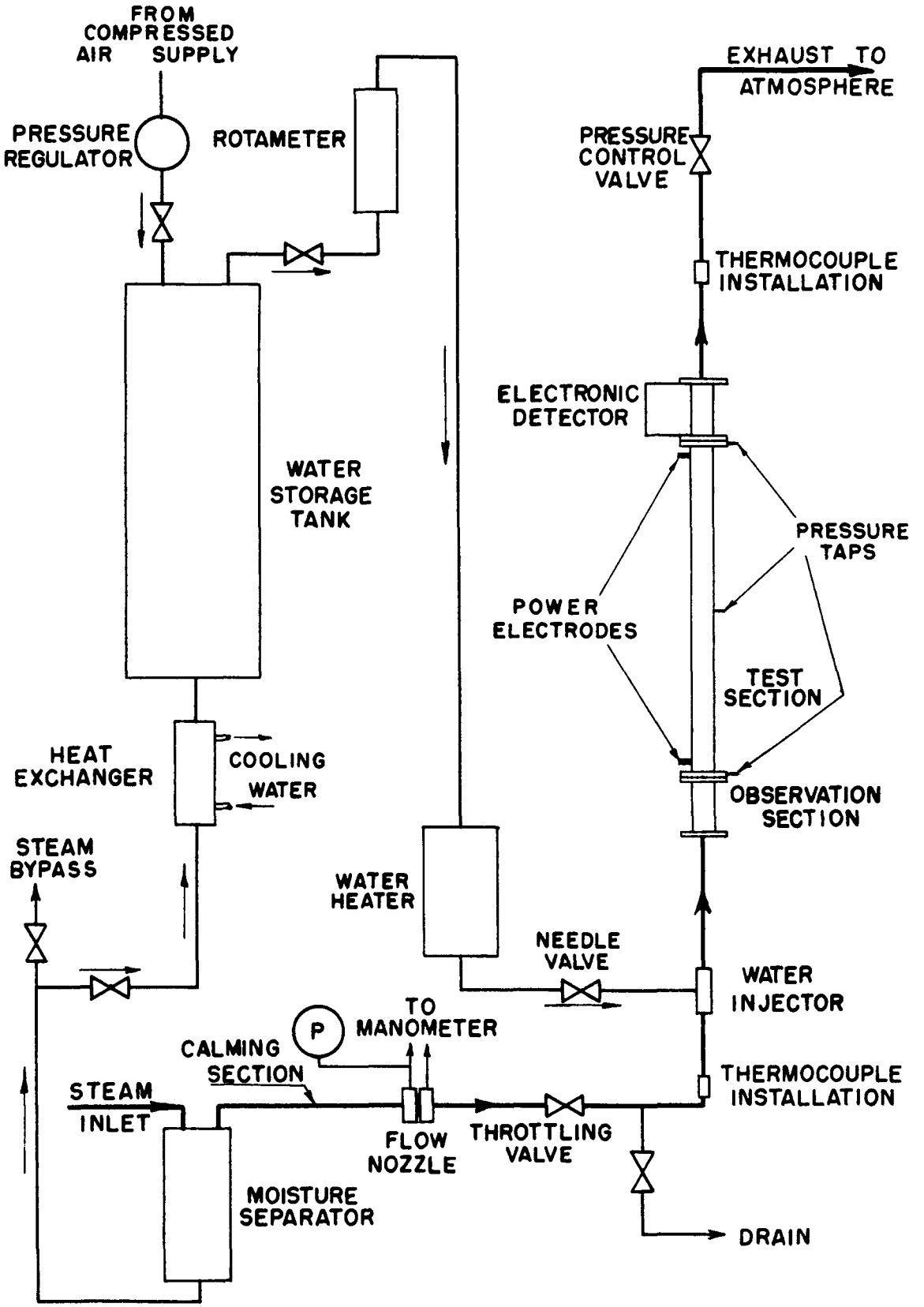

FIG. 18, SCHEMATIC DIAGRAM OF FLOW SYSTEM

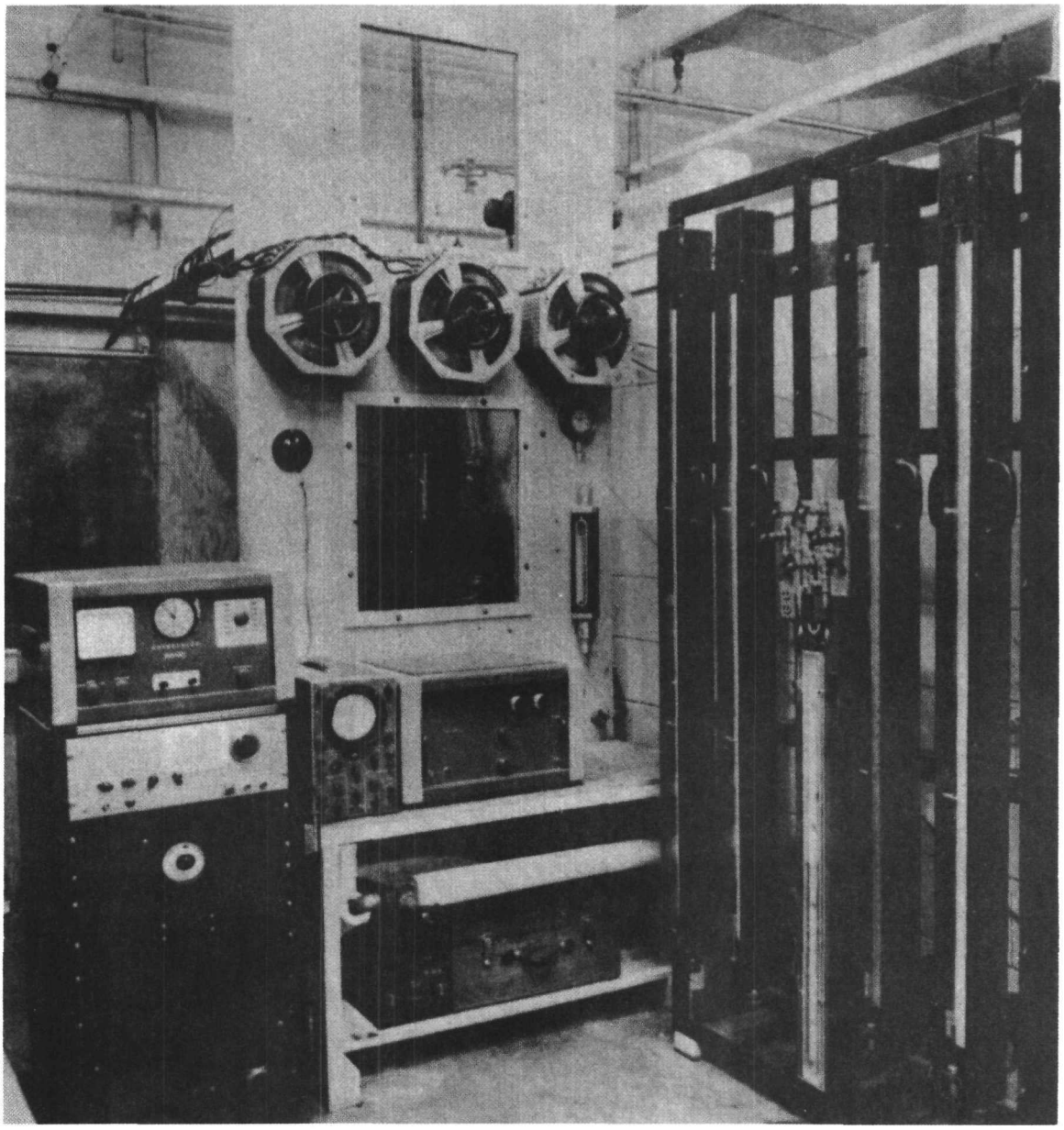

FIG. 19 MIST FLOW HEAT TRANSFER APPARATUS

and sufficiently high quality for accurate flow measurement. Throttling measurements showed that the quality of the steam leaving the separator was greater than ninety-eight percent. Steam flowing from the separator passed through a horizontal calming section of 100 pipe diameters before entering the measuring flow nozzle. The flow nozzle was a standard ASME long radius flow nozzle with an 0.5828 inch diameter throat manufactured by the Bailey Meter Company and installed in a Bailey flow nozzle pipe. The nozzle was calibrated with saturated steam at 150 psig by the manufacturer. Steam flow rates were calculated by means of the formula recommended by the ASME (22).

The static pressure at the entrance to the flow nozzle was measured by means of a Westinghouse Bourdon Tube gauge, 0-160 psig. The gauge was calibrated with a dead weight tester and found to have a constant error of minus one psi over the entire scale. This correction was applied to all readings taken with the gauge.

The pressure differential across the nozzle was measured by a U-tube manometer, using Meriam #3 fluid. This fluid, which has a specific gravity of 2.95, was convenient to use for the low differentials that had to be measured across the nozzle. Since water had to be used in the manometer lines to prevent condensation effects, fluids with specific gravity near 1.0 were too light to use as a manometer fluid. Mercury, on the other hand, was too heavy to permit accurate

measurement of the small differentials. A fluid of 2.95 gravity allowed accurate readings for flows of from 120 to 600 pounds per hour with a manometer 36 inches long.

Steam leaving the flow nozzle was throttled through a one-inch globe valve to approximately 30 psia. This pressure was maintained by the use of the globe valve downstream from the test section. By proper adjustment of the upstream and downstream valves the desired flow rate could be attained at the desired pressure. The value of 30 psia was used throughout all of the tests since it was found to be the lowest level of pressure that could be maintained in the test section at the higher flow rates. It was desired to maintain a constant pressure throughout all of the tests in order to eliminate one variable and to simplify property evaluations.

The temperature of the steam after throttling was measured by means of an iron-constantan thermocouple located in an installation at the elbow. Details of this installation are shown in Fig. 20. The installation was manufactured at Purdue, using the same spool of wire that was used in making the test section thermocouples. Calculation of the conduction effect of the steel tube showed it to be negligible.

At the elbow the steam was directed upward to the vertical test section located five feet downstream.

Water was injected into the steam between the thermocouple installation and the entrance to the test section. The injection was

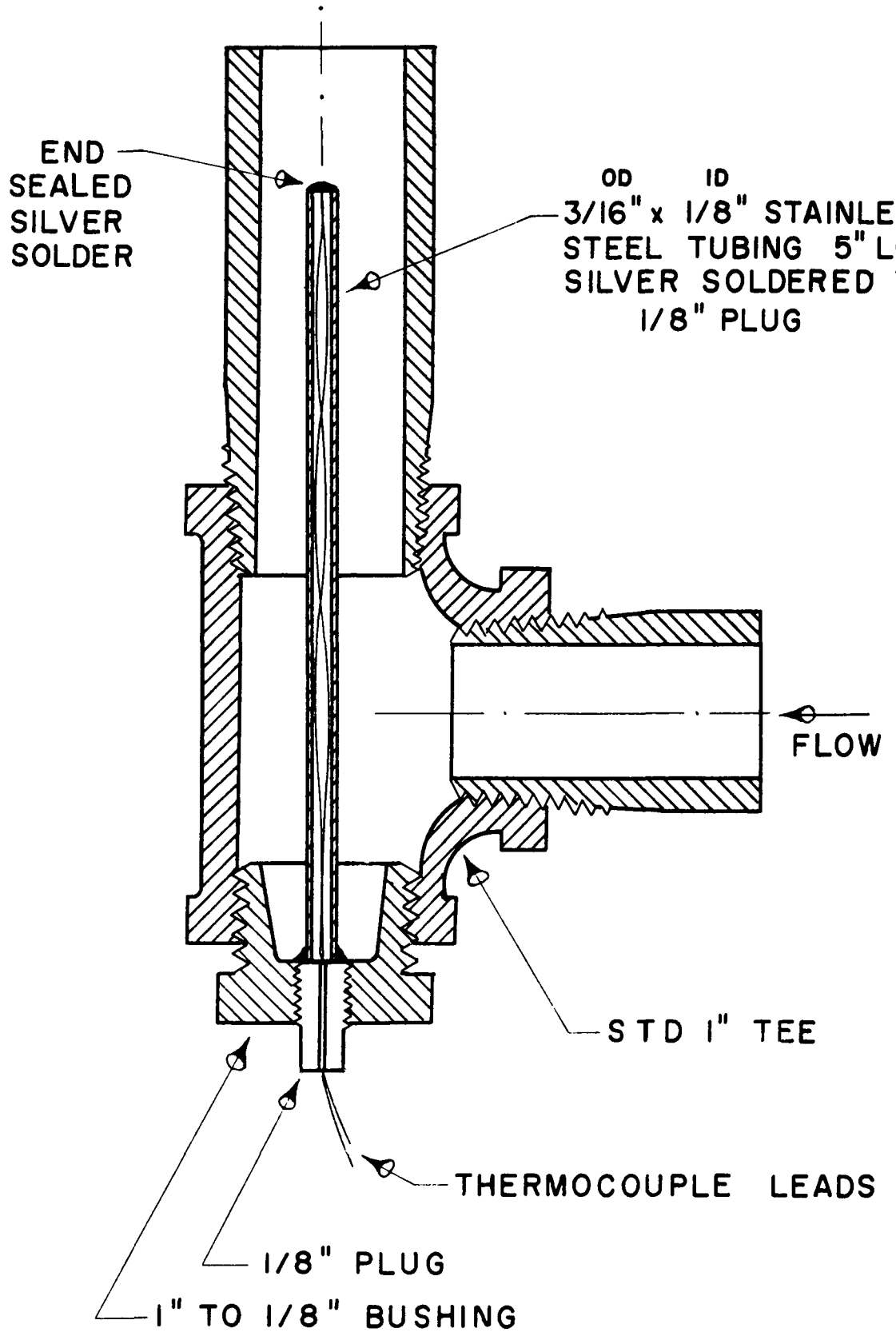

FIG.20 THERMOCOUPLE INSTALLATION

accomplished by means of the device shown in Fig. 21, with the water injected counter-current to the vapor stream. This type of injection system was found to give a fairly steady, uniformly dispersed spray at the entrance to the test section. Water for the injection was supplied from a 30-gallon tank kept at 60 psig by means of compressed air and a pressure regulating valve. This tank was necessary for two reasons. It was found that the pressure of the water lines in the laboratory was very erratic and would cause variations in the injection rate. Also, the water supplied in the water mains was very hard, containing impurities that could soon cause the heated test section to scale up. Water was supplied to the storage tank during shutdowns by the condensing of steam in the heat exchanger as shown in the schematic diagram. Measurements on the water taken from the storage tank showed the average electrical resistivity of 60,000 ohm-centimeters.

A water heater utilizing power furnished from a powerstat was installed to control the temperature of the injection water. The heater was constructed in a manner almost identical to that used in the test section which will be described later. A thermocouple installation similar to that shown in Fig. 20 was used to measure the temperature of the water at inlet to the injector. Because of the low rates of water injection that were eventually used in the runs, the accuracy of this temperature measurement was not critical in making energy balances.

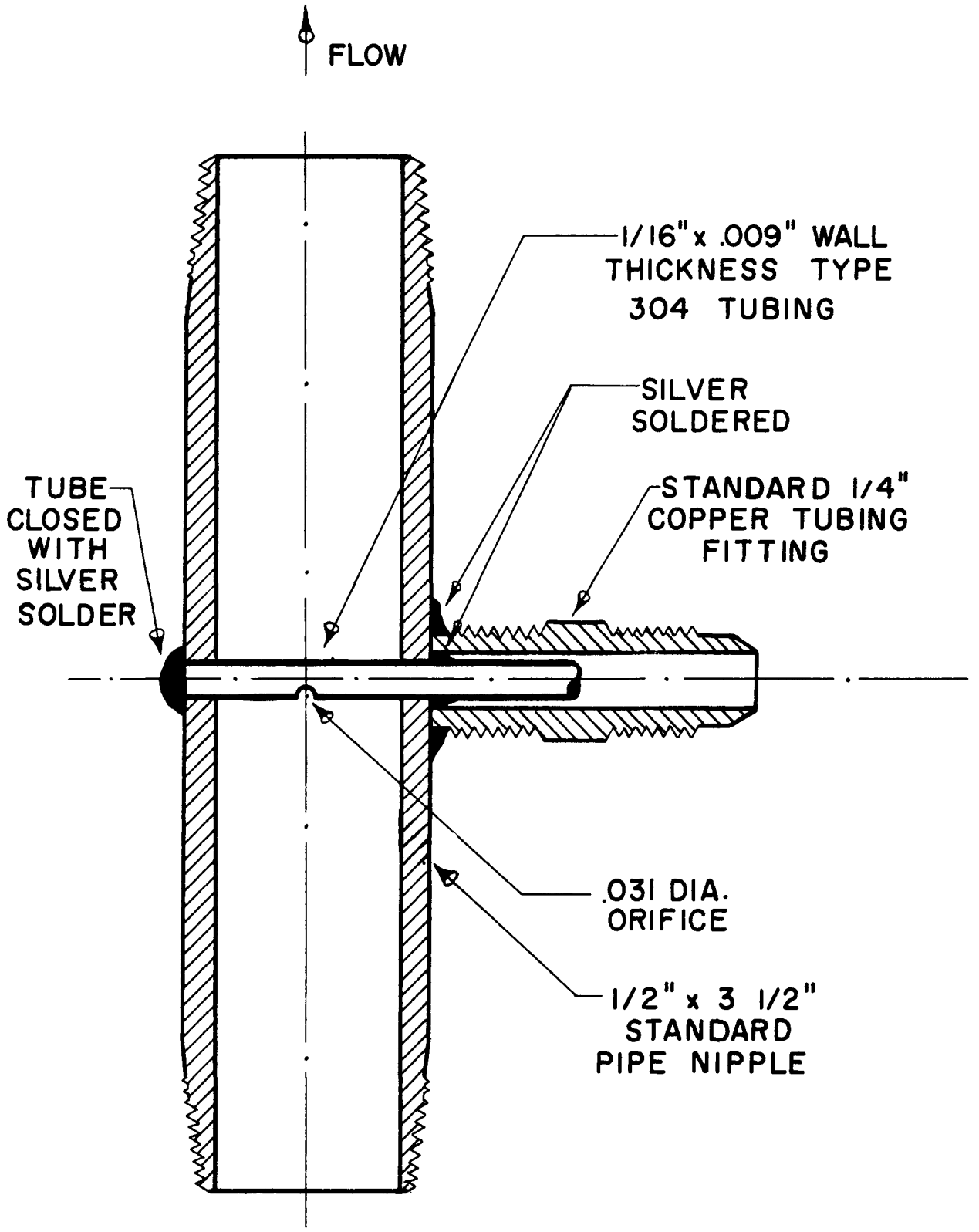

FIG. 21 WATER INJECTOR SECTION

The water supply system was found to be very satisfactory in regard to keeping the injection rate nearly constant. The injection rate was controlled by means of a 1/8 inch needle valve located downstream from the water heater.

The rate of injection of water was measured by means of a Fischer and Porter rotameter, located between the storage tank and the water heater. The rotameter was calibrated by weighing the quantity of water passing through it at the various readings in a measured period of time. The calibration curve for the rotameter is shown in Fig. 22.

In the earlier experimental runs the mist formed by the injection of the water into the steam was passed through a mixing chamber before entering the test section. This mixing chamber was installed in an effort to obtain a uniform mixture entering the test section. Details of the mixing chamber are shown in Fig. 23. It was found that this mixing chamber threw a large portion of the droplets onto the wall and gave a heavy annular film of liquid flowing into the test section. In later runs the mixing chamber was removed and it was found that less water was thrown to the wall. In place of the mixing section a glass observation section was installed to allow observation of the spray entering the test section. This observation section is shown in Fig. 24.

Details of the test section are shown in Fig. 25. It was constructed from a one-inch ID, type K, copper tube, having 1/16 inch

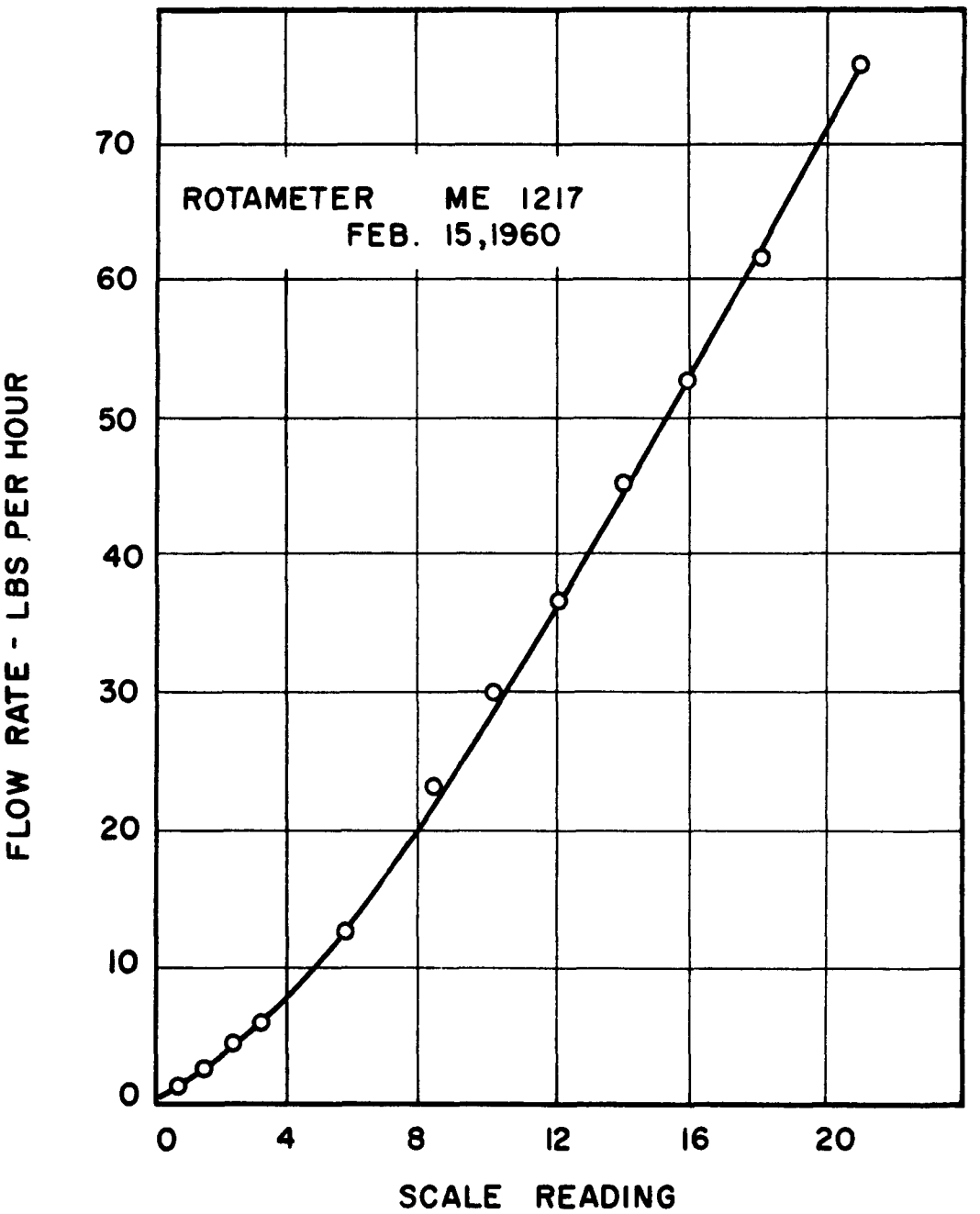

FIG.22 ROTAMETER CALIBRATION CURVE

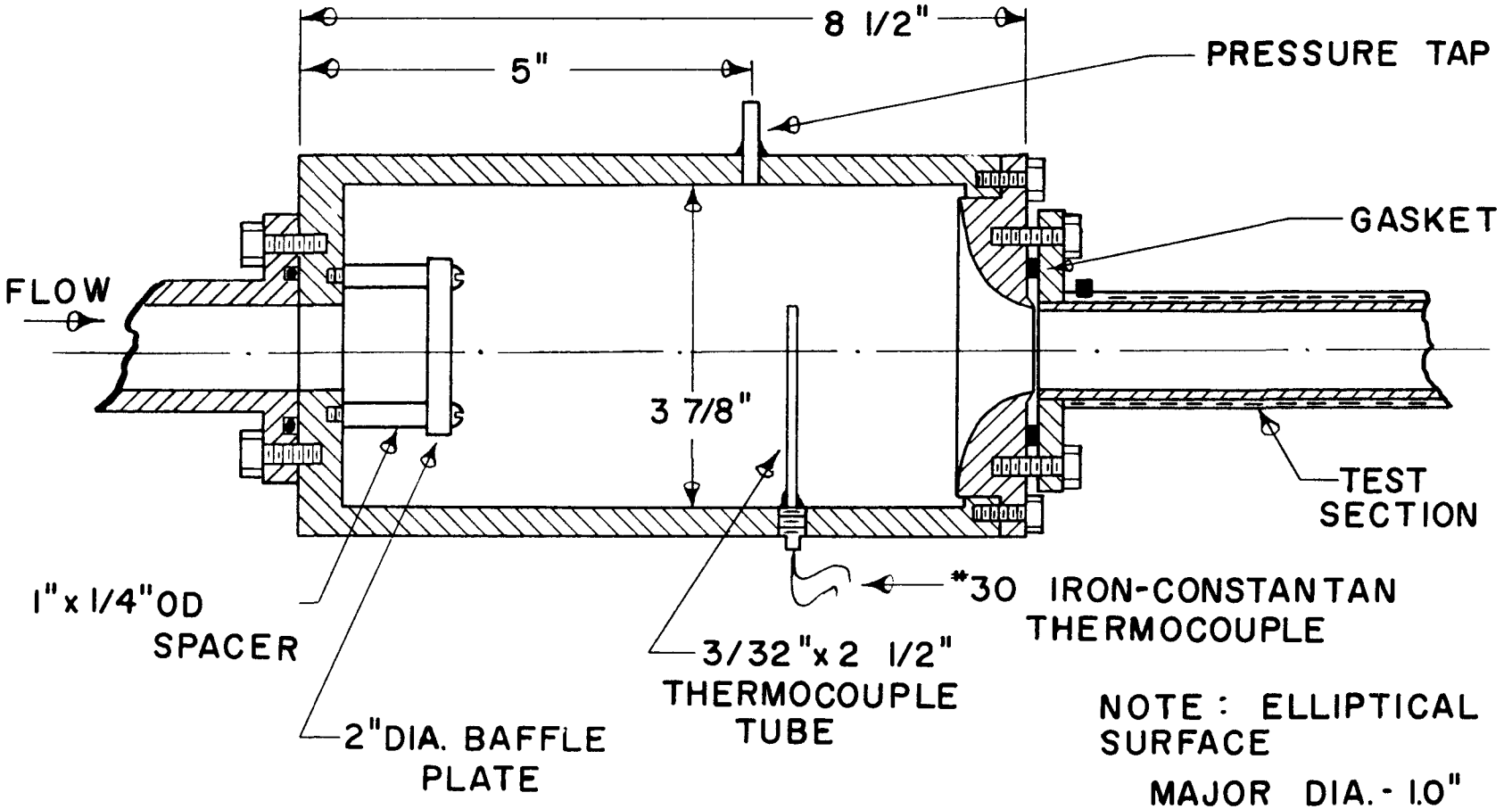

FIG. 23 MIXING CHAMBER

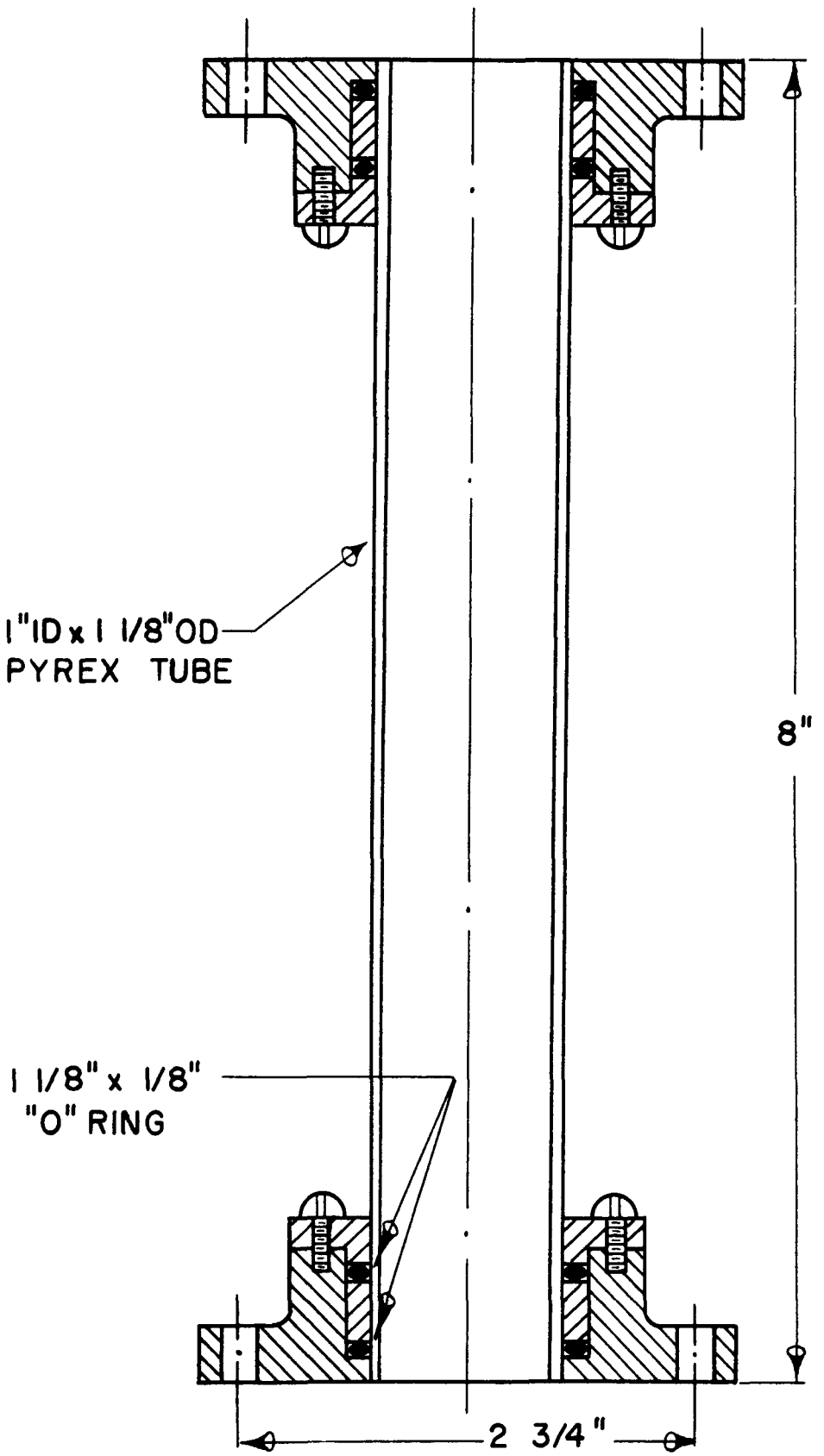

FIG. 24 GLASS OBSERVATION SECTION

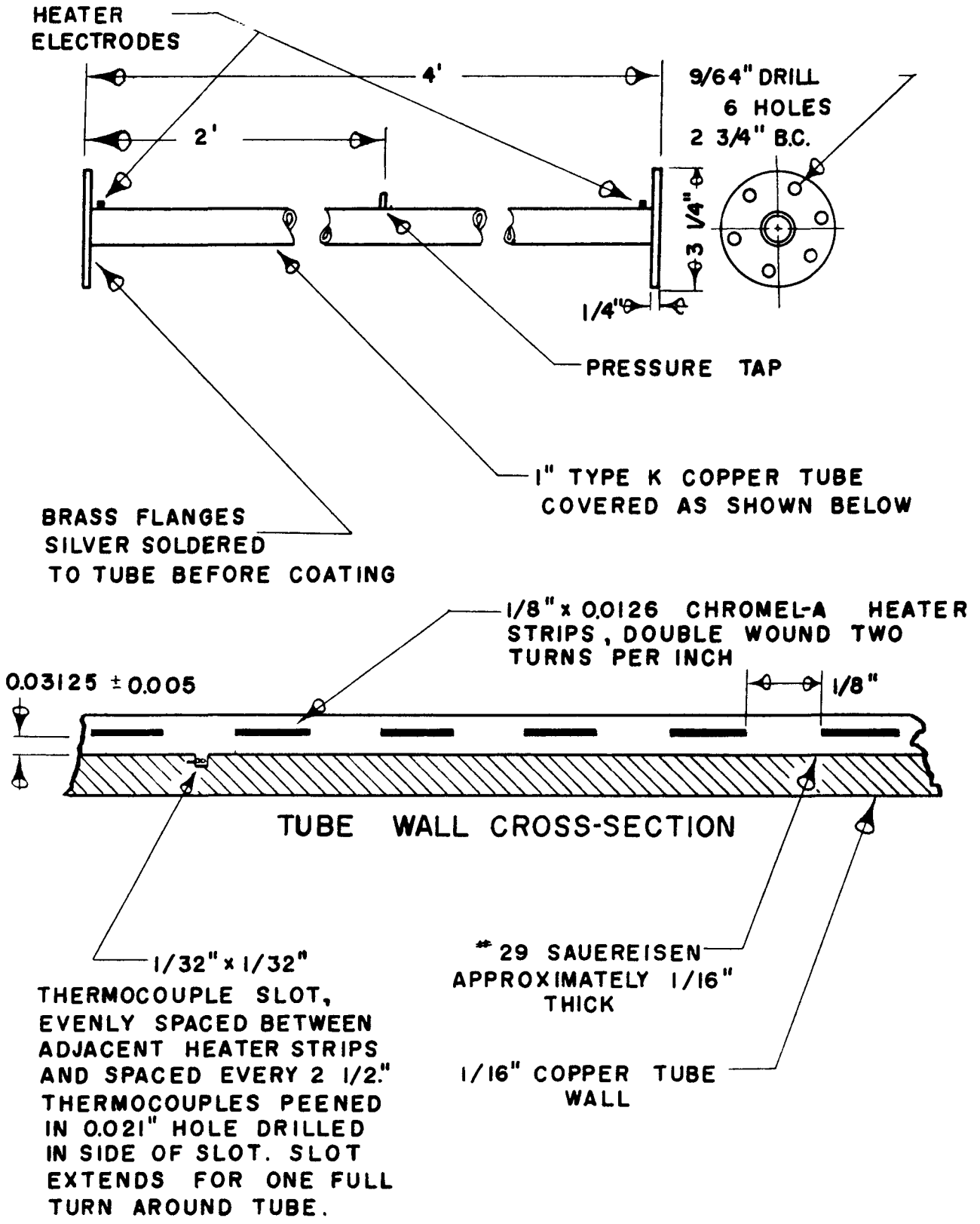

FIG. 25 TEST SECTION DETAIL

thick walls. After installation of flanges the four-foot-long tube was coated with several coats of type 29 Sauereisen Low Expansion Cement. This cement has the unusual characteristic of being a fairly good heat conductor but a poor electrical conductor. After coating, the test section was placed in a lathe and the Sauereisen was sanded down to a thickness of 1/32 plus or minus 0.005 inches. The test section was then wound with 1/8 by 0.0126 inch Chromel A heater ribbon. Two ribbons were wound around the tube in the same direction, each spaced two turns per inch for a total of approximately 96 turns for each ribbon. The ribbons were then joined by a copper strip at each end so as to place them in parallel with each other. The ribbon had a resistance of 0.344 ohms per foot. This arrangement gave a total resistance for the heater section of approximately five ohms, allowing the dissipation of nearly 10,000 watts at 220 volts.

Eighteen iron-constantan thermocouples were installed in the copper by peening between the heater strips as shown in Fig. 25. These #30 gauge, Leeds and Northrup glass-asbestos sheathed thermocouples were laid in grooves made in the copper tube wall at 2-1/2 inch intervals. This was done to prevent errors in temperature measurement caused by conduction along the thermocouple wires. Since the heat was being supplied from the outside, the Sauereisen was at a higher temperature than the copper tube. By installing the thermocouples in the grooves of the copper and by bringing them around the

tube one turn before bringing them out, the conduction errors were minimized.

After the installation of the thermocouples the test section was covered with several coats of the Sauereisen cement so as to cover the heater strips approximately 1/32 inch. This coating was necessary to maintain the even spacing between the heater ribbons, since the ribbons would expand upon heating and would become loose.

In designing the test section it was desirable to know whether the heating arrangement described above would give a near-constant heat flux on the inside of the tube. The 1/8 inch spacing between heater ribbons could conceivably cause variations in the heat flux along the tube length. Also there was the question of whether a thermocouple installed as shown in Fig. 25 would give a temperature reading very close to the temperature of the inside of the tube wall. To check both of these points, calculations were made from a solution to the Laplace equation. The derivations and calculations are shown in Appendix B. These calculations show that for the assumed values of the parameters the wall temperature variations are very small in the tube wall. For practical purposes the tube wall can be assumed to be operating at constant heat flux for regions where the inside film coefficient is not changing too rapidly. The point of location of the thermocouple was found to be at a temperature that differed from the average inner wall temperature by less than 0.2 degrees F.

The thermocouple wiring circuit is shown in Fig. 26. Because of the junctions of the thermocouple wire with the copper terminal strips, it was necessary to compensate for the thermocouple effect produced at that junction. This was done by placing the connections to the cold junction on the same terminal strip with the hot junction thermocouples. The terminal strips were placed between plates of copper, insulated with glass wool, and placed in a location away from sources of heat. This helped to maintain all of the junctions at the terminal strips at approximately the same temperature. Since the cold junction was wired opposite to the hot junctions, any emf produced in this isothermal region was cancelled out by an equal and opposite emf.

The thermocouple emfs were measured by means of a Leeds and Northrup Portable Precision Potentiometer.

Power for the test section heater was supplied through two powerstats, type 1256, manufactured by Superior Electric Company. The powerstats, wired in parallel, were connected to a 220 volt, 60 cycle power source. The power input to the test section was measured by means of a General Electric, type P-3, single-phase wattmeter. A factory calibration of the wattmeter showed it to have a maximum error of 10 watts over the entire scale. This correction was considered insignificant and was ignored in the calculations.

Pressure taps were located at the center of the test section and at the flanges at the entrance and exit to the test section. Care was

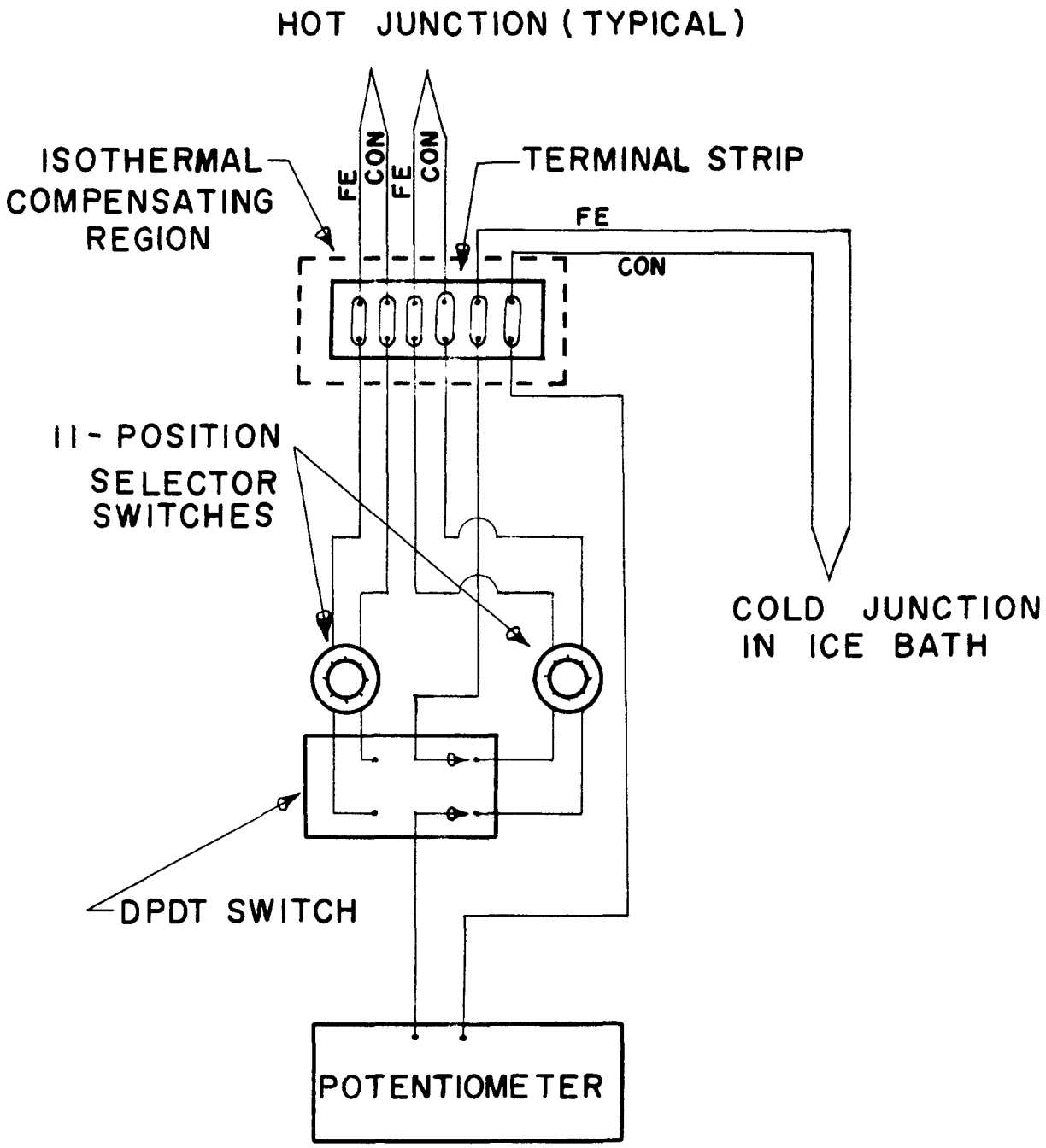

FIG. 26 THERMOCOUPLE WIRING CIRCUIT

taken to see that no obstructions protruded into the flow that would affect the measurement of the static pressure. Pressure drops in the test section were measured with the same manometer used with the flow nozzle for measuring steam flow rate. A valve system permitted the changing from one pressure measurement to another. Static pressures in the mixing chamber and at the center of the test section were measured by the use of Meriam reservoir-type, 60-inch manometers filled with mercury. These are shown in Fig. 19. All manometer lines had to be filled with water to avoid condensation effects in the lines. A constant water level was maintained over each manometer by the use of a reservoir located at the level of the particular pressure tap. These reservoirs were of sufficient capacity to allow changes in manometer fluid level without the lowering of the level in the reservoir to any significant extent. Excess water in any reservoir flowed back through the pressure tap and into the steam line.

A thermocouple installation was located 18 inches downstream from the exit to the test section. By placing the thermocouple far enough from the test section exit to allow mixing to occur, a temperature approximating the bulk temperature of the fluid was measured. Detail of the installation is shown in Fig. 27.

The vertical run of pipe containing the test section was hung from a bracket attached to a laboratory ceiling beam. Gravity was utilized to help maintain the vertical position of the test section

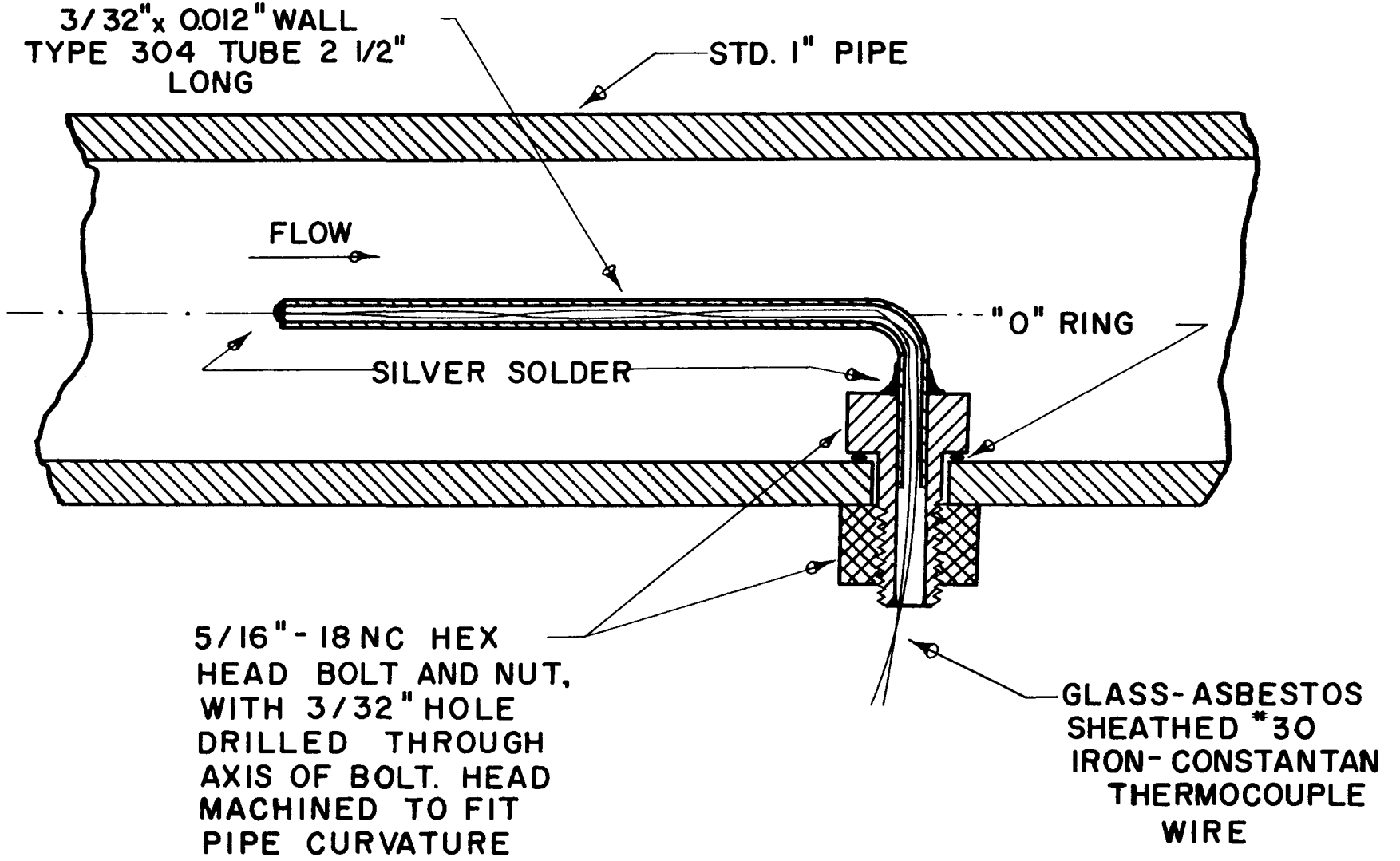

FIG. 27 EXIT THERMOCOUPLE INSTALLATION

and thermal expansion difficulties were avoided.

Because no condenser was available for use in the heat transfer laboratory, the steam was exhausted to the atmosphere. This was particularly undesirable because it did not allow the calculation of mass and energy balances as a check on the measurements.

A bypass system connected to the steam separator at the lower end permitted the flushing out of the steam mains and the separator prior to startup. The heat exchanger used for making condensate was connected to this bypass line. In addition, a line was provided at the base of the vertical run for draining the system.

The entire system, up to the first thermocouple installation, was insulated by standard, one-inch size, 85% magnesia pipe insulation. Downstream from this point the system was insulated with glass wool insulation approximately 1-1/2 inches thick. The glass wool insulation was covered with aluminum foil to reduce radiation losses.

Droplet Detection System

The second major part of the apparatus was built originally to determine the droplet spectrum of the mist flow. The system that was developed was found to be unsatisfactory in making quantitative measurements of droplet size in flowing systems. However, it does appear to be a useful instrument for the detection of entrained material and for monitoring sprays for uniformity and steadiness.

The system was a modification of the electronic spray analyzer developed for the DeVilbiss Company by York, et al (77), and described previously in the literature survey section. The DeVilbiss analyzer had been designed for use in open systems such as a spray nozzle in the open air. Therefore, the probe for this analyzer had to be re-designed for the detection of droplets flowing inside a tube. Detail of this probe is shown in Fig. 28. A block diagram of the entire analyzer is shown in Fig. 29.

The body of the probe was made of Teflon, a material which absorbs a negligible amount of water. In addition, Teflon has a surface resistivity, at 100 percent relative humidity, of 3.6×10^6 megohms, a dielectric constant of only 2.0, and a dielectric strength of 400-500 volts per millimeter. These characteristics made Teflon the best choice of all materials available, for a system operating at moderate temperatures.

The threaded Teflon joint of the probe and the probe wire were sealed with Armstrong A-1 Adhesive. The 0.020 inch ball at the tip of the probe was made by fusing the end of the nickel wire in an electric arc. Upon cooling, a small sphere usually formed at the end of the wire due to surface tension effects. After several trials a nearly perfect sphere of the desired size could usually be obtained. The sphere was checked for imperfections and the size was determined by

FIG. 28 SPRAY ANALYZER PROBE

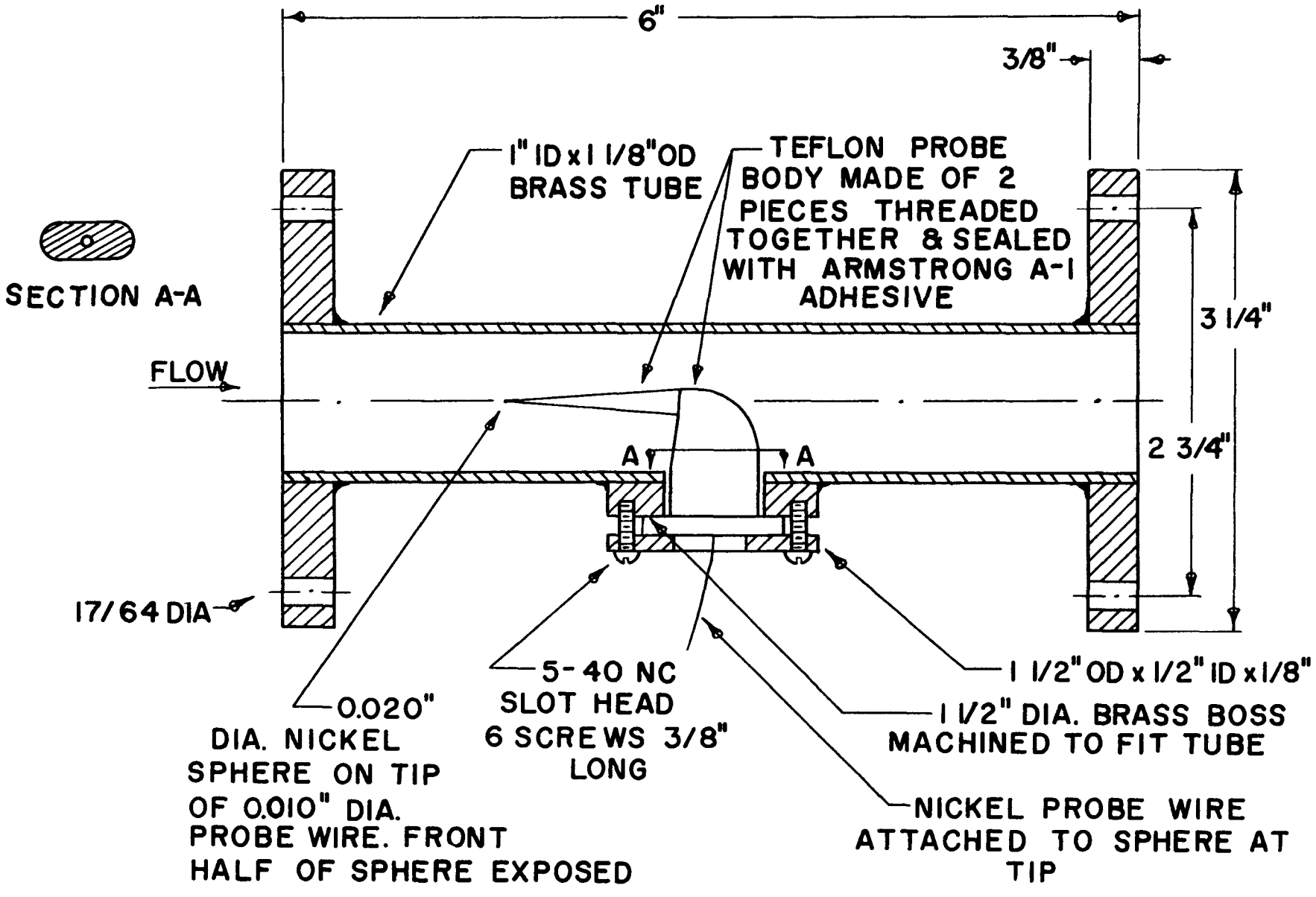

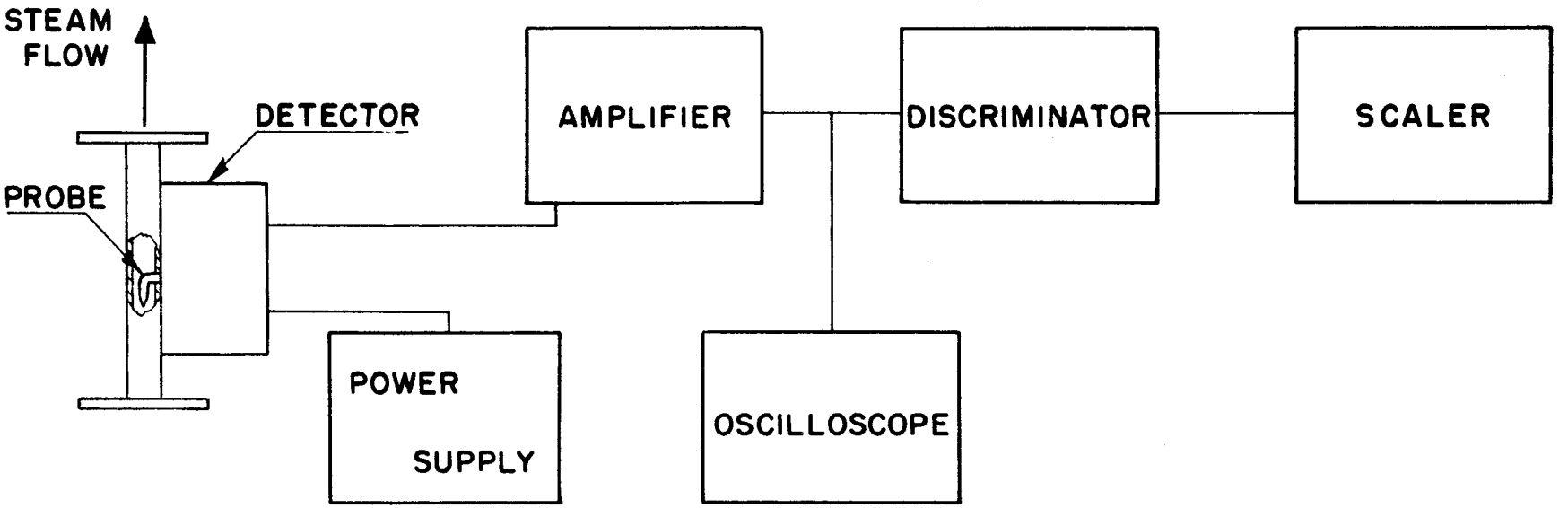

FIG. 29 BLOCK DIAGRAM OF ELECTRONIC SPRAY ANALYZER

the use of a 30x microscope. Both the nickel sphere and the Teflon were found to hold up well in the wet steam atmosphere.

The detector circuit had to be located near the probe to reduce the capacitance of its input. Practical considerations made it desirable to support the detector chassis and housing on the pipe through which the steam was flowing. However, it was found that the small vibrations of the pipe during flow were sufficient to cause noise in the circuit due to the vibration of the 6J6 on the detector chassis. The detector circuit was redesigned to use a 12AY7 tube which has good microphonic characteristics. The diagram of the detector circuit that was finally used in this investigation is shown in Fig. 30. This detector was found to have low microphonic noise characteristics even during high steam flow rates in the pipe. The amplification factor for the detector was measured with an audio oscillator and an oscilloscope and was found to be approximately 0.95.

The signal was transmitted from the detector through 16 feet of coaxial cable to a Tracerlab RLI-4 Pulse Height Analyzer. The Pulse Height Analyzer contained a linear amplifier with a maximum gain of 8,000 and a discriminator circuit. The discriminator was a type which permitted the passing of pulses having heights within a certain band range. By the selection of a certain threshold setting and a window setting, pulses above and below the desired size range were eliminated, and only the desired pulses were passed on to the scaler for

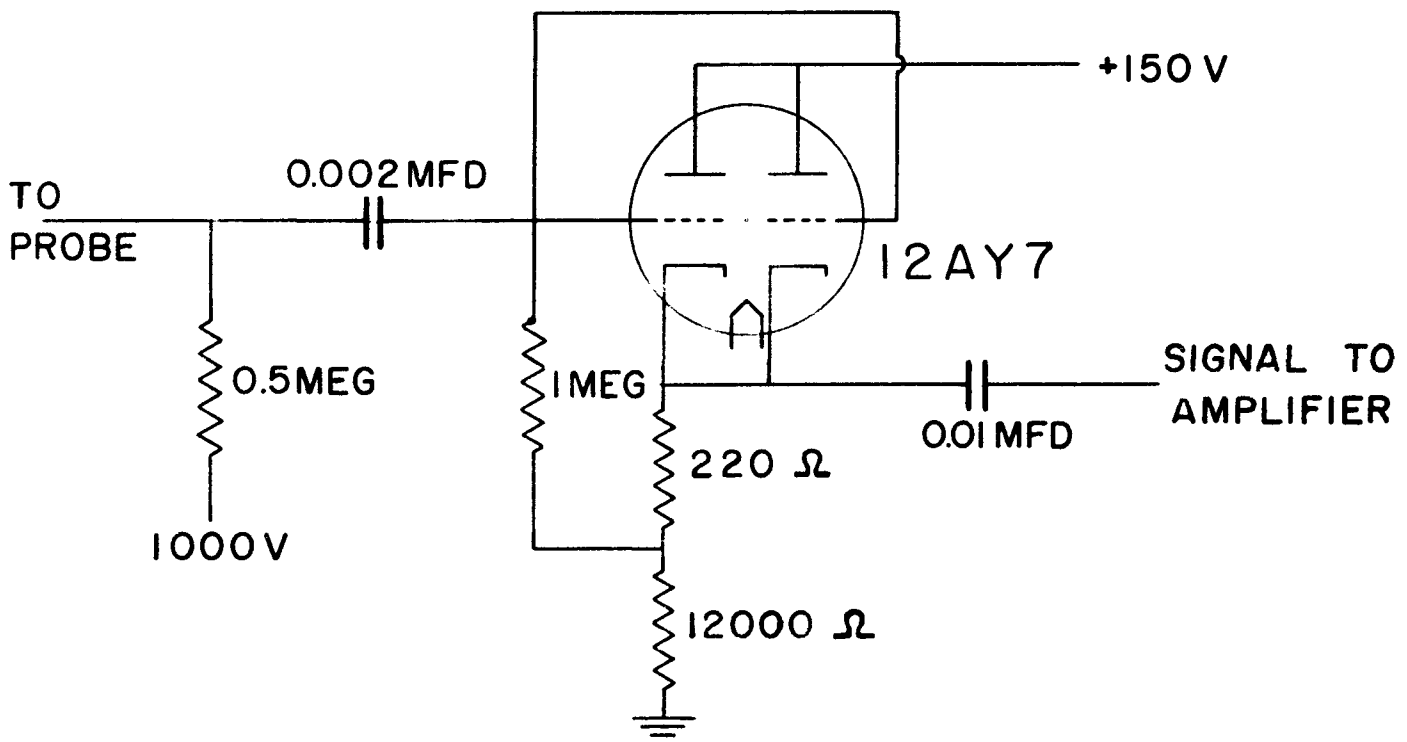

FIG.30 DETECTOR CIRCUIT

counting. The scaler was a Tracerlab Autoscaler with a built-in timer having a least count of 0.01 second. The scaler was connected to a Microflex Counter which increased its preset count capability to 1,638,400 counts. The 1,000 volt potential of the probe was supplied from the scaler power supply. The plate and heater currents for the detector were supplied by a separate standard power supply system built into the DeVilbiss apparatus and described in (77).

A droplet generating device was constructed to calibrate the spray analyzer, following a suggestion made in a personal correspondence from York. The device was similar to devices built by Slykhouse, et al (62), and Dimmock (17)(18). A photograph of the drop generator constructed is shown in Fig. 31.

The generator consisted of a glass tube, tapered to a capillary on which was fastened a small bit of iron wire. The tube was positioned so that the small iron wire winding was located close to the pole of a small electromagnet. Current of varying frequency and potential was supplied to the electromagnet from a Hewlett-Packard Type 200AB Audio Oscillator. Water from a reservoir was forced through the capillary by static pressure due to elevation. With the proper adjustment of frequency and potential the glass capillary could be made to vibrate, throwing droplets away from the tip in one or more steady streams. The drops of a particular stream could be caught in a small

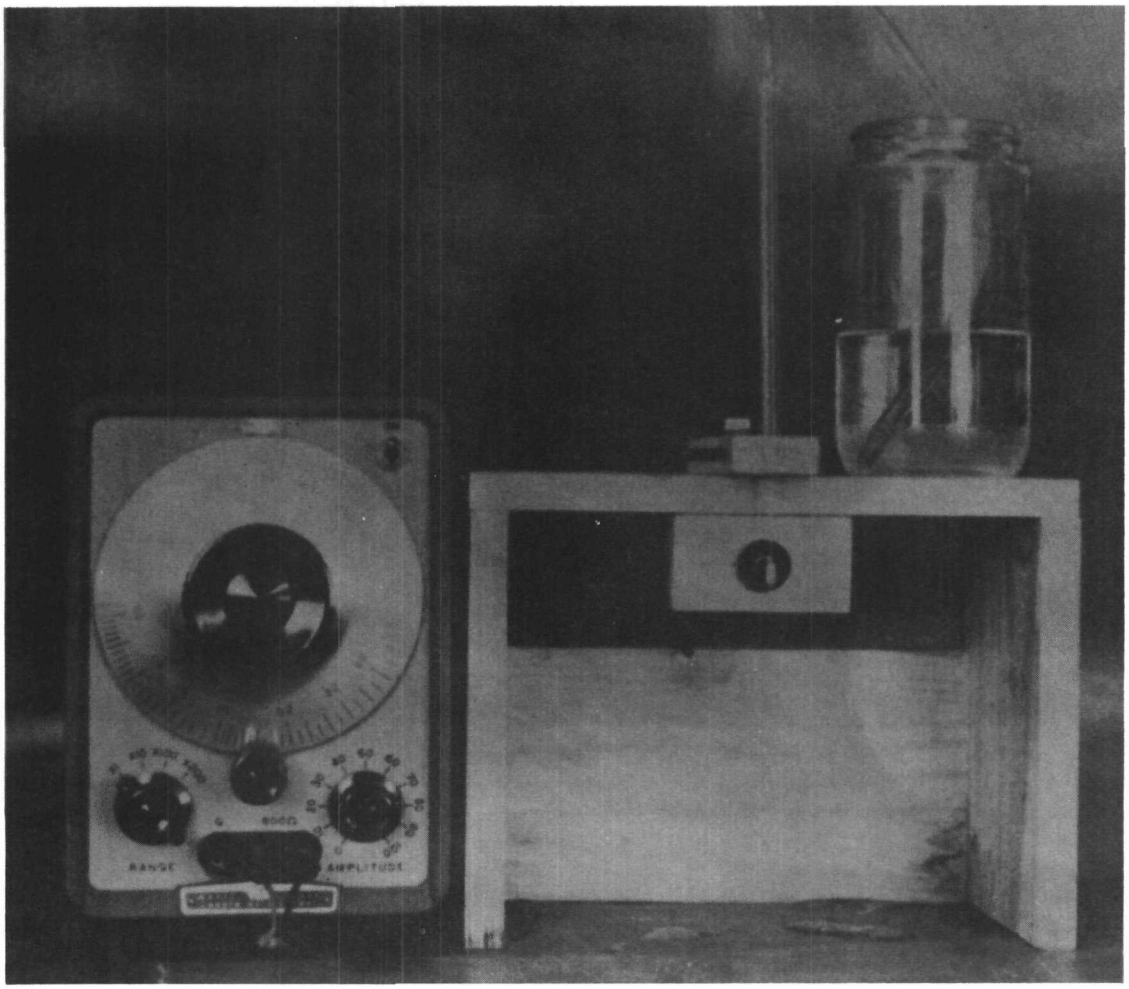

FIG. 31 DROP GENERATING APPARATUS

dish of motor oil and observed under a microscope having a graduated eyepiece.

It was found that the drops in each stream were of a uniform size and that this size could be maintained for long periods of time. The droplet size was determined by the size of the glass capillary, the elevation of the reservoir above the capillary tip, and the adjustment of the frequency and potential on the electromagnet. The frequency and potential adjustment of the audio oscillator determined the number of streams of drops that would come off at the tip and the direction of the streams. After a number of trials and changes, droplets as small as 50 microns and as large as 700 microns were produced in steady streams by the generator and observed with the microscope. Actually, streams of drops smaller than 50 microns were produced by the generator but could not be caught and observed due to their small terminal velocity and rapid evaporation rate.

Calibration of the probe with the drop generator was not easy, since it was very difficult to keep the tip of the probe in the stream of droplets produced by the generator. The streams of droplets, although constant in size, were very unsteady in position and tended to constantly wander. It was difficult to keep the droplets hitting the probe for a sufficiently long period of time to get a good "fix" with the discriminator settings. It appeared from the check points that were made that the analyzer had characteristics very similar to the

DeVilbiss analyzer, after correction for differences in amplification factors.

However, it was found during calibration that the droplets tended to collect on the probe tip, forming a large drop of water that periodically dropped off. It was noted that a large pulse was produced as this drop fell free from the probe tip. Also this liquid that collected on the probe tip seemed to have some effect on the size of the pulse produced by a given size droplet. It was decided to attempt blowing the drops produced by the generator onto the probe tip with a high velocity air stream from a small hose. It was thought that this would keep the probe dry and that the calibration would be more consistent.

It was found that pulses two to four times as great as before were produced with given size drops when the air stream was used. The results seemed to be erratic and difficult to reproduce. Some pulses were found to occur when the droplets hit the probe body near the tip. It was also noted that very large drops passing close to the probe tip caused pulses to occur even though no contact had been made between the drop and the metal sphere. It was at this time that concern developed over the possible effect of droplet spreading or breakup after impact, and over the effect of near misses and impacts on the probe body.

A Tektronix Type 543 Oscilloscope and a Dumont Oscillograph Record Camera were obtained in order to study the pulses produced

by the analyzer when operating with a flowing steam system. Pulses of three general types were found to occur. These are illustrated in Fig. 32.

The pulse shown in (A) is similar in shape to those pulses obtained with the drop generator when the droplets were impacting on the probe tip without blowing. This pulse has the same general shape as the pulses described by York, et al (77) and obtained with the DeVilbiss analyzer. It is also the shape that would be expected from theoretical considerations, ignoring any effect that the droplet might have on the probe potential after the initial effect. Pulses of similar shape were also obtained by blowing metal particles onto the probe by the air stream. It was thought that these pulses were from drops striking the probe at such an angle or position as to not cause breakup or spreading of the drop over the probe tip.

The second type of pulse is shown in (B). These pulses have a slower rise time and much longer decay time than the pulses described in (A). This type of pulse seemed to be the most common found in the photographs. Because the length of the pulses seemed to vary with velocity and because some pulses similar to these were obtained with blowing metal particles, it was thought that this type might be due to near misses or possibly due to contact of the particle with the probe body.

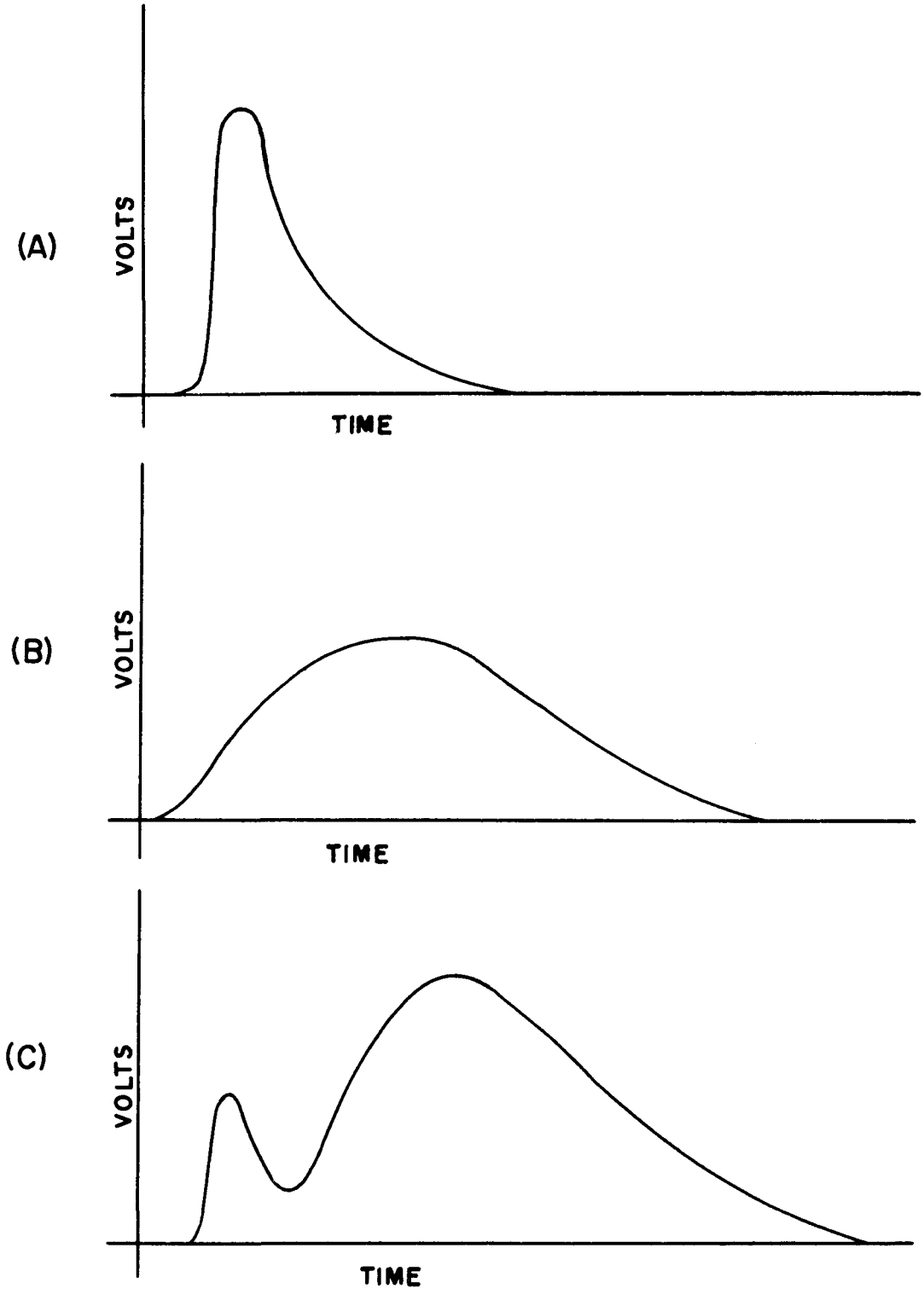

FIG. 32 TYPES OF PULSES OBTAINED WITH SPRAY ANALYZER

The third type of pulse is shown in (C) of Fig. 32. The initial part of the pulse is similar in shape to that described in (A), but a large "tail" follows the initial rise and decay. The ratio of the height of the first pulse to the height of its tail is variable, but generally the tail has much the greater height. The length of the tail seemed to be variable with velocity, but the general shape of the initial pulse (if extended to the axis) did not seem to vary. It was concluded that the initial pulse was caused by droplet contact with the probe and the tail was caused by some kind of spreading or breaking action of the droplet. This was given some substantiation by the fact that no pulses of this type were photographed when metal particles were blown past the probe.

Spectrum analysis of the pulses produced in the steam-water flow showed that a single maximum existed in the counting rates over the various discriminator settings. The counting rate dropped off for settings above and below this point. However, the general shape of the spectrum curve could not be reproduced at different gain settings of the amplifier. This suggested that the discriminator circuit was incapable of determining the maxima of the pulses due to their varying shapes and rise times. No apparent relationship seemed to exist between the measured spectrum curves and the droplet spectrum curves that were thought to exist in the flow. It was concluded therefore that the apparatus was not satisfactory for use in making quantitative

measurements of droplets in its present design. However, it appears to be a useful device for the detection of droplets that may be present in a stream of gas or vapor. A new probe geometry would probably be needed to avoid the difficulties described above.

One of the difficulties that would be encountered in the design of a new probe geometry is the necessity for making a probe with a small collection area. This is evident if one makes a few simple calculations from the data presented in the table below. The table shows the number of drops present per cubic foot of volume for various qualities of steam at 30 psia and for various mass mean drop diameters. Multiplying the proper number in the table by the collection area of the probe and by the velocity of the flow gives the number of drops striking the collection area per unit time.

TABLE 3

Number of Droplets per Cubic Foot in Steam at 30 psia

Mean Mass Diameter (microns)	Quality			
	.95	.90	.85	.80
20	4.418×10^{8}	9.30×10^{8}	1.482×10^{9}	2.099×10^{9}
40	5.535×10^{7}	1.168×10^{8}	1.859×10^{8}	2.62×10^{8}
60	1.632×10^{7}	3.44×10^{7}	5.48×10^{7}	7.76×10^{7}
80	6.90×10^{6}	1.457×10^{7}	2.32×10^{7}	3.279×10^{7}
100	3.525×10^{6}	7.45×10^{6}	1.184×10^{7}	1.674×10^{7}
200	4.415×10^{5}	9.32×10^{5}	1.1481×10^{6}	2.093×10^{6}

Since most electronic scaling systems are limited in counting rates to a few thousand counts per second, it is evident that the probe collection area must be very small, especially for high velocities and low qualities and fine mists.

A general equation was derived to permit calculation of the number of drops per unit volume in a liquid-vapor mixture for any pressure, mean drop size, and quality. The equation is

$$N = \frac{1.91}{\left[\left(\frac{X}{1 - X}\right) \frac{\rho_L}{\rho_g} + 1\right] d^3} .$$

This shows that for a given quality and mean drop size, the number of drops per unit volume depends only on the ratio of the density of the two phases. Near the critical point, where the density of the two phases is nearly the same, the number of drops per unit volume becomes tremendous. In addition, the effect of reduced liquid surface tension at higher temperatures would usually cause mists to be much finer (have a smaller mean drop size) near the critical point. This places a severe design requirement on any type of spray analyzer for use at high pressures.

METHOD OF TESTING

In selecting the method for obtaining the data, it was necessary to consider the characteristic unsteadiness of the system. At times during certain preliminary runs it was noted that the pressure of the inlet steam varied over a period of time. This, of course, resulted in variations in the steam flow rate which led to variations in most of the instrument readings. Ideally, an instrumentation system was needed that would record all readings simultaneously. Since such a system was not available for this project, a method was needed to permit recording of the desired data as rapidly as possible and allow some check against changes that might occur during the recording. It was also necessary to assure that equilibrium had been attained in the system after starting and before data was recorded. This section describes the method that was used to meet these requirements as closely as possible.

Before the starting of each set of runs the barometer was read and its reading recorded. Air was bled from all of the manometer lines and the manometer used to measure the static pressure of the test section was set at a reference position.

Crushed ice was placed in the flask containing the thermocouple cold junction, and the potentiometer was balanced with the standard cell.

The electronic equipment connected with the spray analyzer was turned on and allowed to warm up for at least 30 minutes before being used.

Before admitting steam into the apparatus it was necessary to flush out the water that had accumulated in the steam lines. This was accomplished by opening the steam bypass line at the base of the separator and the drain valve at the base of the vertical run. After most of the water had been cleared from the lines, the drain valve was closed and the throttling valve was opened, permitting steam to pass through the test section. The bypass valve was left open to permit the removal of moisture from the steam separator during operation.

The throttling valve was set to give the desired flow rate of steam through the test section. The pressure in the water supply tank was adjusted to 60 psig by opening the air valve and setting the air pressure regulator. The water injection valve was then opened and set at a position to give the desired water flow rate. The water and steam flow rates were always set simultaneously so as to give a total flow rate of 200, 300, or 400 pounds per hour.

After the steam and water flow rates had been adjusted to desired values, the downstream valve was set so as to make the pressure

at the center tap of the test section as near to 30 psia (61.1 inches Hg absolute) as possible. This was usually accomplished to within $\pm$ 0.5 inches of mercury.

Electric power was then turned on at the main switchbox and the Variacs were adjusted to give the desired power input to the test section. The thermocouples at various positions along the test section were checked with the potentiometer to make sure that there was no local overheating from that particular power setting.

One thermocouple in the test section and the inlet steam thermocouple were checked every five minutes until there was no significant change observed between checks. Then before the thermocouple readings were recorded, the static pressure, steam and water flow rates, and the power setting were checked to make sure that they were at the desired values. After all temperatures had been recorded, checks were made of some of the test section temperatures and the inlet steam temperature to see if they had changed significantly during the time required to record the temperatures. If any temperature had changed significantly, that set of readings was discarded and a new set of readings was taken. The flow rates, pressure, and power input were read after the temperatures had been recorded. If they had not changed significantly from the initial readings, they were recorded on the data sheet. If they had changed, the data for that run were discarded.

A fixed-window and threshold setting was maintained on the discriminator of the spray analyzer for all runs. The time for a count of 4,096 was recorded each run.

After a satisfactory set of readings had been obtained, the pressure drop measurements were taken for that run. In many of the runs the manometer fluctuated significantly during pressure drop measurements, and average readings were recorded. Average readings were obtained by averaging the maximum and minimum values observed over a period of approximately one minute.

In most cases the flow rates were left at the initial settings and the power input to the test section was varied for the next run. After changing the power setting the thermocouples were again checked at five minute intervals and recordings were taken only after steady state appeared to have been attained.

The apparatus was shut down by first turning the Variacs to zero and then turning the throttle valve and water injection valve off.

The static pressure manometer was checked to see if it returned to the reference level set at the beginning of the runs. If it did not, the data sheets for those runs were discarded.

EXPERIMENTAL RESULTS

Mist Flow

Data of the runs that were considered acceptable are tabulated in Appendix C. Runs that are considered to be typical of the data are presented as curves in this section to facilitate the discussion of the results.

Figure 33 shows the temperature variation of the wall for superheated steam flowing through the test section. As theory predicts, the temperature difference is lowest at the start of heating and eventually levels off to a near constant value. The decrease in temperature near the exit is due to conduction losses at the flange. The heat transfer coefficient reaches a minimum of about 56.0 Btu/hr square foot at thermocouple number 16, which is located 40 inches from the test section inlet. This compares with a value of 58.8 predicted by the Colburn (9) equation:

$$\frac{h}{C_p G_g} = 0.023 \left(\frac{\mu_v}{DG}\right)^{0.2} N_{PR}^{\frac{2}{3}} \qquad (17)$$

where the properties, except C_p, are evaluated at the average film temperature:

$$T_f = 0.5 \left(T_w + T_B \right) \quad . \qquad (18)$$

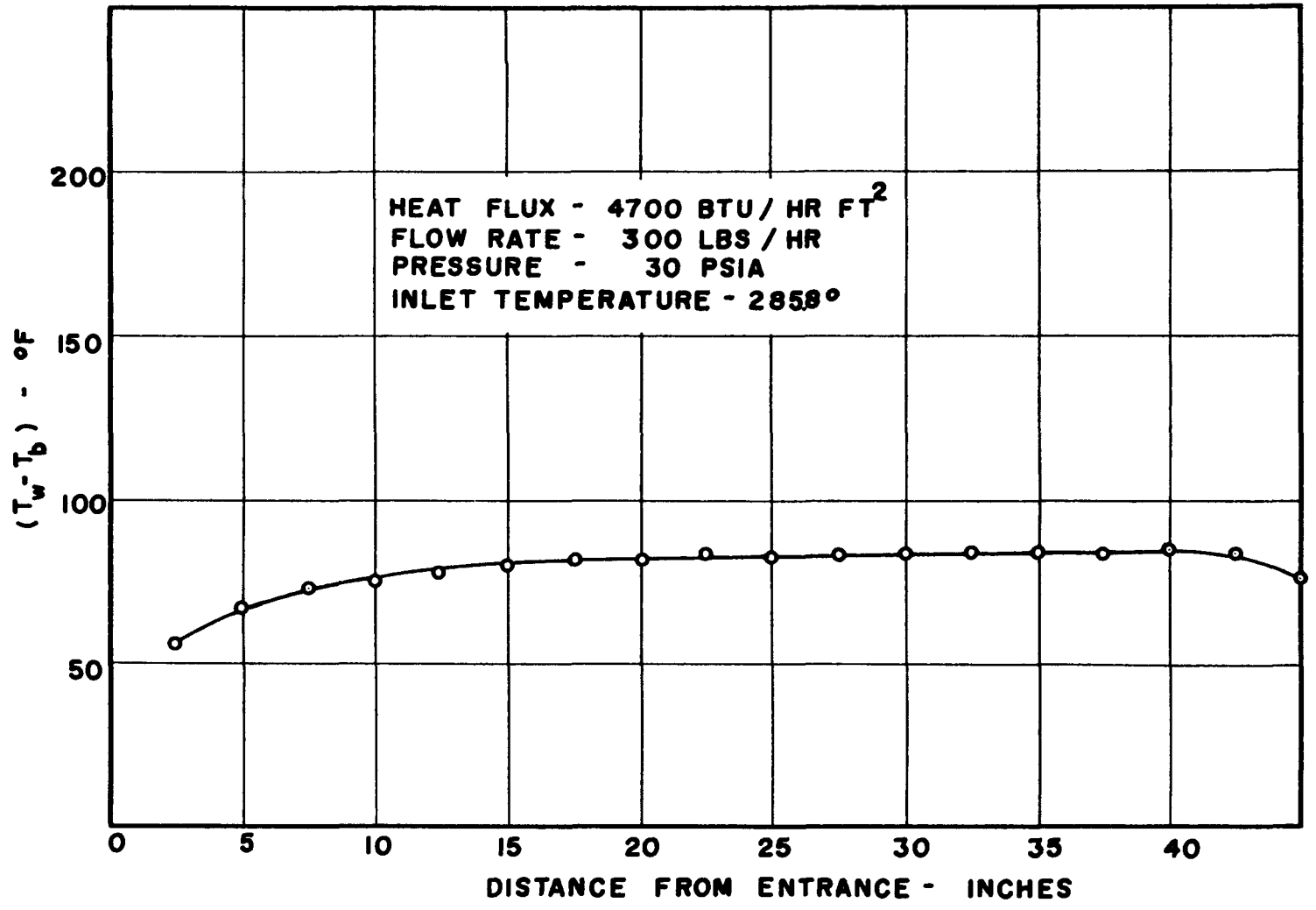

FIG. 33 WALL TEMPERATURE VARIATION FOR SUPERHEATED STEAM

This deviation of approximately five percent from the Colburn equation indicates the general reliability of the measurements taken with the apparatus. However at such low values of heat transfer coefficients, the amount of thermal resistance due to scale in the tube would not be apparent. That is, any small amount of scale present in the tube would not significantly affect the measured values of heat transfer coefficient, provided the coefficients were relatively small compared to the scale coefficients. In the region of annular liquid flow, however, which occurs in some runs, the heat transfer coefficients are large and a small amount of scaling can significantly affect the values obtained.

The tube had been cleaned with a weak acid solution prior to the taking of data and only water that had been condensed from steam was injected into the stream. It was felt therefore that the scale formation in the tube was probably small. Since large coefficients were obtained in some of the runs, however, it was desirable to check the amount of scaling that had occurred. This was accomplished by using a modification of the Wilson method (72). Water was introduced into the system at the separator and passed through the flow manometer, up the test section and out the exhaust through tubing to a drain. A constant heat flux of 8,020 Btu/hr square foot was applied at the test section. The flow rate of the water was varied for nine different runs and wall temperatures and inlet and outlet temperatures were recorded for each of the runs. The averages of the temperature differences $(T_W - T_B)$ for

the ten center thermocouples of the test section were plotted versus the respective manometer readings on log-log paper. This gave a series of points that fell very near to a straight line having a slope of -0.435. The data were then transferred to rectangular coordinate paper with the temperature differences plotted against the manometer readings raised to the -0.435 power. The points again fell very near to a straight line. A line was drawn through the points using the method of least squares. This gave an intercept with the temperature axis of -0.14 degrees F. A study of the method of obtaining the slope on the log-log paper and the round-off errors involved in the least squares method indicated that a maximum deviation of approximately 0.5 degrees F was possible. It was concluded that the value of the scale coefficient was sufficiently high to be insignificant for most of the runs. In the discussion of the results which follows the effect of scale will be ignored unless mentioned for a particular run.

Figure 34 shows the wall temperature variation that was obtained with an annular-mist flow. In most of the runs that have been tabulated the annular film of liquid film is present at the entrance of the test section. This is apparent in Fig. 34, as the wall temperature is very near the saturation temperature up to about the midpoint of the tube. At that point the liquid film apparently disappears and a true mist type flow commences. In this run heat transfer coefficients of approximately 200 Btu/hr square foot F are observed for the mist flow region,

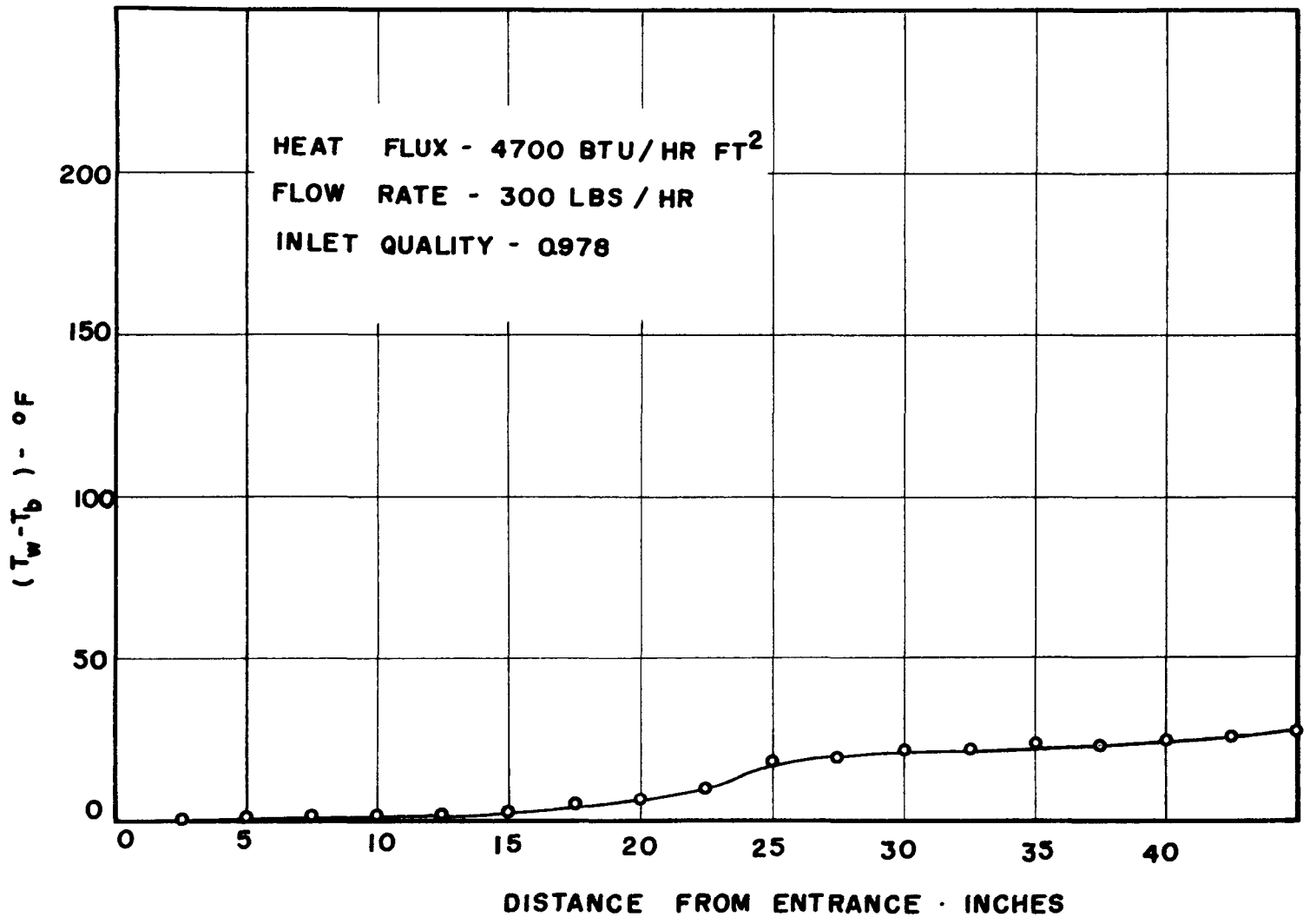

FIG. 34 WALL TEMP. VARIATION FOR ANNULAR-MIST FLOW

compared to coefficients of approximately 5,000 in the annular region. This shows the tremendous effect of the liquid film on the value of the heat transfer coefficient.

Figure 35 shows a wall temperature variation for an annular-mist flow in which the spheroidal state has evidently set in near the exit of the tube. The flow seems to pass sharply from an annular flow to a mist flow with droplet cooling, and then to a flow where the drops seem to have little cooling effect on the wall. Notice the similarity between the curve of the proposed model, Fig. 17, and the curve representing the data, Fig. 35.

The curves shown in Figs. 34 and 35, which are typical of much of the data that was taken, indicate a slight discrepancy with the proposed model. The model predicts an almost linear change of wall temperature from the saturation value to the dry steam value. If the experimental data of Fig. 34 were extrapolated linearly, a temperature corresponding to dry steam would not be attained at the point where the quality is calculated to be 100 percent. This is also observed in Fig. 35, where extension of the "shelf" by a straight line to higher qualities would not reach sufficiently high temperatures at the point of 100 percent quality.

The flatness of the curve in both Figures indicates that the assumption of a constant value of mass transfer coefficient may be incorrect. The arguments given by Vanderwater that transfer of droplets is

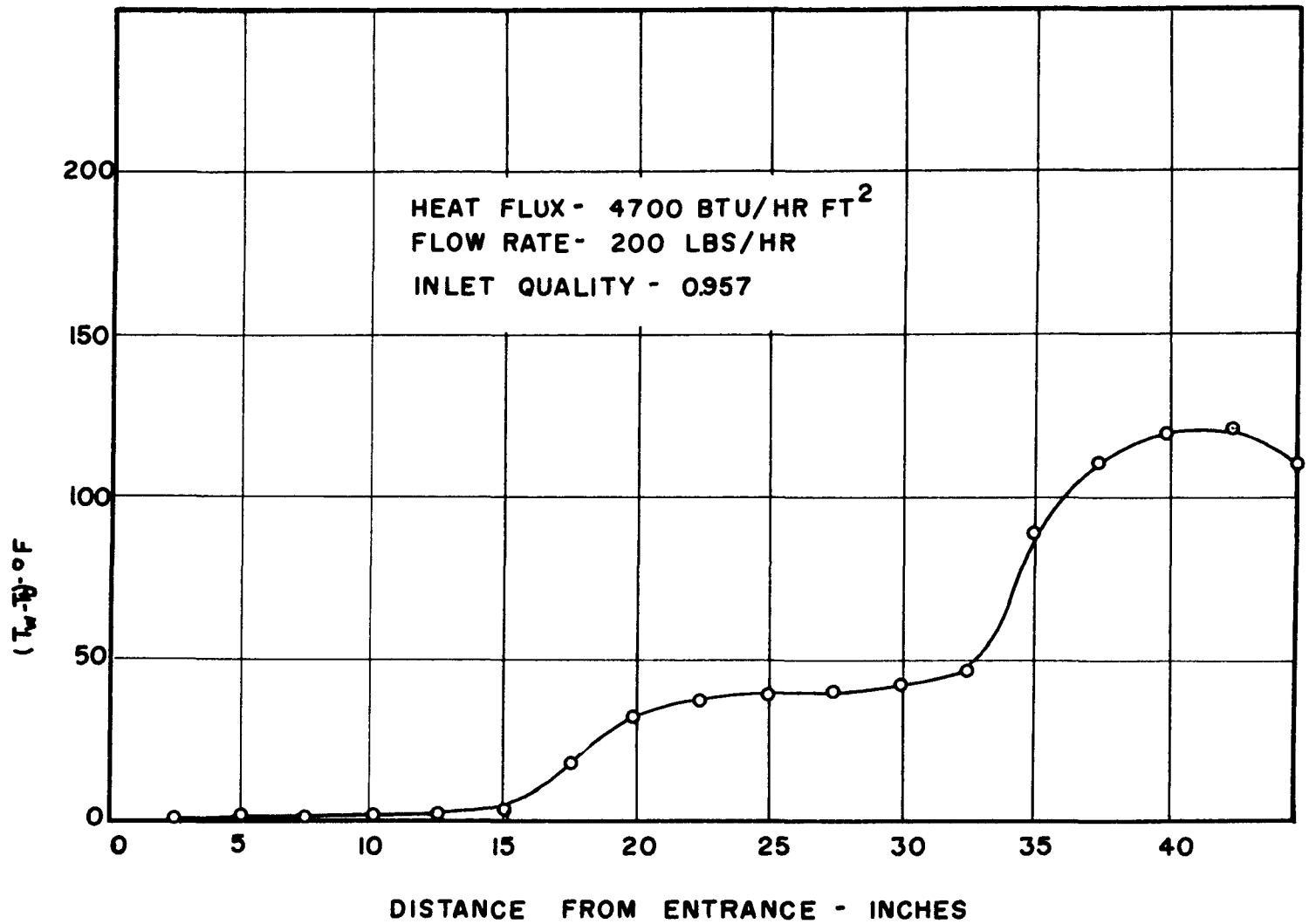

FIG. 35 WALL TEMPERATURE VARIATION FOR ANNULAR-MIST FLOW

hindered by evaporation at the wall seem logical and would indicate that k_d should not be considered constant. Droplet depletion with increasing quality would cause a decreasing amount of new vapor formation at the wall and this in turn should lead to higher values of k_d with length. This could be an explanation for the flattening out of the curves. The complexity of the droplet diffusion process (in addition to an effect which will be discussed next) prohibits the obtaining of a theoretical expression for the variation of k_d with quality for the various flow conditions and wall heat fluxes. Values of k_d were computed from Equation (10) and the data of Fig. 34 and are shown in Fig. 36. This Figure shows the variation in k_d with length that would be necessary to make the proposed model fit the experimental data. It should be remarked that values of k_d computed in this manner are quite sensitive to the amount of moisture present in the stream, so that at high qualities such as occur in this example the values of k_d should be considered as approximate. It is interesting however to compare the value of k_d in Fig. 36 with the value predicted by the equation of Alexander and Coldren (2) which is 6,300 ft/hr, and the value predicted by Reynolds' analogy which is 1,520 ft/hr.

Of course, the tabulated data could be made to fit the prediction of Equation (10) by the choice of an appropriate expression for k_d versus quality; however no single expression was obtained that seemed to apply to all of the data of a particular class. It may be that a general

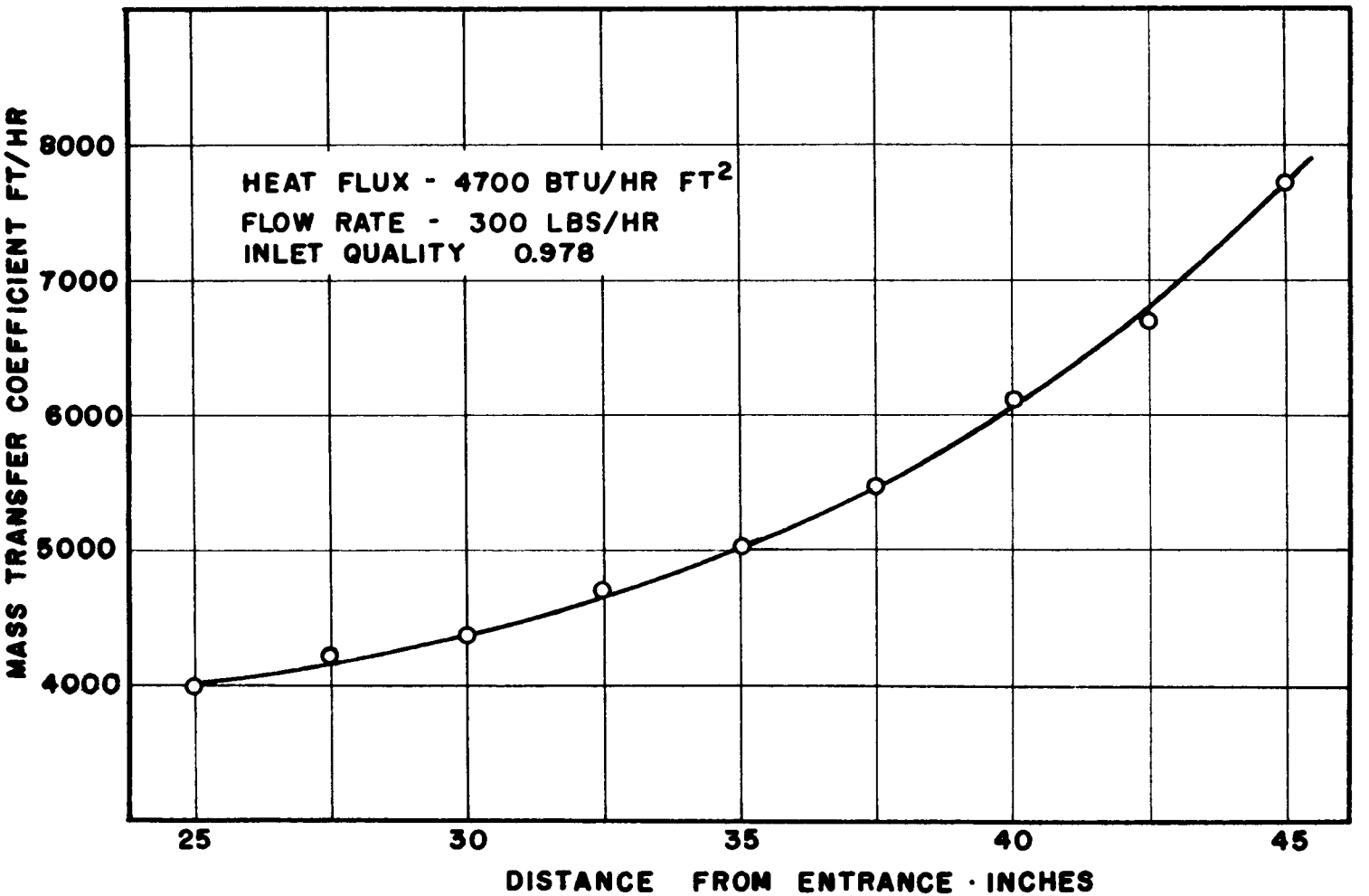

FIG. 36 VARIATION OF K_d ACCORDING TO PROPOSED MODEL & EXPERIMENTAL MEASUREMENTS

expression would have to be of a very complex form.

Equation (10) could be modified into an empirical expression with the use of a function in the second term that would account for variations in k_d, h, and S. An expression of this form might be found with computer techniques that would correlate data over a fairly wide range.

It is important to remember that the assumption of an increasing k_d with length does not prohibit the wall temperature from rising to the value corresponding to dry steam as the droplets are depleted to zero.

A study of the data indicates another factor that seems to influence the change of wall temperature with length in the mist region. This effect is best seen by a study of Figs. 37 and 38. In Fig. 37 are shown the wall temperatures for dry superheated steam and for a mist at the same mass flow rates and wall heat flux. (The flow conditions and the heat flux are the same for the mist in this case as for the mist shown in Fig. 35. The only difference is that the mist flow of Fig. 37 was introduced into the test section after the tube wall had been preheated to a temperature high enough to cause the spheroidal state to exist for the entire tube length. This shows that two temperature patterns are possible at a given flow condition and wall heat flux.) A comparison of the mist curve and the superheated steam curve of Fig. 37 shows them to be similar in shape. The mist flow curve is naturally lower because of the lower inlet temperature of the steam.

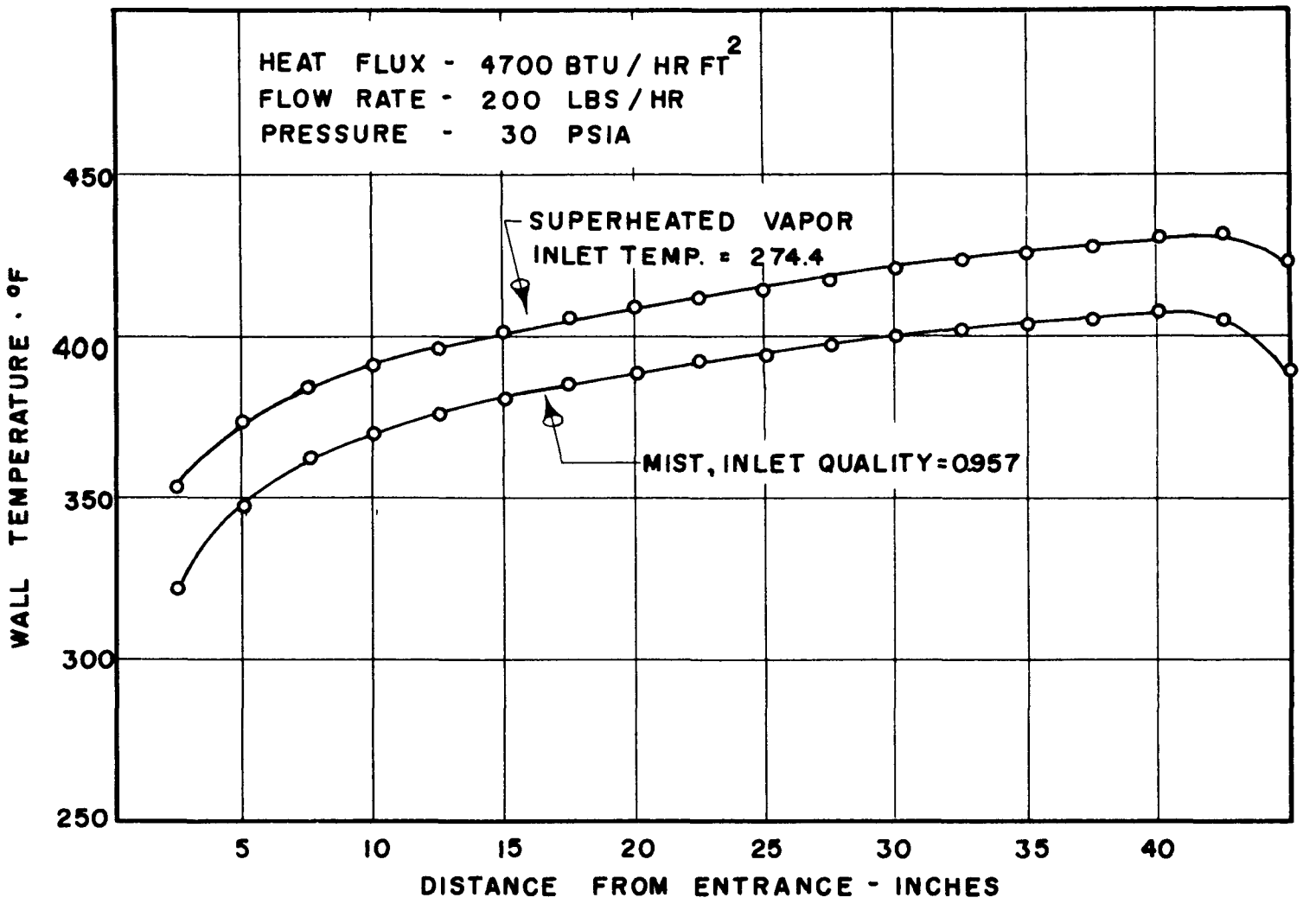

FIG. 37 WALL TEMP FOR DRY STEAM & FOR MIST WITH WALL INITIALLY HEATED

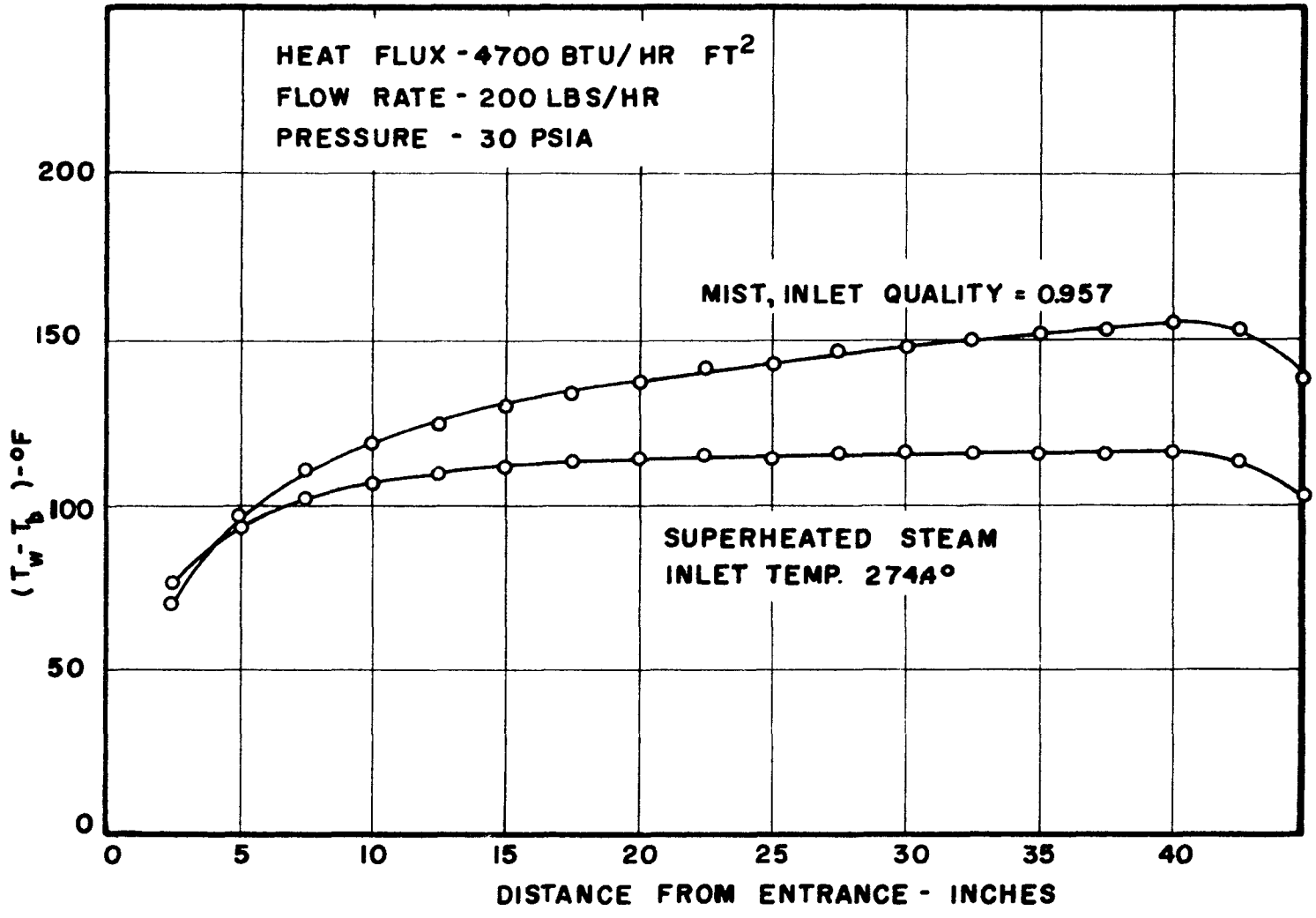

FIG. 38 TEMP. DIFFERENCES FOR DRY & WET STEAM

If the assumption is made that the bulk temperature of the mist is the saturation temperature, as long as moisture is present, and if the bulk temperature of the dry steam is determined from inlet and outlet temperature measurements, then the curve of Fig. 38 results. This Figure shows that the temperature difference for the superheated vapor becomes nearly constant whereas the temperature difference for the mist increases with length. This latter trend is surprising since the amount of moisture present in the steam is supposed to have little effect on the cooling process for the spheroidal condition. Another surprising thing to note is that the temperature difference for the mist is considerably higher than for superheated steam at approximately the same conditions and at the same mass flow rate. It is also interesting to note that the temperature difference for the mist of Fig. 38 is higher than at the same quality in the mist shown in Fig. 36, even though both mists are presumably identical in makeup. This observation was repeated over several runs.

The following explanation is given for this seeming anomaly. The droplets and the vapor are not in thermal equilibrium downstream from the point where the liquid film disappears. The model that was developed predicted that the energy input at the wall would eventually exceed the latent heat in the drops striking the wall. This excess of energy was assumed to go into the vapor phase, superheating it slightly, and then it was assumed to pass into evaporation of droplets at the outer edge of the

core. This latter step evidently does not happen in the test section.

The extremely slow rate of heat transfer between droplets and vapor has been mentioned previously (11), (66). Droplets passing through the test section at 100 fps would be in the test section for only 1/25 of a second and might often stay in the core for the entire time. Unless a particular droplet were of very small size or unless it struck a solid surface below the spheroidal temperature it very likely would not evaporate to any extent, at least at moderate rates of heating at the wall.

It was in this phase of the study that the spray analyzer became a useful tool. The spray analyzer probe had been located downstream from the test section as shown in Fig. 18. The analyzer detected droplets in the flow even in the cases where calculations had indicated that the exit conditions should have been superheated. Since droplets persisted in this superheated vapor at the exit, it is likely that the vapor in the test section was superheated at the points where there was no liquid film but where the apparent quality was less than 100 percent.

The temperature difference for the mist of Fig. 37 was recalculated, assuming that no droplets evaporated in the tube. The result is shown in Fig. 39. This curve is almost identical to the curve for superheated steam shown in Fig. 38, the average difference being approximately four percent. The heat transfer coefficient for this mist flow, based on the assumption of no droplet evaporation, is approximately six percent below

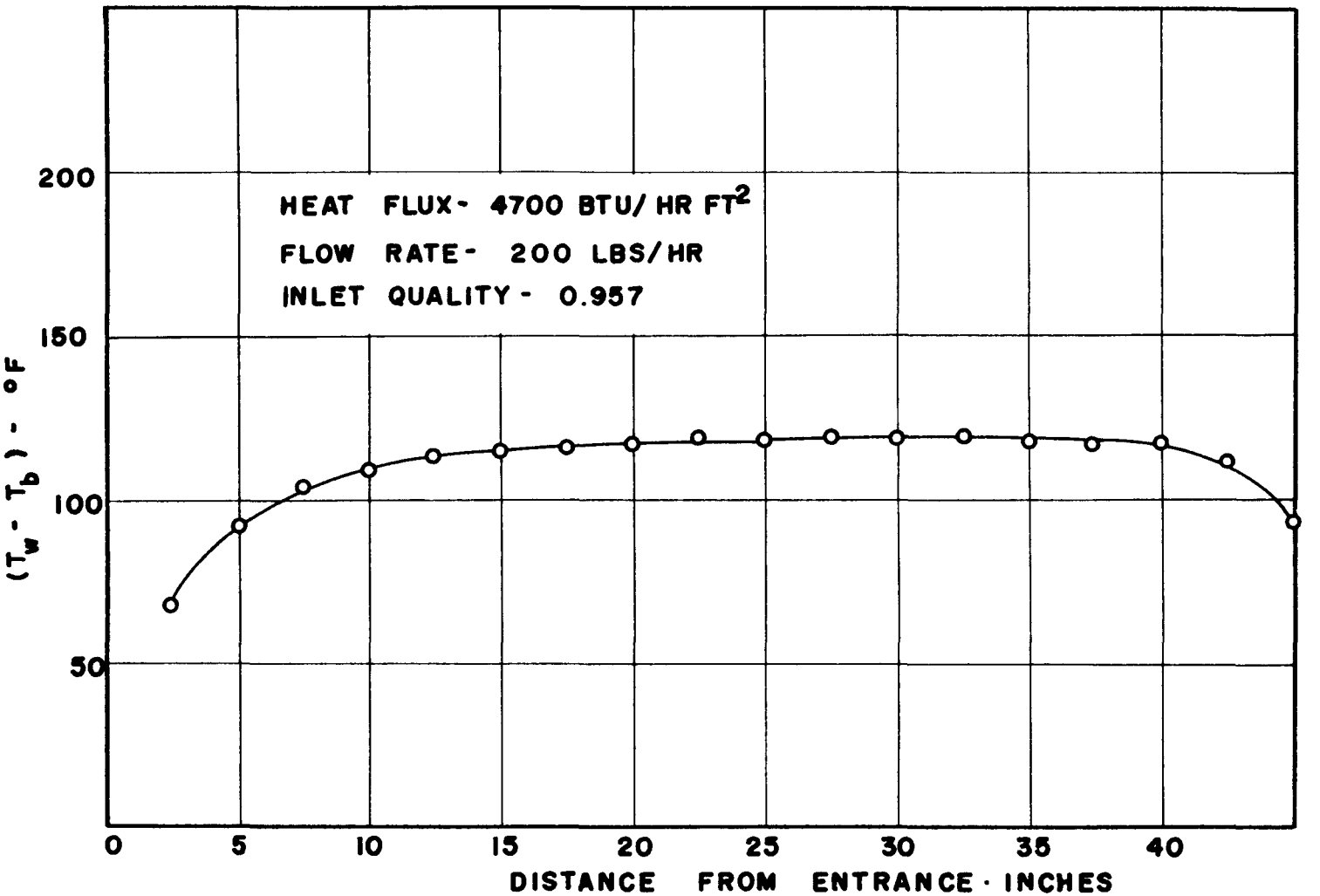

FIG. 39 TEMP. DIFFERENCES FOR MIST IN SPHEROIDAL STATE ASSUMING NO DROPLET EVAPORATION

the value predicted by the Colburn equation for dry saturated steam at the same mass flow rate.

This superheating effect is further shown in Fig. 40 where the mist was heated to a point where energy considerations and the assumption of equilibrium would require the stream to be free of moisture at the point indicated. The upper curve is drawn on the basis of this assumption, using straight line interpolation between the calculated point of 100 percent quality and the measured exit temperature. The values of heat transfer coefficient calculated for the exit region of the tube are approximately 20 percent below the values measured for dry steam at the same flow rate and are approximately 22 percent below the values predicted by the Colburn equation.

The exit thermocouple gave a reading for this run that was too low according to the energy balance calculations. Good energy balances had been obtained previously with dry steam. This low reading of the exit thermocouple occurred in a number of similar runs with wet steam supposedly heated to dryness. It was concluded that this was caused by the moisture still present in the core of the stream impinging on the thermocouple. This probably caused the thermocouple to give a value somewhere between the true vapor temperature and the water droplet temperature. A special type of probe would be required to read the true vapor temperature under such conditions.

The lower curve of Fig. 40 shows the temperature difference that

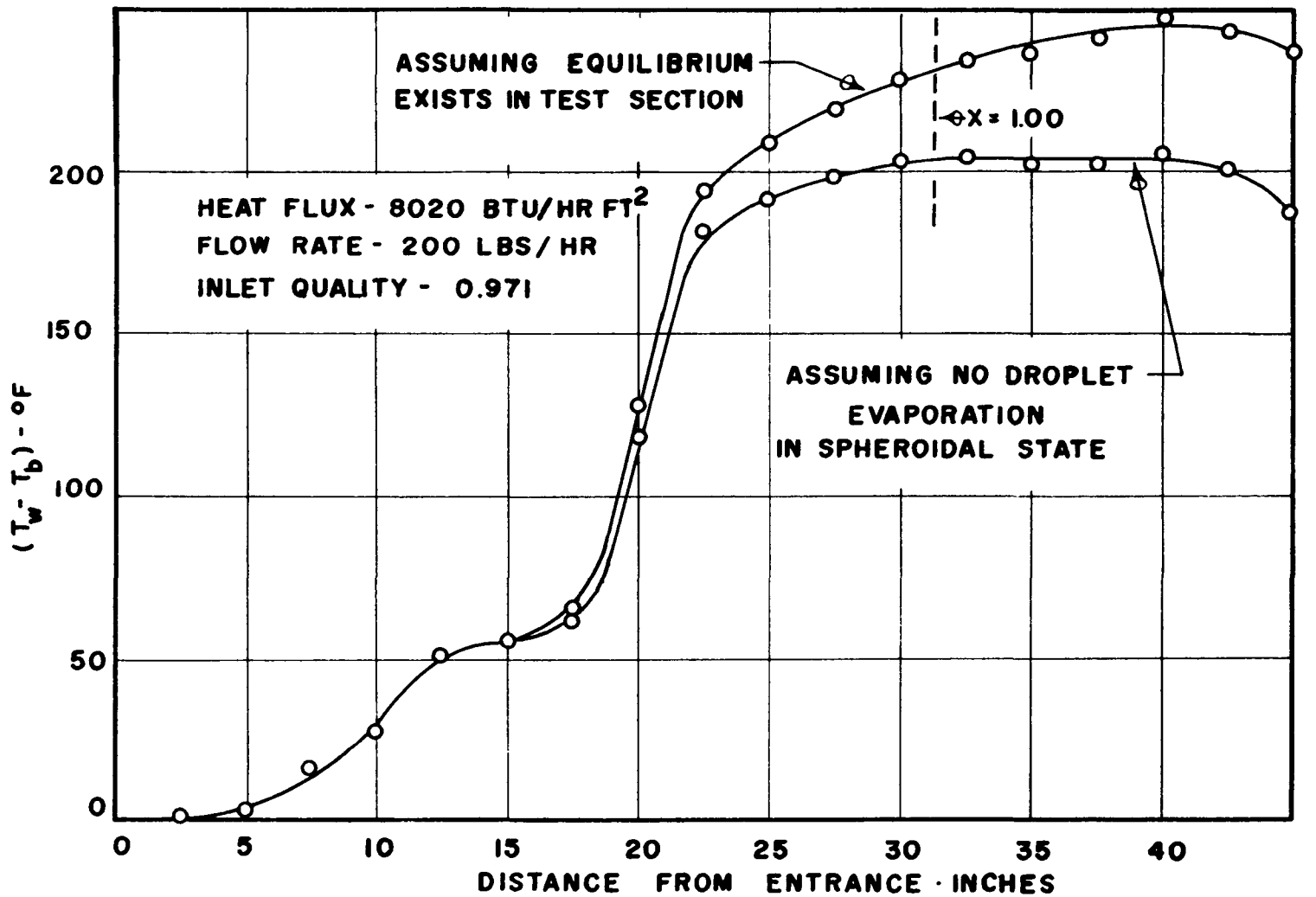

FIG. 40 TEMP. DIFFERENCES FOR A MIST WITH MODERATELY HIGH HEAT FLUX

would exist assuming that no droplets evaporate after a certain point in the tube. The values of the measured film coefficients for this case are within three percent of the predicted value of the Colburn equation and the measured value of superheated steam at the same flow rate.

If non-equilibrium does exist to the extent presumed in the above discussion then it would be improbable that the values of the measured heat transfer coefficients for a mist can be correlated in terms of the physical properties of the system. Indeed, no correlation seemed to exist.

The values of the heat transfer coefficients for mist flow in the non-spheroidal state were generally in the range of 3 to 6 times the value of the dry steam coefficient for the same flow rate. The values of h for mist in the spheroidal state were, for practical purposes, the same as for dry steam at the same flow rate, provided that the bulk temperature used to define the coefficient is based on the assumption that superheating occurs even with droplets present.

The pressure drops in the test section were so small that it was difficult to measure them accurately, even with the Meriam #3 Fluid that was used in the manometers. Fluctuations in the fluid made the manometer difficult to read with consistency.

Average values of all readings for each rate of flow were compared with the values computed by the use of the Moody friction factor. The relatively small acceleration and gravitational effects were ignored

in the comparisons. Since two-phase drops are higher than equivalent single-phase pressure drops, it would be expected that the measured pressure drops would be higher than the values computed from the friction factor. The average measured pressure drops were 9, 16, and 26 percent above the computed values for the 200, 300, and 400 lb per hour runs, respectively. It appears that McAdams' (44) suggestion for the use of a friction factor based on the mean viscosity would give fairly good approximations to the pressure drops in high quality flows.

Annular Flow

In this study of a mist flow it was necessary to insure that the droplets entering the test section were uniformly spread across the tube. The result was that a thin liquid film usually formed on the tube walls upstream from the start of heating. In almost every run, therefore, this film had to be removed by heating before a true mist flow existed in the tube.

Calculations made from the data of the annular flow regions showed that remarkably high heat transfer coefficients existed for this type of flow. In some runs the local coefficients were computed to be as high as 10,000 Btu/hr square foot F. This is much higher than the usual coefficients for water, even for boiling. It is unlikely that boiling existed in these cases due to the extremely low temperature differences. Because of the low temperature differences it was difficult to make accurate

individual measurements, but averages of the coefficients should give a fairly reliable estimate of the values that can be expected with this type of flow. Systematic variations of the coefficients with length, quality, or flow rate were not obvious.

Calculations were made for one run to estimate the film thickness, assuming conduction across the thin film, and assuming that the free surface of the film was at the saturation temperature. Data of run number 45 was used since an annular flow existed for the entire tube length in this case. The average coefficient for the entire tube length was 4,660 Btu/hr square foot F. Assuming the thermal conductivity of water was 0.395 Btu/hr ft F, the thickness of the film was calculated to be 8.5×10^{-5} ft.

In order for the surface temperature of the liquid film to be at the saturation temperature there could be no temperature drop across any vapor sublayer at the free surface of the liquid. In other words, the film would have to have a turbulent surface and the vapor next to the liquid film would also have to be turbulent. Abramson (1) discussed this in his investigation of annular liquid flow.

To check on the existence of a turbulent-free surface it is convenient to use the dimensionless flow parameter of Abramson:

$$w^{+} = \frac{w}{\pi D \mu_{d}} \quad . \tag{20}$$

Assuming that one half of the liquid flowing is in the annular liquid

film, a value of $w^+ = 74$ is computed. Since this is past the limit of the buffer layer ($r^+ = 30$), a turbulent interface could easily exist, according to Abramson. The assumption that one half of the liquid flowing was in the annular film had no particularly logical basis. However, use of the value of liquid flow rate that results from that assumption, along with the estimated value of film thickness, gives an average film velocity of 16 fps, which is a reasonable value and agrees closely with values measured experimentally by Abramson under similar conditions. It seems likely that in most cases where the large values of coefficients were obtained that the turbulent surface condition existed.

It seems probable that the annular liquid film does not end smoothly at an exact location along the tube length but rather ends in a ragged, non-stationary manner. Nucleate boiling very likely occurs at localized spots in this region since a relatively high temperature differential exists just downstream from the end of the liquid film.

CONCLUSIONS AND RECOMMENDATIONS

The following conclusions are made as a result of this study:

1. Two distinct types of heat transfer to a mist flow are possible, depending upon whether the wall temperature is above or below a critical value for the spheroidal state. For the former case the heat transfer coefficients are almost identical to those of dry steam at the same flow rate. For the latter case the heat transfer coefficients are approximately 3 to 6 times the dry steam coefficients. The latter type of heat transfer exists only with certain flow condition and heat flux combinations. High heat fluxes and/or high qualities tend to make the spheroidal state exist. Preheating of the tube wall before injection of water can cause the spheroidal state to exist for conditions where it normally would not. Fluctuations in the flow conditions can cause severe temperature fluctuations in the tube wall as the type of heat transfer changes in a certain region.
2. It appears that equilibrium does not exist between the droplets and vapor in the mist region, and considerable superheating of the vapor or part of the vapor seems to occur even

when drops are present. For this reason heat transfer coefficients for a mist should probably not be based on $(T_w - T_{sat})$, as this leads to coefficients for mists that are lower than those for dry steam at equivalent flow conditions.

3. If the model proposed in this thesis is to adequately predict the wall temperatures for a mist flow, then some method of determining the mass transfer coefficient of the droplets, k_d, must be developed. It appears from a study of the data that k_d cannot be considered a constant.

4. The electronic spray analyzer described in this thesis is not suitable in its present design for quantitative studies of droplet spectrum in steam-water mist flows. A new probe geometry is needed in order to eliminate the undesirable characteristics of the present analyzer. The analyzer was found useful as an instrument for the detection of droplets in a flow. Its value as a monitor of spray uniformity could not be determined from these experiments.

5. Very high heat transfer coefficients were found for annular-mist flow (on the order of 5,000 Btu/hr ft^2 F). It appears that if all of the moisture in a stream could be kept on the wall, then high coefficients could be maintained for very high qualities.

It is recommended that future work be directed toward more fundamental aspects of the problem. It appears that a better method of predicting droplet motion would be necessary before any real progress could be made in the heat transfer problem. Studies need to be made of the droplet behavior at the wall in order to be able to predict the fraction of the droplet that evaporates. A study needs to be made of the temperature necessary for the existence of the spheroidal state for very small drops in a vapor atmosphere.

Since droplet size is likely to be an important factor in any of the above studies, some method is needed to determine the drop sizes in flowing steam-water mixtures. Improvement of the electronic spray analyzer is one possibility. In lieu of such an improvement it appears that photographic methods would likely be the next best choice for the study of droplet spectrums. Development of an entirely new and practical method of droplet size determination under such conditions would represent a real contribution.

Studies should be made into means of directing the liquid entrained in the core toward the wall. If this could be done uniformly and without affecting the pressure drop too severely, it would permit evaporation at moderate heat fluxes to proceed to very high qualities. It is likely that high heat fluxes would disrupt very thin liquid films.

BIBLIOGRAPHY

1. Abramson, A. E., "Investigation of Annular Liquid Flow with Cocurrent Air Flow in Horizontal Tubes", Journal of Applied Mechanics, Vol. 19, 1952, p. 267.

2. Alexander, L. G. and Coldren, C. L., "Droplet Transfer from Suspending Air to Duct Walls", Industrial and Engineering Chemistry, Vol. 43, 1951, p. 1325.

3. Ambrose, T. W., "Literature Survey of Flow Patterns Associated with Two-Phase Flow", HW 52927, 1957.

4. Baker, Ovid, "Simultaneous Flow of Oil and Gas", The Oil and Gas Journal, Vol. 53, July 25, 1954, pp. 185-195.

5. Battelle Memorial Institute, "Injection and Combustion of Liquid Fuels", WADC Technical Report 56-344 and ASTIA Document No. AD 118142, March, 1957.

6. Bennett, J. A. R., "Two-Phase Flow in Gas-Liquid Systems--A Literature Survey", AERE CE/R 2497, Atomic Energy Research Establishment, Harwell, Berkshire, England, 1958.

7. Bevans, R. S., "Mathematical Expressions for Drop Size Distribution in Sprays", Conference on Fuel Sprays, University of Michigan, Mar. 30-31, 1949.

8. Boggs, J. H., and Fitch, E. C., "Reconnaissance Survey of Two-Phase, Two-Component Fluid Flow and Transportation of Solid Particles in Fluid Streams", Fluid Dynamics Project, Oklahoma State University, 1957.

9. Colburn, A. P., "A Method of Correlating Forced Convection Heat Transfer Data and a Comparison with Fluid Friction", Transactions AIChE, Vol. 29, 1933, p. 174.

10. Collier, J. G., "A Review of Two-Phase Heat Transfer", (1935-1957), AERE CE/R 2496, Atomic Energy Research Establishment, Harwell, Berkshire, England, 1958.

11. Combustion Engineering, Inc., Steam Tables-- Properties of Saturated and Superheated Steam, Third Edition, 1940, p. 37.

12. Dallavalle, J. M., Micromeritics--The Technology of Fine Particles, Pittman, 1948.

13. Davidson, W. F., Hardie, P. H., Humphreys, C. G. R., Markson, A. A., Mumford, A. R., and Ravese, T., "Studies of Heat Transfer Through Boiler Tubing at Pressures from 500 to 3000 Pounds", Transactions ASME, Vol. 65, 1943, p. 553.

14. DeJuhasz, K. J., Bibliography on Sprays, New York, The Texas Company, 1948.

15. DeJuhasz, K. J., Spray Literature Abstracts, New York, The American Society of Mechanical Engineers, 1959.

16. Dengler, C. E., "Heat Transfer and Pressure Drop for Evaporation of Water in a Vertical Tube", Ph.D. Thesis, MIT, 1952.

17. Dimmock, N. A., "Production of Uniform Droplets", Nature (England) Vol. 166, 1950, pp. 686-687.

18. Dimmock, N. A., "The Controlled Production of Streams of Identical Droplets", Memo M-115, National Gas Turbine Establishment, England, 1951.

19. Drew, T. B., and Mueller, A. C., "Boiling", Transactions AIChE, Vol. 33, 1937, p. 449.

20. Elliott, H. W., "Cloud Droplet Camera", Report MI-701, National Research Council of Canada, Dec. 1947.

21. Fikry, M. M., "Heat Transfer to Wet Steam Flowing in a Horizontal Tube", Ph.D. Thesis, University of London, October 1952.

22. Fluid Meters--Their Theory and Application, Report of ASME Research Committee on Fluid Meters, Fifth Edition, 1959.

23. Friedlander, S. K., and Johnstone, H. F., "Deposition of Suspended Particles from Turbulent Gas Streams", Industrial and Engineering Chemistry, Vol. 49, 1957, p. 1151.

24. Geist, J. M., "An Electronic Spray Analyzer for Electrically Conducting Particles", Ph.D. Thesis, University of Michigan, 1950.

25. Geist, J. M., York, J. L., and Brown, G. G., "Electronic Spray Analyzer for Electrically Conducting Particles", Industrial and Engineering Chemistry, Vol. 43, 1951, p. 1371.

26. Gorton, C. W., "Heat Transfer to Drops of Liquid in the Spheroidal State", Ph.D. Thesis, Purdue University, 1953.

27. Green, H. L., and Lane, W. R., Particulate Clouds: Dusts, Smokes, Mists, London, E. and F. N. Spon Ltd., 1957.

28. Gresham, W. A., Foster, P. A., and Kyle, R. J., "Review of the Literature on Two-Phase (Gas-Liquid) Fluid Flow in Pipes, Part I", WADC-TR-55-422, Part I, June 1955.

29. Gunther, F. C., "Photographic Study of Surface Boiling Heat Transfer to Water with Forced Convection", Transactions ASME, Vol. 73, 1951, p. 115.

30. Hermanns, J. J., Flow Properties of Disperse Systems, Amsterdam, North-Holland Publishing Co., 1953.

31. Hottel, H. C., Williams, G. C., and Simpson, H. C., "Combustion of Droplets of Heavy Liquid Fuels", Fifth Symposium on Combustion, New York, Reinhold Publishing Corp., 1955.

32. Ingebo, R. D., "Vaporization Rates and Drag Coefficients for Isooctane Sprays in Turbulent Air Streams", NACA TN 3265, Oct. 1954.

33. Isbin, H. S., Moen, R. H., and Mosher, D. R., "Two-Phase Pressure Drops", AECU-2994, Nov. 1954.

34. Keenan, J. H., and Keyes, F. G., Thermodynamic Properties of Steam, First Edition, New York, John Wiley and Sons, 1936.

35. Laufer, John, "The Structure of Turbulence in Fully Developed Pipe Flow", NACA TN 2954, June 1953.

36. Leonard, W. D., "Pressure Drop of Mist Flow of Air and Water in a Vertical Pipe", M.S. Thesis, Oklahoma State University, 1957.

37. Lockhart, R. W., and Martinelli, R. C., "Proposed Correlation of Data for Isothermal Two-Phase, Two-Component Flow in Pipes", Chemical Engineering Progress, Vol. 45, 1949, p. 39.

38. Longwell, J. P., and Weiss, M. A., "Mixing and Distribution of Liquids in High Velocity Air Streams", Industrial and Engineering Chemistry, Vol. 45, 1953, p. 667.

39. Lumley, J. L., "Some Problems Connected with the Motion of Small Particles in Turbulent Fluid", Ph.D. Thesis, Johns Hopkins University, 1957.

40. Martinelli, R. C., Boelter, L. M. K., Taylor, T. H. M., Thomsen, E. G., and Morrin, E. H., "Isothermal Pressure Drop for Two-Phase,Two Component Flow in a Horizontal Pipe", Transactions ASME, Vol. 66, 1944, p. 139.

41. Martinelli, R. C., Putnam, J. A., and Lockhart, R. W., "Two-Phase, Two Component Flow in the Viscous Region", Transactions AIChE, Vol. 42, 1946, p. 681.

42. Martinelli, R. C., and Nelson, D. B., "Prediction of Pressure Drop During Forced Circulation Boiling of Water", Transactions ASME, Vol. 70, 1948, p. 695.

43. McAdams, W. H., Woods, W. K., and Bryan, R. L., Transactions ASME, Vol. 63, 1941, p. 545.

44. McAdams, W. H., Woods, W. K., and Heroman, L. C., "Vaporization Inside Horizontal Tubes II--Benzine Oil Mixtures", Transactions ASME, Vol. 64, 1942, p. 193.

45. McCullough, S. and Perkins, P. J., "Flight Camera for Photographing Cloud Droplets in Natural Suspensions in the Atmosphere", NACA RM E50K01a, June 29, 1951.

46. McFadden, P. W., and Grosh, R. J., "High Flux Heat Transfer Studies: An Analytical Investigation of Laminar Film Boiling", ANL 6060, Oct. 1959.

47. Miesse, C. C., "Recent Advances in Spray Technology", Applied Mechanics Reviews, Aug. 1956, p. 321.

48. Mugele, R. A., and Evans, H. D., "Droplet Size Distribution in Sprays", Industrial and Engineering Chemistry, Vol. 43, 1951, p. 1317.

49. Mumm, J. F., "Heat Transfer to Boiling Water Forced Through a Uniformly Heated Tube", ANL-5276, Nov. 1954.

50. NAE LR-98, Classified Report, National Aeronautical Establishment, Ottawa, Canada, 1954.

51. NGTE-M 127, Classified Report, National Gas Turbine Establishment, Pyestock, England, Sept. 1951.

52. Nukiyama, S., and Tanasawa, Y., "Experiments on the Atomization of Liquids in an Air Stream", Reports #1-6, Transactions of the Society of Mechanical Engineers, Japan, Vols. 4, 5, and 6, 1938 1939, 1940, Translation by The Defence Research Board, Department National Defence, Ottawa, Canada, Mar. 18, 1950.

53. Pennsylvania State University, The Penn State Bibliography on Sprays, New York, The Texas Company, 1953.

54. Pilcher, M., and Thomas, R. E., "Drop Size Distribution of Fuel Sprays", Advances in Chemistry #20, American Chemical Society, 1958, p. 155.

55. Rosin, P., and Rammler, E., "The Laws Governing the Fineness of Powdered Coal", Journal of the Institute of Fuel, England, Vol. 7, 1933, p. 29.

56. Ryley, D. J., "The Flow of Wet Steam", The Engineer, Vol. 193, 1952, p. 332 and p. 363.

57. Ryley, D. J., "The Growth of Small Water Droplets in Steam Nozzles", The Engineer, Vol. 195, 1953, p. 686.

58. Ryley, D. J., "Behavior of Water Globules in Steam", The Engineer, Vol. 198, 1954, p. 74.

59. Santalo, M. A., "Two-Phase Flow", Applied Mechanics Reviews, Oct. 1958, p. 523.

60. Savic, P., "The Cooling of a Hot Surface by Drops Boiling in Contact with It", Report MT-37, National Research Council of Canada, Ottawa, April 1958.

61. Savic, P., and Boult, G. J., "The Fluid Flow Associated with the Impact of Liquid Drops with Solid Surfaces", Report MT-26, National Research Council of Canada, May 1955. Also AGARD AG 19/P9 Paper presented at the 7th meeting of the wind tunnel and model testing panel, NATO, Ottawa, Canada, June 1955.

62. Slykhouse, T. E., and York, J. L., "Uniform-Drop-Generator Method for Calibrating Spray Analyzer", 1886:1-1-P, Engineering Research Institute, University of Michigan, July 1954.

63. Soo, S. L., "Statistical Properties of Momentum Transfer in Two-Phase Flow", Chemical Engineering Science, Vol. 5, 1956, p. 57.

64. Soo, S. L., Ihrig, H. K., and El Kouh, A. F., "Experimental Determination of Statistical Properties of Two-Phase Turbulent Motion", ASME Paper 59-A-59.

65. Soo, S. L., and Tien, C. L., "Effect of the Wall on Two-Phase Turbulent Motion", ASME Paper 59-APMW-18.

66. Stodola, A., and Lowenstein, L. C., Steam and Gas Turbines, Vol. 2, New York, Peter Smith Co., 1945, p. 1049.

67. Tchen, C. M., "Mean Value and Correlation Problems Connected with the Motion of Small Particles in a Turbulent Fluid", Ph.D. Thesis, Delft, 1947.

68. Torobin, L. B., and Gauvin, W. H., "Fundamental Aspects of Solid-Gas Flows", Parts I, II, and III, Canadian Journal of Chemical Engineering, Vol. 37, Aug., Oct., Dec. 1959.

69. Vanderwater, R. G., "An Analysis of Burnout in Two-Phase, Liquid-Vapor Flow", Ph.D. Thesis, University of Minnesota, 1956.

70. Von Karman, T., "The Analogy Between Fluid Friction and Heat Transfer", Transactions ASME, Vol. 61, 1939, p. 765.

71. Weiss, D. H., "Pressure Drop in Two-Phase Flow", ANL 4916, Oct. 1952.

Missing Page 165
from
Original Document

Missing Page 166
from
Original Document

$$\frac{\rho_d d}{6} u_d \frac{d(u_d)}{dx} = \frac{1}{2} \rho_g \frac{(\Delta u)^2}{4} \frac{27}{(\overline{N}_{Re})^{0.84}} .$$

The Reynolds number on which the drag coefficient is based is

$$\overline{N}_{Re} = \frac{\Delta u \, d\rho_g}{\mu_v} .$$

Substituting,

$$\frac{u_d d(u_d)}{(\Delta u)^2} (\overline{N}_{Re})^{0.84} = 20.25 \frac{\rho_g}{d\rho_d} dx ,$$

$$\frac{u_d d(u_d)}{(u_g - u_d)^{1.16}} = 20.25 \frac{\rho_g}{d\rho_d} \left(\frac{d\rho_g}{\mu_v}\right)^{-0.84} dx .$$

This is of the form of Integral #91, Dwights Tables of Integrals with $a = u_g$, $b = -1$, and $n = 1.16$.

$$\int \frac{x dx}{(a + bx)^n} = \frac{1}{b^2} \left[\frac{-1}{(n-2)(a+bx)^{n-2}} + \frac{a}{(n-1)(a+bx)^{n-1}} \right] .$$

Since $(a + bx) = (u_g - u_d)$ = slip velocity, the integration is made from $(a + bx) = u_g$ and $x = 0$ to $(a + bx) = (1 - S)u_g$ and $x = L$. This will give the relationship between the slip velocity S and the distance L from the point where the droplets have a zero velocity. This assumes, of course, that the velocity of the vapor is constant, a situation that may not be true in the real case. Integrating, we obtain

$$\left[\frac{1}{(0.84)(\Delta u)^{-0.84}} + \frac{u_g}{(0.16)(\Delta u)^{0.16}}\right]_{\Delta u = u_g}^{\Delta u = (1-S)u_g}$$

$$= \left[-20.25\ \frac{\rho_g}{d\rho_d}\left(\frac{d\rho_g}{\mu_v}\right)^{-0.84} X\right]_{x=0}^{x=L}$$

$$\frac{1}{0.84\,u_g^{-0.84}} + \frac{u_g}{(0.16)(u_g)^{0.16}} - \frac{1}{(0.84)\left[(1-S)\,u_g\right]^{-0.84}}$$

$$- \frac{u_g}{(0.16\left[(1-S)\,u_g\right]^{0.16}} = -20.25\,\frac{\rho_g}{d\rho_d}\left[\frac{d\rho_v}{\mu_v}\right]^{-0.84} L\,.$$

Multiplying through by $(u_g)^{-0.84}$,

$$\frac{1}{0.84} + \frac{1}{0.16} - \frac{(1-S)^{0.84}}{0.84} - \frac{1}{(0.16)(1-S)^{0.16}} = -20.25\,\frac{\rho_g}{d\rho_d}\,(\overline{N_{Re}})^{-0.84} L\,.$$

Since the equation cannot be solved for S in terms of L, it is solved for L:

$$L = 0.0585\,\frac{\rho_d}{\rho_g}\,d\,\overline{N}_{Re}^{0.84}\left[(1-S)^{0.84} + 5.25\,(1-S)^{-0.16} - 6.25\right]\,.$$

This is the distance that a droplet must travel before it attains the particular slip velocity ratio S with the vapor stream.

APPENDIX B

Determination of Temperatures in Tube Wall

The test section was heated by means of spirally wound heater ribbon as shown in Fig. 25. It was desirable to know whether the tube wall could be considered to be operating at a constant heat flux condition. Also it was desirable to know if the thermocouples would read temperatures close to the inside wall temperature.

This was checked by assuming that a section of the tube wall could be approximated by the figure shown below.

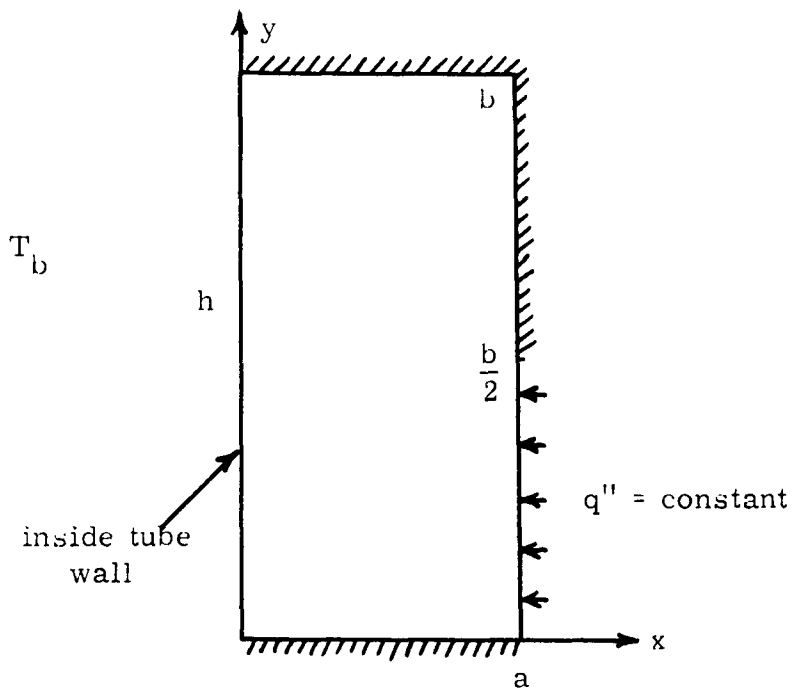

Heat is assumed to flow directly from the heater strip to the outside of the copper tube without spreading out. This essentially ignores the effect of the Sauereisen layer between the copper and the heater ribbon. This, however, will give a solution that is on the conservative side. Due to this assumption and symmetry, the body can be assumed to be insulated on all faces except the inner and out walls. A constant value of heat transfer coefficient h is assumed to exist at the inner wall, x = 0. The heat flux q'' at the lower half of the outer surface of the figure will be twice the value of the average heat flux for the tube since the heater strips cover exactly one half of the total surface area of the test section.

For steady state, two-dimensional heat conduction with no sinks,

$$\frac{\partial^2 \theta}{\partial x^2} + \frac{\partial^2 \theta}{\partial y^2} = 0 \quad , \qquad \text{where } \theta = T - T_B \ .$$

The boundary conditions are

$$\frac{\partial \theta}{\partial y} = 0 \qquad \text{at } y = 0, b \qquad x = x$$

$$-k\frac{\partial \theta}{\partial x} = f(y) \qquad \text{at } x = a \qquad y = y$$

$$k\frac{\partial \theta}{\partial x} = h\theta \qquad \text{at } x = 0 \qquad y = y \ .$$

Assuming that the solution is of the form $\theta = X(x)\,Y(y)$, we obtain

$$Y'' + \lambda^2 Y = 0 \qquad X'' - \lambda^2 X = 0 \ .$$

Taking the first equation, we have

$$Y = A \sin \lambda y + B \cos \lambda y \ .$$

Using the boundary condition at y = 0, y = b gives

$$\lambda = \frac{n\pi}{b} \qquad n = 0, 1, 2, 3 \ldots\ldots$$

$$Y = B \cos \frac{n\pi y}{b} \ .$$

For the second equation we have

$$X = Ce^{\lambda x} + De^{-\lambda x} \ .$$

Using the boundary conditions for x = 0

$$X' = -\frac{h}{k} X \ .$$

This leads to

$$X = \frac{E}{1 - \frac{hb}{n\pi k}} \left\{ 2 \cosh \frac{n\pi X}{b} - \frac{2hb}{n\pi k} \sinh \frac{n\pi x}{b} \right\} .$$

Since θ is of the form X(x) Y(y), the solution is of the form

$$\frac{An}{1 - \frac{hb}{n\pi k}} \cos \frac{n\pi y}{b} \left\{ \cosh \frac{n\pi x}{b} - \frac{hb}{n\pi k} \sinh \frac{n\pi x}{b} \right\} \ .$$

In order to satisfy the non-homogeneous boundary condition along x = a, an infinite number of terms of this form is taken

$$\theta = \sum_{n=0}^{\infty} \frac{An}{1 - \frac{hb}{n\pi k}} \cos \frac{n\pi y}{b} \left\{ \cosh \frac{n\pi x}{b} - \frac{hb}{n\pi k} \sinh \frac{n\pi x}{b} \right\} \ .$$

Since $f(a, y) = -k \frac{\partial \theta}{\partial X}$,

$$f(a,y) = -k\sum_{n=0}^{\infty} \frac{A_n}{1-\frac{hb}{n\pi k}} \cos\frac{n\pi y}{b}\left\{\frac{n\pi}{b}\sinh\frac{n\pi a}{b} - \frac{h}{k}\cosh\frac{n\pi a}{b}\right\}$$

If

$$A_n = -2\,\frac{(1-\frac{hb}{n\pi k})}{bk}\left(\frac{1}{\frac{n\pi}{b}\sinh\frac{n\pi a}{b} - \frac{h}{k}\cosh\frac{n\pi a}{b}}\right)\int_o^b f(y')\cos\frac{n\pi y'}{b}\,dy'$$

for $n = 1, 2, 3, 4$

and if $A_o = \dfrac{+\,(1-\frac{hb}{n\pi k})}{bh}\displaystyle\int_o^b f(y')\,dy'$

then this would be a cosine series for $f(a,y)$. Thus a solution which satisfies all boundary conditions is

$$\theta = \frac{1}{bh}\int_o^b f(y')\,dy' - \frac{2}{bk}\sum_{n=1}^{\infty}\left\{\frac{\cosh\frac{n\pi X}{b} - \frac{hb}{n\pi k}\sinh\frac{n\pi X}{b}}{\frac{n\pi}{b}\sinh\frac{n\pi a}{b} - \frac{h}{k}\cosh\frac{n\pi a}{b}}\right\}\cos\frac{n\pi y}{b}\int_o^b f(y')\cos\frac{n\pi y'}{b}\,dy'.$$

The first term represents the average temperature of the tube wall which is a function only of the heat flux and the film coefficient. The second term determines the variation from that average value and is a function of the thermal conductivity of the tube as well as the heat flux and the film coefficient.

Since the heat flux is assumed to be constant over one-half of the outer wall, and zero over the other half, the final equation can be written in a more simple form:

$$\theta = \frac{q''}{2h} - \frac{2}{bk} \sum_{n=1}^{\infty} \left\{ \frac{\cosh \frac{n\pi X}{b} - \frac{hb}{n\pi k} \sinh \frac{n\pi X}{b}}{\frac{n\pi}{b} \sinh \frac{n\pi a}{b} - \frac{h}{k} \cosh \frac{n\pi a}{b}} \right\} \cos \frac{n\pi y}{b} \; q'' \int_{o}^{\frac{b}{2}} \cos \frac{n\pi y'}{b} \, dy'.$$

A solution to this equation has been made using the tube dimensions for a and b and assuming that h = 100 Btu/hr ft^2 F and k = 200 Btu/hr ft F. The solution shows a sinusoidal variation of temperature along the inner tube wall with a peak to peak amplitude of approximately 0.4 degrees, for an average tube wall heat flux of 20,000 Btu/hr ft^2. The same assumptions show that point of location of the thermocouple differs from the average inside tube wall temperature by less than 0.2 degrees. Calculations using a value of h = 1,000 Btu/hr ft^2 F did not result in a significant change in the temperatures.

The calculations show that there is little variation in the tube wall temperature for the assumed conditions. Since by definition $q'' = h\Delta T$, the small variation in tube wall temperature would lead to approximately a constant heat flux condition for the inside tube wall. It was concluded that the wall could be assumed to be approximately at constant heat flux. The thermocouple readings were assumed to be equal to the inside wall temperature at that position.

APPENDIX C

Tabulated Data

Run Number 1

200 Pounds per Hour

Power Input	100 watts
Steam Flow Rate	193 lbs/hr
Water Injection Rate	7 lbs/hr
Steam Inlet Temperature	280.5° F
Inlet Quality	0.968
Test Section Static Pressure	61.5 inches Hg, abs
Test Section Pressure Drop	.0645 inches Hg/ft
Exit Temperature	249.4° F

T.C. No.	Quality	Wall Temperature	Heat Transfer Coefficient
1	0.969	252.7	1590
2	0.970	253.9	975
3	0.970	255.4	656
4	0.971	259.8	336
5	0.972	264.8	212
6	0.973	270.4	154
7	0.974	273.7	132
8	0.975	274.6	126
9	0.976	277.3	113
10	0.977	277.7	112
11	0.977	278.3	109
12	0.978	279.3	106
13	0.979	279.3	105
14	0.980	280.5	101
15	0.981	282.6	94
16	0.982	283.0	93
17	0.983	282.8	93
18	0.984	280.7	101

Run Number 2

200 Pounds per Hour

Power Input	1500 watts
Steam Flow Rate	200 lbs/hr
Water Injection Rate	Zero
Steam Inlet Temperature	280.4° F
Inlet Quality	Superheated
Test Section Static Pressure	61.1 inches Hg, abs
Test Section Pressure Drop	0.0930 inches Hg/ft
Exit Temperature	323.6° F

T.C. No.	Wall Temperature	Heat Transfer Coefficient
1	352.8	41.6
2	372.9	50.0
3	383.7	46.0
4	390.4	44.2
5	395.7	43.1
6	400.4	42.3
7	404.8	41.6
8	408.6	41.1
9	411.5	41.0
10	413.3	41.3
11	417.4	40.7
12	420.1	40.6
13	422.7	40.6
14	424.9	40.8
15	427.3	40.9
16	430.6	40.6
17	430.6	41.5
18	422.5	45.8

Run Number 3

200 Pounds per Hour

Power Input	1500 watts
Steam Flow Rate	195 lbs/hr
Water Injection Rate	5 lbs/hr
Steam Inlet Temperature	280.5° F
Inlet Quality	0.982
Test Section Static Pressure	60.9 inches Hg, abs
Test Section Pressure Drop	.0787 inches Hg/ft
Exit Temperature	252.8° F

T. C. No.	Quality	Wall Temperature	Heat Transfer Coefficient
1	0.983	252.8	1810
2	0.984	258.3	581
3	0.986	263.9	343
4	0.987	273.4	203
5	0.988	283.4	142
6	0.990	294.5	106
7	0.991	298.0	98.2
8	0.993	300.5	93.2
9	0.994	306.8	83.0
10	0.995	322.1	65.3
11	0.997	364.2	41.2
12	0.998	372.1	38.5
13	0.999	377.5	36.9
14		381.6	35.7
15		385.8	34.6
16		390.5	33.5
17		390.9	33.4
18		384.3	35.0

Run Number 4

200 Pounds per Hour

Power Input	1500 watts
Steam Flow Rate	192 lbs/hr
Water Injection Rate	8 lbs/hr
Steam Inlet Temperature	280.2° F
Inlet Quality	0.964
Test Section Static Pressure	60.8 inches Hg, abs
Test Section Pressure Drop	.0716 inches Hg/ft
Exit Temperature	249.1° F

T. C. No.	Quality	Wall Temperature	Heat Transfer Coefficient
1	0.965	251.6	3140
2	0.966	252.8	1740
3	0.968	255.5	870
4	0.969	258.5	560
5	0.971	262.2	388
6	0.972	270.4	231
7	0.973	280.1	156
8	0.975	285.9	131
9	0.976	290.4	116
10	0.977	291.9	112
11	0.979	293.4	108
12	0.980	291.4	113
13	0.981	290.7	115
14	0.983	287.2	126
15	0.984	288.5	122
16	0.985	288.3	122
17	0.987	289.8	118
18	0.988	284.9	134

Run Number 5

200 Pounds per Hour

Power Input	1500 watts
Steam Flow Rate	191 lbs/hr
Water Injection Rate	9 lbs/hr
Steam Inlet Temperature	278.7° F
Inlet Quality	0.957
Test Section Static Pressure	61.5 inches Hg, abs
Test Section Pressure Drop	0.115 inches Hg/ft
Exit Temperature	250.5° F

(In this run the tube wall was preheated)

T. C. No.	Quality	Wall Temperature	Heat Transfer Coefficient
1	0.958	320.8	67.2
2	0.959	347.8	48.5
3	0.961	361.8	42.4
4	0.962	369.4	39.6
5	0.963	375.1	37.8
6	0.965	380.3	36.2
7	0.966	384.3	35.2
8	0.968	387.9	34.2
9	0.969	391.8	33.3
10	0.970	392.8	33.0
11	0.972	396.5	32.2
12	0.973	399.0	31.6
13	0.974	401.1	31.2
14	0.976	402.8	30.8
15	0.977	404.4	30.6
16	0.979	406.9	30.0
17	0.980	404.1	30.6
18	0.981	388.5	34.0

Run Number 6

200 Pounds per Hour

Power Input	1500 watts
Steam Flow Rate	191 lbs/hr
Water Injection Rate	9 lbs/hr
Steam Inlet Temperature	278.7° F
Inlet Quality	0.957
Test Section Static Pressure	61.4 inches Hg, abs
Test Section Pressure Drop	0.108 inches Hg/ft
Exit Temperature	249.8° F

T. C. No.	Quality	Wall Temperature	Heat Transfer Coefficient
1	0.958	252.2	3360
2	0.959	252.5	2760
3	0.961	252.5	2760
4	0.962	252.5	2610
5	0.963	253.6	1620
6	0.965	255.1	1070
7	0.966	268.9	258
8	0.968	283.7	142
9	0.969	288.6	124
10	0.970	290.2	119
11	0.972	290.8	117
12	0.973	293.6	109
13	0.974	297.9	99.1
14	0.976	340.1	52.4
15	0.977	361.8	42.2
16	0.979	371.0	39.0
17	0.980	372.5	38.4
18	0.981	361.8	42.1

Run Number 7

200 Pounds per Hour

Power Input	1500 watts
Steam Flow Rate	190 lbs/hr
Water Injection Rate	10 lbs/hr
Steam Inlet Temperature	280.1° F
Inlet Quality	0.952
Test Section Static Pressure	60.3 inches Hg, abs
Test Section Pressure Drop	.0716 inches Hg/ft
Exit Temperature	248.5° F

T.C. No.	Quality	Wall Temperature	Heat Transfer Coefficient
1	0.953	250.8	4270
2	0.954	250.6	5230
3	0.956	250.7	4700
4	0.957	250.4	6720
5	0.958	250.6	5230
6	0.960	250.5	5880
7	0.961	252.4	1680
8	0.963	252.7	1520
9	0.964	256.6	672
10	0.965	258.4	534
11	0.967	260.9	416
12	0.968	262.8	356
13	0.969	264.2	320
14	0.971	264.4	315
15	0.972	265.7	290
16	0.973	276.5	174
17	0.974	275.7	179
18	0.976	269.4	236

Run Number 8

200 Pounds per Hour

Power Input	1500 watts
Steam Flow Rate	189 lbs/hr
Water Injection Rate	11 lbs/hr
Steam Inlet Temperature	280° F
Inlet Quality	0.946
Test Section Static Pressure	61.3 inches Hg, abs
Test Section Pressure Drop	0.0573 inches Hg/ft
Exit Temperature	249.3° F

T.C. No.	Quality	Wall Temperature	Heat Transfer Coefficient
1	0.947	251.7	4270
2	0.948	251.7	4270
3	0.950	251.7	4270
4	0.951	251.4	5870
5	0.953	251.6	4700
6	0.954	251.9	3360
7	0.955	253.2	1740
8	0.957	253.1	1810
9	0.958	255.8	886
10	0.959	256.8	745
11	0.961	256.7	770
12	0.962	257.5	671
13	0.963	257.8	644
14	0.965	258.0	618
15	0.966	257.8	635
16	0.967	259.4	522
17	0.969	259.1	540
18	0.970	259.9	494

Run Number 9

200 Pounds per Hour

Power Input	2000 watts
Steam Flow Rate	200 lbs/hr
Water Injection Rate	zero
Steam Inlet Temperature	276.5° F
Inlet Quality	Superheated
Test Section Static Pressure	60.7 inches Hg, abs
Test Section Pressure Drop	0.0787 inches Hg/ft
Exit Temperature	336.5° F

T.C. No.	Wall Temperature	Heat Transfer Coefficient
1	382.7	58.6
2	407.0	49.2
3	420.7	45.6
4	429.0	44.1
5	435.0	43.1
6	438.0	43.4
7	446.9	41.8
8	450.1	41.9
9	456.9	38.4
10	457.4	39.2
11	462.7	38.7
12	466.5	38.6
13	470.1	38.5
14	473.4	38.6
15	476.3	38.7
16	480.9	38.4
17	480.9	39.2
18	469.5	43.1

Run Number 10

200 Pounds per Hour

Power Input	2000 watts
Steam Flow Rate	193 lbs/hr
Water Injection Rate	7 lbs/hr
Steam Inlet Temperature	279.6° F
Inlet Quality	0.9672
Test Section Static Pressure	61.0 inches Hg, abs
Test Section Pressure Drop	.0645 inches Hg/ft
Exit Temperature	250.9° F

T.C. No.	Quality	Wall Temperature	Heat Transfer Coefficient
1	0.968	257.3	909
2	0.970	266.5	392
3	0.972	274.8	260
4	0.974	286.6	180
5	0.976	292.6	150
6	0.978	300.0	126
7	0.979	302.1	123
8	0.981	302.1	123
9	0.983	310.3	106
10	0.985	318.5	93.1
11	0.987	376.7	50.3
12	0.989	393.0	44.6
13	0.990	412.3	39.2
14	0.992	421.4	37.1
15	0.994	427.9	35.8
16	0.996	433.8	34.6
17	0.998	435.4	34.3
18	0.999	424.8	36.4

Run Number 11

200 Pounds per Hour

Power Input	2000 watts
Steam Flow Rate	192 lbs/hr
Water Injection Rate	8 lbs/hr
Steam Inlet Temperature	280.4° F
Inlet Quality	0.964
Test Section Static Pressure	61.4 inches Hg, abs
Test Section Pressure Drop	.0716 inches Hg/ft
Exit Temperature	250.1° F

T.C. No.	Quality	Wall Temperature	Heat Transfer Coefficient
1	0.966	254.0	1930
2	0.967	259.6	715
3	0.969	268.3	361
4	0.971	273.4	280
5	0.973	279.8	218
6	0.975	303.6	120
7	0.976	308.1	111
8	0.978	308.9	109
9	0.980	312.0	104
10	0.982	312.1	103
11	0.984	313.6	101
12	0.986	313.5	101
13	0.987	313.9	100
14	0.989	317.1	95.5
15	0.991	342.1	69.4
16	0.993	394.7	44.1
17	0.995	411.0	39.6
18	0.997	406.0	40.9

Run Number 12

200 Pounds per Hour

Power Input	2000 watts
Steam Flow Rate	190 lbs/hr
Water Injection Rate	10 lbs/hr
Steam Inlet Temperature	280.5° F
Inlet Quality	0.970
Test Section Static Pressure	61.6 inches Hg, abs
Test Section Pressure Drop	.0645 inches Hg/ft
Exit Temperature	250.1° F

T.C. No.	Quality	Wall Temperature	Heat Transfer Coefficient
1	0.971	252.8	3340
2	0.973	252.5	3970
3	0.975	252.6	3740
4	0.977	253.2	2760
5	0.979	259.1	776
6	0.981	275.6	256
7	0.982	286.9	176
8	0.984	292.1	154
9	0.986	297.1	137
10	0.988	299.3	131
11	0.990	301.7	125
12	0.992	301.1	126
13	0.993	300.8	127
14	0.995	297.7	135
15	0.997	299.2	131
16	0.999	298.0	134
17		299.2	131
18		296.0	140

Run Number 13

200 Pounds per Hour

Power Input	2000 watts
Steam Flow Rate	190 lbs/hr
Water Injection Rate	10 lbs/hr
Steam Inlet Temperature	279.1° F
Inlet Quality	0.954
Test Section Static Pressure	61.8 inches Hg, abs
Test Section Pressure Drop	.0645 inches Hg/ft
Exit Temperature	249.5° F

T.C. No.	Quality	Wall Temperature	Heat Transfer Coefficient
1	0.955	252.5	4540
2	0.957	252.3	5300
3	0.959	252.8	3740
4	0.961	256.4	1200
5	0.963	262.7	548
6	0.965	278.9	229
7	0.967	287.9	173
8	0.968	292.1	155
9	0.970	295.1	144
10	0.972	293.1	151
11	0.974	294.1	148
12	0.976	293.4	150
13	0.977	294.0	148
14	0.979	292.2	154
15	0.981	293.7	149
16	0.983	294.8	145
17	0.985	295.4	143
18	0.987	292.4	153

Run Number 14

200 Pounds per Hour

Power Input	2000 watts
Steam Flow Rate	189 lbs/hr
Water Injection Rate	11 lbs/hr
Steam Temperature	278.8° F
Inlet Quality	0.946
Test Section Static Pressure	60.8 inches Hg, abs.
Test Section Pressure Drop	0.0573 inches Hg/ft
Exit Temperature	248.8° F

T.C. No.	Quality	Wall Temperature	Heat Transfer Coefficient
1	0.948	251.5	4550
2	0.949	251.8	3740
3	0.951	252.0	3350
4	0.953	252.8	3360
5	0.955	254.4	1480
6	0.957	256.4	995
7	0.959	260.6	600
8	0.960	266.1	395
9	0.962	274.3	262
10	0.964	273.4	272
11	0.966	272.5	283
12	0.968	275.4	252
13	0.970	276.0	245
14	0.971	279.5	215
15	0.973	281.9	199
16	0.975	287.2	171
17	0.977	286.4	174
18	0.979	284.6	183

Run Number 15

200 Pounds per Hour

Power Input	2000 watts
Steam Flow Rate	187 lbs/hr
Water Injection Rate	13 lbs/hr
Steam Inlet Temperature	279.1° F
Inlet Quality	0.934
Test Section Static Pressure	60.9 inches Hg, abs
Test Section Pressure Drop	.0645 inches Hg/ft
Exit Temperature	249.5° F

T.C. No.	Quality	Wall Temperature	Heat Transfer Coefficient
1	0.935	253.8	1770
2	0.937	254.3	1550
3	0.939	255.0	1320
4	0.941	257.2	908
5	0.943	262.4	521
6	0.945	268.9	340
7	0.946	275.4	252
8	0.948	273.0	278
9	0.950	271.8	293
10	0.952	266.5	388
11	0.954	266.5	388
12	0.956	268.5	346
13	0.957	269.4	328
14	0.959	270.5	318
15	0.961	270.5	317
16	0.963	273.5	270
17	0.965	275.0	254
18	0.967	276.2	243

Run Number 16

200 Pounds per Hour

Power Input	2500 watts
Steam Flow Rate	200 lbs/hr
Water Injection Rate	Zero
Steam Inlet Temperature	278.5° F
Inlet Quality	Superheated
Test Section Static Pressure	60.8 inches Hg, abs
Test Section Pressure Drop	0.0787 inches Hg/ft
Exit Temperature	355.1° F

T.C. No.	Wall Temperature	Heat Transfer Coefficient
1	410.9	59.5
2	440.6	50.0
3	457.2	46.5
4	467.4	45.0
5	475.7	44.0
6	483.2	43.2
7	490.0	42.7
8	495.6	42.3
9	501.7	42.0
10	503.3	42.6
11	509.8	42.1
12	514.6	42.0
13	519.7	41.8
14	523.9	41.9
15	527.9	42.0
16	534.0	41.2
17	534.6	42.4
18	521.5	46.7

Run Number 17

200 Pounds per Hour

Power Input	2500 watts
Steam Flow Rate	194 lbs/hr
Water Injection Rate	6 lbs/hr
Steam Inlet Temperature	276.9° F
Inlet Quality	0.975
Test Section Static Pressure	61.1 inches Hg, abs
Test Section Pressure Drop	0.0930 inches Hg/ft
Exit Temperature	266.8° F

(In this run the tube wall was preheated)

T.C. No.	Quality	Wall Temperature	Heat Transfer Coefficient
1	0.977	385.3	59.5
2	0.979	416.2	48.4
3	0.981	441.9	41.8
4	0.984	452.6	39.6
5	0.986	460.8	38.1
6	0.988	468.2	36.8
7	0.991	475.0	35.7
8	0.993	480.1	34.9
9	0.995	486.0	34.0
10	0.998	487.9	33.8
11		494.2	33.0
12		498.4	32.7
13		502.1	32.5
14		506.3	32.2
15		510.3	32.0
16		516.0	31.5
17		515.1	31.9
18		496.6	34.8

Run Number 18

200 Pounds per Hour

Power Input	2500 watts
Steam Flow Rate	193 lbs/hr
Water Injection Rate	7 lbs/hr
Steam Inlet Temperature	280.8° F
Inlet Quality	0.971
Test Section Static Pressure	60.6 inches Hg, abs
Test Section Pressure Drop	0.0787 inches Hg/ft
Exit Temperature	258.8° F

T.C. No.	Quality	Wall Temperature	Heat Transfer Coefficient
1	0.973	251.5	5020
2	0.975	253.5	2230
3	0.977	266.0	498
4	0.980	277.7	299
5	0.982	301.0	157
6	0.984	305.5	144
7	0.987	316.0	121
8	0.989	377.2	63.0
9	0.991	443.3	41.5
10	0.994	458.3	38.5
11	0.996	469.0	36.4
12	0.998	478.2	35.1
13		485.0	34.2
14		489.1	33.8
15		494.8	33.3
16		502.9	32.4
17		500.8	32.9
18		486.3	33.7

Run Number 19

200 Pounds per Hour

Power Input	2500 watts
Steam Flow Rate	190 lbs/hr
Water Injection Rate	10 lbs/hr
Steam Inlet Temperature	280.3° F
Inlet Quality	0.951
Test Section Static Pressure	61.5 inches Hg, abs
Test Section Pressure Drop	.0645 inches Hg/ft
Exit Temperature	249.8° F

T.C. No.	Quality	Wall Temperature	Heat Transfer Coefficient
1	0.953	253.5	3970
2	0.955	253.5	3970
3	0.957	257.8	1130
4	0.960	277.2	303
5	0.962	295.9	178
6	0.964	310.0	135
7	0.967	312.9	129
8	0.969	312.2	130
9	0.971	315.4	124
10	0.974	315.4	124
11	0.976	317.4	120
12	0.978	316.7	121
13	0.980	316.4	122
14	0.983	312.1	130
15	0.985	312.2	130
16	0.988	311.2	132
17	0.990	312.1	130
18	0.992	310.1	135

Run Number 20

200 Pounds per Hour

Power Input	2500 watts
Steam Flow Rate	187 lbs/hr
Water Injection Rate	13 lbs/hr
Steam Inlet Temperature	279.8° F
Inlet Quality	0.934
Test Section Static Pressure	61.5 inches Hg, abs
Test Section Pressure Drop	0.0645 inches Hg/ft
Exit Temperature	249.3° F

T.C. No.	Quality	Wall Temperature	Heat Transfer Coefficient
1	0.936	252.5	4720
2	0.938	253.6	2860
3	0.941	253.7	2760
4	0.943	254.0	2500
5	0.946	256.1	1510
6	0.948	263.8	616
7	0.950	277.1	304
8	0.953	279.1	282
9	0.955	280.4	270
10	0.958	280.4	270
11	0.960	278.3	290
12	0.962	278.3	290
13	0.965	273.9	344
14	0.967	273.4	352
15	0.970	271.6	382
16	0.972	276.4	311
17	0.975	280.6	268
18	0.977	286.3	225

Run Number 21

200 Pounds per Hour

Power Input	3000 watts
Steam Flow Rate	193 lbs/hr
Water Injection Rate	7 lbs/hr
Steam Inlet Temperature	279.8° F
Inlet Quality	0.970
Test Section Static Pressure	61.0 inches Hg, abs
Test Section Pressure Drop	0.0645 inches Hg/ft
Exit Temperature	301.5° F

T.C. No.	Quality	Wall Temperature	Heat Transfer Coefficient
1	0.972	268.5	533
2	0.975	272.6	435
3	0.978	285.6	275
4	0.981	300.5	193
5	0.983	308.6	166
6	0.986	319 1	165
7	0.989	382.0	73.6
8	0 992	464.4	45.3
9	0.995	488.5	40.7
10	0.997	497 3	39.2
11		509.2	38 3
12		516.9	38.0
13		524.0	37.8
14		530.3	37 7
15		535 4	37 8
16		543.0	37.5
17		543 8	38 2
18		5?9.7	43.3

Run Number 22

200 Pounds per Hour

Power Input	3000 watts
Steam Flow Rate	190 lbs/hr
Water Injection Rate	10 lbs/hr
Steam Inlet Temperature	280.4° F
Inlet Quality	0.952
Test Section Static Pressure	60.9 inches Hg, abs
Test Section Pressure Drop	.0716 inches Hg/ft
Exit Temperature	249.7° F

T.C. No.	Quality	Wall Temperature	Heat Transfer Coefficient
1	0.954	253.1	3230
2	0.957	253.5	2850
3	0.960	261.1	970
4	0.963	278.8	338
5	0.965	291.7	233
6	0.968	306.9	171
7	0.971	325.0	129
8	0.973	327.9	125
9	0.977	331.3	120
10	0.979	330.2	121
11	0.982	330.4	121
12	0.984	330.3	121
13	0.988	383.3	72.7
14	0.991	461.7	45.8
15	0.993	476.0	43.0
16	0.996	488.0	40.8
17	0.999	492.9	39.9
18		479.5	42.3

Run Number 23

200 Pounds per Hour

Power Input	3000 watts
Steam Flow Rate	190 lbs/hr
Water Injection Rate	10 lbs/hr
Steam Inlet Temperature	280.3° F
Inlet Quality	0.950
Test Section Static Pressure	61.6 inches Hg, abs
Test Section Pressure Drop	.0716 inches Hg/ft
Exit Temperature	250.4° F

T.C. No.	Quality	Wall Temperature	Heat Transfer Coefficient
1	0.952	254.7	2550
2	0.955	262.5	836
3	0.958	272.4	452
4	0.961	292.7	232
5	0.964	311.8	159
6	0.967	322.2	136
7	0.969	326.6	128
8	0.971	329.0	124
9	0.974	332.6	119
10	0.977	330.7	121
11	0.980	332.8	118
12	0.983	332.0	120
13	0.986	338.2	111
14	0.989	389.8	69.8
15	0.991	443.6	50.2
16	0.994	480.8	42.2
17	0.998	492.5	40.1
18	0.999	483.6	41.6

Run Number 24

200 Pounds per Hour

Power Input	3000 watts
Steam Flow Rate	189 lbs/hr
Water Injection Rate	11 lbs/hr
Steam Inlet Temperature	279° F
Inlet Quality	0.946
Test Section Static Pressure	61.9 inches Hg, abs
Test Section Pressure Drop	0.0787 inches Hg/ft
Exit Temperature	250.4° F

T.C. No.	Quality	Wall Temperature	Heat Transfer Coefficient
1	0.948	269.8	519
2	0.951	270.0	513
3	0.954	270.0	513
4	0.957	267.1	606
5	0.959	269.9	516
6	0.962	270.4	503
7	0.965	280.7	328
8	0.968	285.0	286
9	0.971	294.7	222
10	0.973	304.8	181
11	0.976	308.1	170
12	0.979	314.8	152
13	0.982	324.3	132
14	0.985	424.9	55.8
15	0.987	480.8	42.2
16	0.990	498.8	39.2
17	0.993	502.8	38.6
18	0.996	487.5	39.3

Run Number 25

200 Pounds per Hour

Power Input	3000 watts
Steam Flow Rate	187 lbs/hr
Water Injection Rate	13 lbs/hr
Steam Inlet Temperature	278.7° F
Inlet Quality	0.933
Test Section Static Pressure	60.6 inches Hg, abs
Test Section Pressure Drop	.0715 inches Hg/ft
Exit Temperature	246.6° F

T.C. No.	Quality	Wall Temperature	Heat Transfer Coefficient
1	0.935	253.2	2940
2	0.937	253.7	2560
3	0.939	255.6	1701
4	0.941	259.0	1070
5	0.943	265.8	610
6	0.945	278.4	340
7	0.947	294.4	218
8	0.949	295.4	213
9	0.951	301.5	188
10	0.953	302.2	185
11	0.955	301.1	189
12	0.957	303.5	181
13	0.959	302.2	185
14	0.961	303.2	181
15	0.963	301.3	188
16	0.965	305.4	174
17	0.967	307.6	168
18	0.969	309.9	161

Run Number 26

200 Pounds per Hour

Power Input	3000 watts
Steam Flow Rate	187 lbs/hr
Water Injection Rate	13 lbs/hr
Steam Inlet Temperature	279.4° F
Inlet Quality	0.934
Test Section Static Pressure	61.5 inches Hg, abs
Test Section Pressure Drop	0.0645 inches Hg/ft
Exit Temperature	249.3° F

T.C. No.	Quality	Wall Temperature	Heat Transfer Coefficient
1	0.936	256.5	1700
2	0.939	257.2	1520
3	0.943	258.0	1350
4	0.945	264.8	693
5	0.947	276.7	374
6	0.950	286.9	269
7	0.953	295.8	215
8	0.956	295.8	215
9	0.959	297.3	208
10	0.961	294.9	222
11	0.964	297.8	206
12	0.967	300.5	195
13	0.970	304.9	179
14	0.973	306.3	174
15	0.975	309.6	164
16	0.978	314.6	151
17	0.981	319.2	141
18	0.984	318.6	143

Run Number 27

200 Pounds per Hour

Power Input	3500 watts
Steam Flow Rate	187 lbs/hr
Water Injection Rate	13 lbs/hr
Steam Inlet Temperature	279.8° F
Inlet Quality	0.937
Test Section Static Pressure	61.3 inches Hg, abs
Test Section Pressure Drop	0.0705 inches Hg/ft
Exit Temperature	248.9° F

T.C. No.	Quality	Wall Temperature	Heat Transfer Coefficient
1	0.940	256.6	1890
2	0.943	265.9	741
3	0.946	265.5	761
4	0.949	264.6	810
5	0.953	267.4	675
6	0.956	278.7	404
7	0.959	296.0	250
8	0.963	299.7	231
9	0.966	311.8	185
10	0.969	354.3	99.8
11	0.972	468.1	52.2
12	0.976	483.9	48.6
13	0.979	487.4	47.9
14	0.982	488.5	47.6
15	0.985	521.0	41.9
16	0.989	538.3	39.4
17	0.992	541.9	38.9
18	0.995	522.8	41.6

Run Number 28

200 Pounds per Hour

Power Input	4000 watts
Steam Flow Rate	180 lbs/hr
Water Injection Rate	20 lbs/hr
Steam Inlet Temperature	278.7° F
Inlet Quality	0.891
Test Section Static Pressure	61.2 inches Hg, abs
Test Section Pressure Drop	.0645 inches Hg/ft
Exit Temperature	249.5° F

T.C. No.	Quality	Wall Temperature	Heat Transfer Coefficient
1	0.894	255.5	2600
2	0.898	255.4	2650
3	0.902	255.6	2550
4	0.906	254.7	3100
5	0.909	255.3	2710
6	0.913	254.4	3340
7	0.917	256.5	2130
8	0.921	254.0	3610
9	0.924	254.4	3250
10	0.928	255.1	2770
11	0.932	257.5	1830
12	0.936	261.0	1230
13	0.939	267.3	765
14	0.943	266.9	783
15	0.947	267.1	774
16	0.951	267.0	778
17	0.954	267.4	760
18	0.958	270.4	647

Run Number 29

200 Pounds per Hour

Power Input	4400 watts
Steam Flow Rate	187 lbs/hr
Water Injection Rate	13 lbs/hr
Steam Inlet Temperature	278.3° F
Inlet Quality	0.933
Test Section Static Pressure	61.2 inches Hg, abs
Test Section Pressure Drop	.0645 inches Hg/ft
Exit Temperature	249.6° F

T. C. No.	Quality	Wall Temperature	Heat Transfer Coefficient
1	0.936	258.3	2110
2	0.940	259.6	1580
3	0.944	260.5	1440
4	0.949	265.4	964
5	0.952	275.7	570
6	0.957	294.2	328
7	0.961	310.0	241
8	0.965	314.0	226
9	0.969	319.8	207
10	0.974	318.4	211
11	0.978	326.4	189
12	0.982	331.8	177
13	0.986	334.6	170
14	0.990	349.5	145
15	0.994	396.9	98.0
16	0.998	504.2	56.6
17		556.6	46.9
18		557.5	46.9

Run Number 30

200 Pounds per Hour

Power Input	6300 watts
Steam Flow Rate	180 lbs/hr
Water Injection Rate	20 lbs/hr
Steam Inlet Temperature	278.9° F
Inlet Quality	0.891
Test Section Static Pressure	61.7 inches Hg, abs
Test Section Pressure Drop	.0645 inches Hg/ft
Exit Temperature	249.9° F

T. C. No.	Quality	Wall Temperature	Heat Transfer Coefficient
1	0.896	259.3	2490
2	0.902	258.8	2650
3	0.908	259.1	2550
4	0.914	257.9	3000
5	0.920	257.9	3000
6	0.926	256.9	3000
7	0.932	262.6	1770
8	0.938	274.2	913
9	0.944	294.8	471
10	0.950	341.7	228
11	0.956	362.3	186
12	0.962	374.8	167
13	0.968	376.4	165
14	0.974	365.4	181
15	0.980	370.6	173
16	0.986	377.9	163
17	0.992	479.2	90.5
18	0.998	610.0	59.3

Run Number 31

300 Pounds per Hour

Power Input	1500 watts
Steam Flow Rate	300 lbs/hr
Water Injection Rate	Zero
Steam Inlet Temperature	289.8° F
Inlet Quality	Superheated
Test Section Static Pressure	61.0 inches Hg, abs
Test Section Pressure Drop	0.1720 inches Hg/ft
Exit Temperature	317.1° F

T.C. No.	Wall Temperature	Heat Transfer Coefficient
1	342.1	85.2
2	355.9	69.9
3	362.9	64.6
4	367.1	62.5
5	370.6	60.9
6	374.4	59.2
7	377.5	58.0
8	379.9	57.5
9	382.7	56.6
10	383.3	57.3
11	386.0	56.5
12	387.9	56.3
13	389.6	56.2
14	391.0	56.3
15	392.4	56.5
16	395.2	55.6
17	395.6	56.4
18	390.5	61.3

Run Number 32

300 Pounds per Hour

Power Input	1500 watts
Steam Flow Rate	290 lbs/hr
Water Injection Rate	10 lbs/hr
Steam Inlet Temperature	289.2° F
Inlet Quality	0.978
Test Section Static Pressure	61.5 inches Hg, abs
Test Section Pressure Drop	0.1432 inches Hg/ft
Exit Temperature	249.4° F

T. C. No.	Quality	Wall Temperature	Heat Transfer Coefficient
1	0.979	251.5	9400
2	0.980	251.7	5870
3	0.981	251.7	5870
4	0.982	252.0	4270
5	0.983	252.2	3360
6	0.983	253.8	1570
7	0.984	256.6	810
8	0.985	257.7	681
9	0.986	261.0	443
10	0.987	269.2	254
11	0.988	270.2	241
12	0.989	272.7	212
13	0.990	273.2	208
14	0.991	274.6	196
15	0.992	273.8	218
16	0.992	275.4	189
17	0.993	276.7	179
18	0.994	277.5	173

Run Number 33

300 Pounds per Hour

Power Input	1500 watts
Steam Flow Rate	287 lbs/hr
Water Injection Rate	13 lbs/hr
Steam Inlet Temperature	290.1° F
Inlet Quality	0.966
Test Section Static Pressure	61.4 inches Hg, abs
Test Section Pressure Drop	0.158 inches Hg/ft
Exit Temperature	249.2° F

T. C. No.	Quality	Wall Temperature	Heat Transfer Coefficient
1	0.967	251.9	4700
2	0.968	251.9	4700
3	0.969	251.9	4270
4	0.969	251.7	5220
5	0.970	251.7	5220
6	0.971	251.2	9400
7	0.972	252.0	3610
8	0.973	252.3	2940
9	0.974	253.9	1420
10	0.975	256.5	795
11	0.976	257.8	644
12	0.977	260.0	494
13	0.978	260.0	494
14	0.979	261.8	416
15	0.979	261.8	412
16	0.980	263.7	353
17	0.981	265.1	329
18	0.982	266.8	284

Run Number 34

300 Pounds per Hour

Power Input	2000 watts
Steam Flow Rate	290 lbs/hr
Water Injection Rate	10 lbs/hr
Steam Inlet Temperature	289.4° F
Inlet Quality	0.978
Test Section Static Pressure	61.3 inches Hg, abs
Test Section Pressure Drop	0.151 inches Hg/ft
Exit Temperature	250.1° F

T. C. No.	Quality	Wall Temperature	Heat Transfer Coefficient
1	0.979	251.7	6360
2	0.980	252.6	3350
3	0.982	252.9	2990
4	0.983	252.6	3350
5	0.984	253.9	1930
6	0.985	253.9	1930
7	0.987	262.4	539
8	0.988	275.4	256
9	0.989	274.2	268
10	0.990	285.7	182
11	0.992	288.8	166
12	0.993	328.0	81.9
13	0.994	364.2	56.0
14	0.995	369.2	53.5
15	0.997	372.0	52.3
16	0.998	378.9	49.5
17	0.999	381.3	48.6
18		375.1	51.0

Run Number 35

300 Pounds per Hour

Power Input	2000 watts
Steam Flow Rate	287 lbs/hr
Water Injection Rate	13 lbs/hr
Steam Inlet Temperature	289.6° F
Inlet Quality	0.966
Test Section Static Pressure	61.0 inches Hg, abs
Test Section Pressure Drop	0.158 inches Hg/ft
Exit Temperature	248° F

T. C. No.	Quality	Wall Temperature	Heat Transfer Coefficient
1	0.967	251.2	9080
2	0.968	251.4	7060
3	0.969	251.5	5780
4	0.971	251.2	7950
5	0.972	251.2	7950
6	0.973	251.7	4540
7	0.974	254.1	1630
8	0.976	255.7	1180
9	0.977	257.4	884
10	0.978	258.6	757
11	0.979	259.3	691
12	0.980	265.1	424
13	0.981	265.9	402
14	0.983	268.5	344
15	0.984	268.2	350
16	0.986	271.3	299
17	0.987	272.2	286
18	0.989	273.1	274

Run Number 36

300 Pounds per Hour

Power Input	2000 watts
Steam Flow Rate	286 lbs/hr
Water Injection Rate	14 lbs/hr
Steam Inlet Temperature	290.6° F
Inlet Quality	0.962
Test Section Static Pressure	61.8 inches Hg, abs
Test Section Pressure Drop	.151 inches Hg/ft
Exit Temperature	248.8° F

T. C. No.	Quality	Wall Temperature	Heat Transfer Coefficient
1	0.963	252.7	4240
2	0.964	252.9	3530
3	0.965	252.9	3530
4	0.967	252.5	4540
5	0.968	253.2	3030
6	0.969	256.5	1180
7	0.970	261.4	617
8	0.972	261.4	617
9	0.973	265.3	445
10	0.974	266.8	402
11	0.975	266.8	402
12	0.976	267.7	379
13	0.978	268.1	370
14	0.979	268.9	353
15	0.980	270.5	323
16	0.981	272.9	288
17	0.983	273.7	278
18	0.984	273.7	276

Run Number 37

300 Pounds per Hour

Power Input	2500 watts
Steam Flow Rate	283 lbs/hr
Water Injection Rate	17 lbs/hr
Steam Inlet Temperature	289.4° F
Inlet Quality	0.950
Test Section Static Pressure	61.2 inches Hg, abs
Test Section Pressure Drop	0.143 inches Hg/ft
Exit Temperature	248.5° F

T. C. No.	Quality	Wall Temperature	Heat Transfer Coefficient
1	0.951	252.5	4450
2	0.953	252.5	4220
3	0.954	252.5	4220
4	0.956	252.5	4220
5	0.957	252.8	3480
6	0.959	253.4	2762
7	0.960	255.8	1510
8	0.962	257.6	1130
9	0.964	259.8	853
10	0.965	261.0	756
11	0.967	261.5	729
12	0.968	263.2	629
13	0.970	264.5	568
14	0.971	265.7	524
15	0.973	265.5	527
16	0.974	266.2	504
17	0.976	268.1	450
18	0.977	267.8	455

Run Number 38

300 Pounds per Hour

Power Input	3000 watts
Steam Flow Rate	287 lbs/hr
Water Injection Rate	13 lbs/hr
Steam Inlet Temperature	290.2° F
Inlet Quality	0.966
Test Section Static Pressure	61.1 inches Hg, abs
Test Section Pressure Drop	0.158 inches Hg/ft
Exit Temperature	248.5° F

T. C. No.	Quality	Wall Temperature	Heat Transfer Coefficient
1	0.967	251.8	8080
2	0.969	252.5	5100
3	0.971	253.9	2850
4	0.973	254.2	2620
5	0.975	256.5	1620
6	0.977	260.8	932
7	0.978	275.3	390
8	0.981	288.4	255
9	0.982	294.1	222
10	0.984	292.7	229
11	0.986	293.7	223
12	0.988	302.0	167
13	0.990	324.5	131
14	0.992	393.7	67.5
15	0.994	412.8	59.6
16	0.997	433.3	53.0
17	0.999	436.6	52.0
18		426.8	54.9

Run Number 39

300 Pounds per Hour

Power Input	4000 watts
Steam Flow Rate	280 lbs/hr
Water Injection Rate	20 lbs/hr
Steam Inlet Temperature	289.5° F
Inlet Quality	0.938
Test Section Static Pressure	60.8 inches Hg, abs
Test Section Pressure Drop	0.165 inches Hg/ft
Exit Temperature	247.9° F

T. C. No.	Quality	Wall Temperature	Heat Transfer Coefficient
1	0.940	253.4	4180
2	0.943	253.5	4060
3	0.945	253.6	3820
4	0.947	253.5	3940
5	0.950	254.1	3330
6	0.952	254.5	2960
7	0.955	258.0	1650
8	0.958	256.9	1910
9	0.960	261.4	1140
10	0.962	265.9	816
11	0.965	268.7	691
12	0.967	272.8	567
13	0.970	274.0	540
14	0.973	280.9	418
15	0.975	280.9	418
16	0.977	291.5	312
17	0.980	294.3	292
18	0.982	299.1	263

Run Number 40

300 Pounds per Hour

Power Input	5000 watts
Steam Flow Rate	280 lbs/hr
Water Injection Rate	20 lbs/hr
Steam Inlet Temperature	289.8° F
Inlet Quality	0.938
Test Section Static Pressure	60.7 inches Hg, abs
Test Section Pressure Drop	0.178 inches Hg/ft
Exit Temperature	248° F

T. C. No.	Quality	Wall Temperature	Heat Transfer Coefficient
1	0.940	254.2	4090
2	0.944	254.5	3800
3	0.947	255.6	3030
4	0.950	255.6	2980
5	0.953	256.8	2440
6	0.956	259.3	1760
7	0.959	269.7	830
8	0.963	277.1	604
9	0.966	289.5	413
10	0.969	297.2	346
11	0.972	301.6	316
12	0.975	312.5	262
13	0.977	312.9	259
14	0.981	329.4	205
15	0.985	340.8	180
16	0.988	436.0	87.7
17	0.991	517.7	61.0
18	0.996	510.5	62.7

Run Number 41

300 Pounds per Hour

Power Input	6000 watts
Steam Flow Rate	270 lbs/hr
Water Injection Rate	30 lbs/hr
Steam Inlet Temperature	288.5° F
Inlet Quality	0.897
Test Section Static Pressure	61.0 inches Hg, abs
Test Section Pressure Drop	0.201 inches Hg/ft
Exit Temperature	248.5° F

T. C. No.	Quality	Wall Temperature	Heat Transfer Coefficient
1	0.900	256.1	3580
2	0.903	256.4	3340
3	0.907	256.6	3230
4	0.911	256.2	3390
5	0.915	257.2	2890
6	0.919	257.6	2730
7	0.922	263.0	1550
8	0.926	258.9	2290
9	0.930	266.2	1230
10	0.934	274.1	824
11	0.937	273.9	826
12	0.941	281.4	628
13	0.945	283.7	585
14	0.949	295.3	434
15	0.952	296.3	425
16	0.956	303.8	365
17	0.960	308.5	336
18	0.964	318.5	286

Run Number 42

400 Pounds per Hour

Power Input	1500 watts
Steam Flow Rate	390 lbs/hr
Water Injection Rate	10 lbs/hr
Steam Inlet Temperature	293.4° F
Inlet Quality	0.991
Test Section Static Pressure	61.1 inches Hg, abs
Test Section Pressure Drop	0.279 inches Hg/ft
Exit Temperature	249.2° F

T. C. No.	Quality	Wall Temperature	Heat Transfer Coefficient
1	0.992	251.3	9400
2	0.992	252.0	3610
3	0.993	252.0	3610
4	0.994	251.5	5220
5	0.994	252.8	2140
6	0.995	255.4	959
7	0.996	256.8	745
8	0.996	255.2	979
9	0.997	257.6	644
10	0.998	263.7	351
11	0.998	269.4	245
12	0.999	274.7	192
13	1.000	275.0	189
14		276.8	175
15		283.4	141
16		293.2	108
17		294.2	106
18		303.8	87.0

Run Number 43

400 Pounds per Hour

Power Input	2000 watts
Steam Flow Rate	386 lbs/hr
Water Injection Rate	14 lbs/hr
Steam Inlet Temperature	294.2° F
Inlet Quality	0.979
Test Section Static Pressure	61.5 inches Hg, abs
Test Section Pressure Drop	0.268 inches Hg/ft
Exit Temperature	248.5° F

T. C. No.	Quality	Wall Temperature	Heat Transfer Coefficient
1	0.980	251.3	3180
2	0.981	252.4	4890
3	0.982	252.4	4890
4	0.982	251.7	9080
5	0.983	252.2	5300
6	0.984	252.5	3960
7	0.985	253.9	2120
8	0.986	253.0	2890
9	0.987	259.7	705
10	0.988	263.8	485
11	0.989	265.7	421
12	0.990	266.9	390
13	0.991	268.0	363
14	0.992	269.5	333
15	0.993	269.9	326
16	0.994	273.1	279
17	0.994	273.9	269
18	0.995	275.4	252

Run Number 44

400 Pounds per Hour

Power Input	2000 watts
Steam Flow Rate	389 lbs/hr
Water Injection Rate	11 lbs/hr
Steam Inlet Temperature	291.8° F
Inlet Quality	0.987
Test Section Static Pressure	61.0 inches Hg, abs
Test Section Pressure Drop	0.294 inches Hg/ft
Exit Temperature	248.8° F

T. C. No.	Quality	Wall Temperature	Heat Transfer Coefficient
1	0.988	251.4	9080
2	0.989	251.6	7060
3	0.990	252.2	3970
4	0.991	252.6	3030
5	0.991	253.5	2120
6	0.992	258.1	825
7	0.993	263.3	493
8	0.994	266.4	395
9	0.995	270.0	321
10	0.996	275.2	254
11	0.997	279.0	220
12	0.998	284.7	183
13	0.999	291.5	153
14	1.000	297.0	135
15		319.3	91.6
16		337.2	72.7
17		339.4	70.8
18		339.1	71.0

Run Number 45

400 Pounds per Hour

Power Input	3000 watts
Steam Flow Rate	375 lbs/hr
Water Injection Rate	25 lbs/hr
Steam Inlet Temperature	293.7° F
Inlet Quality	0.945
Test Section Static Pressure	60.9 inches Hg, abs
Test Section Pressure Drop	0.265 inches Hg/ft
Exit Temperature	247.6° F

T. C. No.	Quality	Wall Temperature	Heat Transfer Coefficient
1	0.946	252.5	5110
2	0.948	252.5	4850
3	0.949	252.5	4850
4	0.951	252.2	5380
5	0.952	252.3	5110
6	0.953	251.8	6460
7	0.955	253.4	3030
8	0.956	251.5	7460
9	0.958	251.8	5700
10	0.959	251.8	5700
11	0.961	251.8	5380
12	0.962	252.2	4410
13	0.963	252.2	4220
14	0.965	252.5	3730
15	0.966	252.2	4040
16	0.968	253.1	4040
17	0.969	252.5	3460
18	0.970	251.7	4850

Run Number 46

400 Pounds per Hour

Power Input	3000 watts
Steam Flow Rate	386 lbs/hr
Water Injection Rate	14 lbs/hr
Steam Inlet Temperature	294.5° F
Inlet Quality	0.979
Test Section Static Pressure	61.1 inches Hg, abs
Test Section Pressure Drop	0.315 inches Hg/ft
Exit Temperature	250.2° F

T. C. No.	Quality	Wall Temperature	Heat Transfer Coefficient
1	0.980	252.3	6930
2	0.982	253.9	3130
3	0.983	254.5	2550
4	0.984	254.1	2850
5	0.986	254.7	2360
6	0.987	259.5	1080
7	0.989	273.7	418
8	0.990	290.5	236
9	0.991	300.9	192
10	0.993	366.3	83.5
11	0.994	385.5	71.6
12	0.995	392.3	68.1
13	0.997	395.0	66.9
14	0.998	396.5	66.6
15	0.999	398.1	65.4
16		401.5	64.0
17		402.6	63.5
18		395.6	66.5

Run Number 47

400 Pounds per Hour

Power Input	4500 watts
Steam Flow Rate	375 lbs/hr
Water Injection Rate	25 lbs/hr
Steam Inlet Temperature	293.7° F
Inlet Quality	0.945
Test Section Static Pressure	61.0 inches Hg, abs
Test Section Pressure Drop	0.280 inches Hg/ft
Exit Temperature	247.8° F

T. C. No.	Quality	Wall Temperature	Heat Transfer Coefficient
1	0.947	253.6	5060
2	0.949	253.8	4590
3	0.951	253.8	4590
4	0.953	253.2	5450
5	0.955	253.9	4320
6	0.958	253.4	4900
7	0.960	256.5	2410
8	0.962	253.4	4740
9	0.964	265.5	2330
10	0.966	260.8	1390
11	0.968	262.7	1170
12	0.971	272.0	671
13	0.973	273.7	620
14	0.975	281.1	471
15	0.977	282.3	454
16	0.979	291.9	349
17	0.981	297.3	309
18	0.983	304.7	267

Run Number 48

400 Pounds per Hour

Power Input	4500 watts
Steam Flow Rate	386 lbs/hr
Water Injection Rate	14 lbs/hr
Steam Inlet Temperature	294.4° F
Inlet Quality	0.979
Test Section Static Pressure	61.4 inches Hg, abs
Test Section Pressure Drop	0.344 inches Hg/ft
Exit Temperature	266.2° F

T. C. No.	Quality	Wall Temperature	Heat Transfer Coefficient
1	0.981	259.7	1710
2	0.983	260.0	1650
3	0.985	260.1	1630
4	0.987	277.0	565
5	0.989	411.8	91.4
6	0.992	423.0	85.4
7	0.994	439.3	78.0
8	0.996	444.8	76.0
9	0.998	446.5	75.0
10		455.6	74.3
11		466.7	68.0
12		473.5	65.9
13		480.0	64.0
14		484.1	62.9
15		488.3	61.7
16		497.5	59.4
17		498.7	59.1
18		487.6	61.8

Run Number 49

400 Pounds per Hour

Power Input	5000 watts
Steam Flow Rate	375 lbs/hr
Water Injection Rate	25 lbs/hr
Steam Inlet Temperature	295.2° F
Inlet Quality	0.944
Test Section Static Pressure	61.6 inches Hg, abs
Test Section Pressure Drop	.301 inches Hg/ft
Exit Temperature	247.7° F

T. C. No.	Quality	Wall Temperature	Heat Transfer Coefficient
1	0.946	254.6	4300
2	0.948	254.6	4300
3	0.951	254.6	4190
4	0.953	254.5	4300
5	0.955	255.3	3480
6	0.958	256.6	2780
7	0.960	263.6	1250
8	0.962	263.9	1210
9	0.965	274.5	675
10	0.967	279.9	553
11	0.969	285.7	461
12	0.972	292.8	383
13	0.974	295.4	361
14	0.977	300.2	326
15	0.979	301.4	318
16	0.981	312.9	260
17	0.984	314.4	253
18	0.986	329.8	204

Run Number 50

400 Pounds per Hour

Power Input	6000 watts
Steam Flow Rate	375 lbs/hr
Water Injection Rate	25 lbs/hr
Steam Inlet Temperature	294° F
Inlet Quality	0.946
Test Section Static Pressure	61.1 inches Hg, abs
Test Section Pressure Drop	0.301 inches Hg/ft
Exit Temperature	248.5° F

T. C. No.	Quality	Wall Temperature	Heat Transfer Coefficient
1	0.948	254.6	5180
2	0.951	255.1	4580
3	0.954	255.5	4100
4	0.957	255.0	4580
5	0.960	255.5	4020
6	0.962	255.7	3780
7	0.965	260.6	1950
8	0.968	259.4	2180
9	0.971	366.8	169
10	0.974	457.6	95.0
11	0.976	496.8	79.6
12	0.979	499.6	78.9
13	0.982	505.3	77.1
14	0.985	520.1	72.9
15	0.988	525.5	71.5
16	0.990	541.3	67.6
17	0.993	544.7	66.7
18	0.996	529.7	70.4

APPENDIX D

Methods of Computation

As mentioned previously, one of the undesirable features of the apparatus was the fact that the steam was not condensed and measured at the exhaust of the system. Since the steam was simply thrown into the atmosphere, complete energy balances were impossible to make for the wet steam runs. For this reason, superheated steam runs were used to make energy balances and these values of heat losses were used as corrections for the wet steam data. It is admitted that this was not a precise method of determining or estimating losses, but, since in most cases the losses were small, it is felt that the reliability of the tabulated heat transfer coefficients was not greatly affected.

Superheated steam runs were made with thermocouple installations at the elbow at the base of the vertical run, and at the entrance and exit to the test section. Dry steam data from 15 runs were analyzed and averaged and this led to the decision to make the following constant correction for all runs:

Heat loss from elbow to test section entrance - 600 Btu/hr.

Heat loss from test section entrance to test section outlet - 300 Btu/hr.

Heat loss from test section outlet to thermocouple installation - 100 Btu/hr.

A study of the following methods of computation will show that the corrections could affect the local quality by less than one percent and the value of the heat transfer coefficient by less than 10 percent.

The quality at the entrance to the test section was computed by assuming that the superheated steam and the injection water mix at constant pressure. An energy balance gives:

$$W_s h_s + W_w h_w = (W_s + W_w)(h_f + X h_{fg}) \quad .$$

Thus

$$X = \frac{W_s h_s + W_w h_w}{(W_w + W_s) h_{fg}} - \frac{h_f}{h_{fg}} \quad .$$

The values of enthalpy were taken from Keenan and Keyes (34).

The heat flux was computed by taking the measured power input to the test section, converting it to Btu/hr, correcting by the constant heat loss factor, and dividing by the area of heating. Thus

$$\frac{(\text{Power in watts})\,(3,414) - 300}{1.025} = q'' \quad .$$

The heat transfer coefficient was obtained by dividing the heat flux obtained above by the temperature difference between the wall and bulk temperature of the fluid. In the tabulated data the heat transfer coefficient was obtained by assuming that the bulk temperature of the fluid was the saturation temperature corresponding to the pressure, for regions where the apparent quality was less than 100 percent. For regions where the apparent quality was greater than 100 percent the bulk

temperature was assumed to be based on a linear interpolation between the saturation temperature and the exit thermocouple reading, correcting for the heat loss between the test section outlet and the thermocouple.

The local pressure used in determining the local saturation temperature was based on a linear interpolation between the pressure taps.

The apparent quality at any particular thermocouple location was determined from the expression

$$X = X_o + \frac{q''\pi DL}{W h_{fg}} \quad .$$

Heating was assumed to start $\frac{1}{2}$ inch from the inlet of the test section and to end $\frac{1}{2}$ inch from the exit.

Bulk temperatures for the superheated steam runs were determined from the inlet and outlet thermocouple temperature readings corrected for losses, and assuming a linear increase in bulk temperature during heating.

APPENDIX E

Nomenclature

a	-	acceleration, ft per sec^2
A	-	projected area of droplet or particle, ft^2
b	-	parameter in distribution equation or coefficient in Vanderwater equation for mass transfer coefficient
B	-	$B = \frac{3\pi\mu_v d}{m}$
c	-	dimensionless coefficient
C	-	local concentration of diffusing substance, lbs per ft^3
C_E	-	electrical capacitance, farads
C_D	-	drag coefficient
C_p	-	specific heat at constant pressure, Btu per lb ^oF
d	-	diameter of droplet or particle, ft
d_{32}	-	Sauter mean diameter, microns
d_m	-	maximum stable droplet diameter, ft
$\bar{d}$	-	size parameter in distribution equation
D	-	inside diameter of duct, ft
E'	-	re-entrainment function in Vanderwater equation
f	-	Fanning friction factor
f'_m	-	apparent friction factor of Fig. 2
g	-	acceleration of gravity, ft per sec^2

g_c - dimensional constant, lbs mass ft per lb force hr^2

G - mass velocity, lbs per sec ft^2

G_d - mass velocity of dispersed phased, lbs per sec ft^2

G_g - mass velocity of gas or vapor phase, lbs per hr ft^2

G_L - mass velocity of liquid phase, lbs per hr ft^2

h - heat transfer coefficient, Btu per hr ft^2 ^oF

h_f - saturation enthalpy of liquid phase, Btu per lb

h_{fg} - enthalpy of vaporization, Btu per lb

h_s - enthalpy of steam, Btu per lb

h_w - enthalpy of water, Btu per lb

j - exponent in Vanderwater equation for mass transfer coefficient

k - thermal conductivity, Btu per hr ft ^oF

k_d - mass transfer coefficient for droplets, ft per hr

K - parameter in Fig. 9 $K = \frac{\pi}{18} \bar{N}_{Re} \frac{d}{\ell_1} \frac{\rho_L}{\rho_g}$

ℓ_1 - scale of turbulence, ft

L - distance from a reference position, ft

L^+ - non-dimensional stopping distance, $L^+ = \frac{L u_{avg}}{\nu} \sqrt{\frac{f}{2}}$

L' - distance upstream from point of 100 percent quality, ft

m - mass of droplet or particle, lbs

M - rate of transfer of diffusing substance, lbs per hr

N_{Pr} - Prandtl number

N_{Re} - Reynolds number for flow of gas or vapor phase

$\bar{N}_{Re}$ - Reynolds' number based on particle diameter and relative velocity

N_{Nu} - Nusselt number

P_{avg} - average static pressure of mixture, psfa

P_i - inlet static pressure of mixture, psfa

q - heat flow, Btu per hour

q'' - heat flux, Btu per hr ft^2

Q - electric charge, Coulombs

Q_L - volume rate of liquid flowing, cfs

Q_g - volume rate of gas or vapor flowing, cfs

r^+ - non-dimensional distance from wall, $r^+ = \frac{r u_{avg}}{\nu} \sqrt{\frac{f}{2}}$

R_1 - first root of zero order Bessel function of first kind

S - ratio of average liquid velocity to average stream velocity

T_B - bulk temperature, ^oF

T_f - average film temperature, ^oF

T_w - wall temperature, ^oF

u_{avg} - average axial velocity of gas or vapor phase, ft per sec

u_d - axial velocity of dispersed phase, ft per sec

u_g - axial velocity of gas or vapor phase, ft per sec

u_o - initial velocity of particle, ft per sec

u^* - friction velocity $u^* = u_{avg} \sqrt{\frac{f}{2}}$, ft per sec

$\bar{u}$ - average axial velocity of gas or vapor phase, ft per hr

Δu - relative velocity between droplet or particle and the gas or vapor phase, ft per sec

U - peak velocity of turbulent gas fluctuation, ft per sec

U_B - local overall heat transfer coefficient for boiling, Btu per hr ft^2 ^oF

v - volume fraction of drops or particles having diameters greater than d

v' - root mean square of the radial component of the fluctuating gas velocity, ft per sec

Δv - relative velocity between liquid and air, meters per sec

V - voltage, volts

V_B - boiling velocity, ft per sec

w - flow rate of liquid, lbs per sec

w^+ - non-dimensional flow rate $w^+ = \frac{w}{\pi D \mu_d}$

W - total flow rate, lbs per hour

W_L - flow rate of dispersed phase, lbs per min

W_g - flow rate of gas or vapor phase, lbs per min

W_S - flow rate of steam, lbs per hour

W_w - flow rate of water, lbs per hour

x - distance, ft

X - quality

X_o - initial quality at reference position

y - distance, ft

y_m - apparent quality, Fig. 2

Z - droplet or particle displacement from mean position, ft

Z_m - maximum displacement from mean, ft

Z_o - $Z_o = \frac{U}{\omega}$

δ - size distribution parameter

α_d - eddy diffusivity of droplet or particle, ft^2 per sec

α_g - eddy diffusivity of gas or vapor phase, ft^2 per sec

θ - time, sec or temperature difference $\theta = T - T_B$, ^oF

μ - dynamic viscosity of liquid phase, dyne sec per cm^2

μ_d - dynamic viscosity of liquid phase, lbs per sec ft

μ_L - dynamic viscosity of liquid phase, centipoise

μ_m - mean viscosity of mixture, lbs per sec ft

μ_v - dynamic viscosity of gas or vapor phase, lbs per sec ft

ν - kinematic viscosity, ft^2 per sec

ρ - density, lbs per ft^3

ρ_{avg} - average density of mixture, lbs per ft^3

ρ_d - density of dispersed phase, gm per cm^3

ρ_g - density of gas or vapor phase, lbs per ft^3

ρ_L - density of dispersed phase, lbs per ft^3

σ - surface tension of liquid, dynes per cm

σ_L - surface tension of liquid, lbs per sec^2

τ - shear stress, lbs per ft^2

τ_w - shear stress at wall, lbs per ft^2

ω - angular frequency, radians per sec

$\left[\frac{dP}{dL}\right]_{TPF}$ - two phase friction pressure gradient

$\left[\frac{dP}{dL}\right]_{O}$ - pressure gradient for liquid only flowing at the total flow rate

$\left[\frac{\Delta P}{\Delta L}\right]_{TP}$ - pressure drop for two phase flow, psi per ft

$\left[\frac{\Delta P}{\Delta L}\right]_{L}$ - pressure drop if liquid were flowing alone, psi per ft

$\left[\frac{\Delta P}{\Delta L}\right]_{G}$ pressure drop if gas were flowing alone, psi per ft

APPENDIX F

List of Equipment

Item	Manufacturer	Serial No.
Autoscaler, Model SCIC	Tracerlab	735
Manometer, 36" Cleanout Type	Meriam	-
Manometers (4), Type W, Model A338A	Meriam	18443 16663 16843 16797
Oscillograph, Type 543	Tektronix	637
Oscillograph Record Camera, Type 297	Dumont	275
Potentiometer, Portable Precision	Leeds and Northrup	546326
Powerstats (3), Type 1256, 7.5 kva	Superior	670 1491
Pressure Gauge, Air 0-150 psig	Trerice	-
Pressure Gauge, Steam, 0-160 psig	Ashcroft	41775
Pressure Regulator, Type F-M	Rego	848
Pulse Height Analyzer, RLI-4	Tracerlab	322
Rotameter	Fischer Porter	3-2288
Wattmeter, Type P-3 0-12,000 watts	General Electric	2607437